CHAPTER 5

INTERPRETATION OF THE CONE PRESSUREMETER TEST IN SAND

5.1 Introduction

The dominant reason for the development of the cone pressuremeter had been to provide information originally on soil stiffness, and more recently on strength and *in situ* horizontal stress. In this chapter, analyses for the determination of relative density (and hence friction angle) and *in situ* horizontal stress are applied to the database of calibration chamber tests in sand. The database draws together tests in Hokksund feldspathic sand reported in Chapter 3, Dogs Bay carbonate sand reported in Chapter 4 and Leighton Buzzard silica sand reported by Schnaid (1990) in the same chamber, and is representative of a wide range of sand types encountered in the field.

In clays, analytical methods of obtaining soil properties from the CPM have proved successful (Houlsby and Withers, 1988; Campanella *et al.*, 1990; Houlsby and Nutt, 1992). The volume change characteristics of sands, coupled with the large cavity strains induced by the CPM, however, present additional complexities in cavity expansion theory. Analytical solutions, whether closed form (Yu and Houlsby, 1991), numerical (Houlsby and Yu, 1990) or numerical/empirical (Collins *et al.*, 1992) are shown to be of limited success in modelling CPM behaviour in sands.

The use of empirical correlations developed from calibration chamber tests is an alternative

approach to CPM interpretation. It is shown in this chapter that two well defined, independent CPM measurements, the cone resistance and the limit pressure, are dependent upon only two soil parameters, relative density and horizontal stress. Correlations are presented which link these variables and can be solved to give reasonable estimates of relative density and *in situ* horizontal stress. The important finding of this chapter is that these correlations can be applied to all three sands tested in the calibration chamber within the range of stresses at which testing was carried out.

5.2 Analytical methods of CPM interpretation

5.2.1 Small strain elastic-plastic analysis

Among the few reported sets of field testing with the cone pressuremeter are the tests in sand reported and interpreted in a paper by Withers *et al.* (1989). The paper is important because it is the first attempt to produce a comprehensive approach to CPM interpretation in sand. Withers *et al.* present a detailed explanation of the mechanism of cone penetration and pressuremeter inflation, and this has been discussed in Chapter 1 and summarised in Figure 1.8. Making use of the Hughes *et al.* (1977) analysis, they adopted graphical methods of calculating friction and dilation angles of the sand. From the analytical expression of the expansion curve, it was shown that

$$\log \psi = S_e \log(\varepsilon + c_e) + constant \qquad ...(5.1)$$

where ψ is the inflation pressure and c_e is negligibly small compared with ε, the pressuremeter strain defined as $(R - R_0) / R_0$. Note that this definition of strain is only applicable to small strains, and in the CPM test it is better to use $\varepsilon = \ln(R / R_0)$. In the self-boring pressuremeter test, S_e is a slope of the linear portion of the plot of equation (5.1) defined as

$$S_e = \frac{1 - N}{1 + n} \quad \text{for cylindrical expansion} \qquad ...(5.2)$$

where $$N = \frac{1 - \sin\phi}{1 + \sin\phi} \quad ...(5.3)$$

and $$n = \frac{1 - \sin\nu}{1 + \sin\nu} \quad ...(5.4)$$

N and n can be linked by the stress dilatancy theory of Rowe (1962) by the equation

$$N = nN_{cv} \quad ...(5.5)$$

Hence a knowledge of ϕ_{cv} (the angle of internal friction when soil fails at constant volume), and a measurement of S_e leads to estimates of ϕ and ν. This graphical approach was applied to the CPM field tests where an early deviation from linearity (*i.e* S_e not constant) was observed in the plot of log ψ against log ε resulting in unrealistically high estimates of ϕ and ν. Withers *et al.* (1989) attributed this to significant creep strains in the soil at large CPM expansions. Indeed, creep has been shown in the previous chapter to influence the pressure expansion curve, however, it is most likely that the small strain analysis of Hughes *et al.* (1977), developed for the SBPM is simply not applicable to the CPM test where the soil has been grossly disturbed prior to pressuremeter inflation.

It would be more realistic to expect the unloading portion of the pressuremeter curve to be less sensitive to initial disturbance, and the graphical method of Withers *et al.* was extended to incorporate the small strain unloading analysis of Houlsby *et al.* (1986). A greater degree of linearity was observed in the unloading curves of the CPM in the plot of $\ln(\psi / \psi_l)$ against $\ln[(\varepsilon_e - \varepsilon) / (1+\varepsilon_e)]$ where ε_e is the maximum pressuremeter strain. Unrealistically low values of ϕ and ν, however, were obtained from this analysis, and Withers *et al.* concluded that neither expansion nor contraction theory was suitable for CPM interpretation of ϕ and ν.

5.2.2 Large strain elastic-plastic analysis

Use of the unloading curve of the cone pressuremeter was taken further by Houlsby and Yu (1990). Assuming that the CPM test can be simulated by the expansion and contraction of a cylindrical cavity under conditions of plane strain and axial symmetry, a numerical analysis was developed which allowed for the large strains typical of a CPM test. It was found that the plastic unloading slope in a plot of $\ln\psi$ against $-\ln(\varepsilon_{max} - \varepsilon)$ is primarily controlled by the soil strength parameters and to a small extent to soil stiffness, where ψ is the cavity pressure and ε_{max} and ε are the maximum and current cavity strains respectively.

The pressuremeter curves for two typical tests in Dogs Bay sand, one loose and one dense, are shown in Figure 5.1 in logarithmic form. The unloading curve of the test in loose sand is linear with a slope of

$$S_d = -\frac{N - \frac{1}{N}}{N + \frac{1}{n}} \qquad ...(5.6)$$

where N and n are given by equations (5.3) and (5.4) respectively. If N and n are related as in equation (5.5), then the following expression for friction angle results

$$\sin\phi = \left(\sin\phi_{cv} + \frac{1+\sin\phi_{cv}}{S_d}\right) - \sqrt{\left(\sin\phi_{cv} + \frac{1+\sin\phi_{cv}}{S_d}\right)^2 - 1} \qquad ...(5.7)$$

The measured values of S_d in the loose samples result in estimates of ϕ for Dogs Bay sand of about 9° and in Hokksund sand of about 16°, clearly unrealistic values. In dense sands, it is shown in Figures 5.1(b) and 5.2(b) that the unloading curves in the logarithmic plots are not linear and no estimates of ϕ can be made at all. The same conclusion was drawn by Houlsby and Yu (1990) based on the calibration chamber tests of Schnaid (1990).

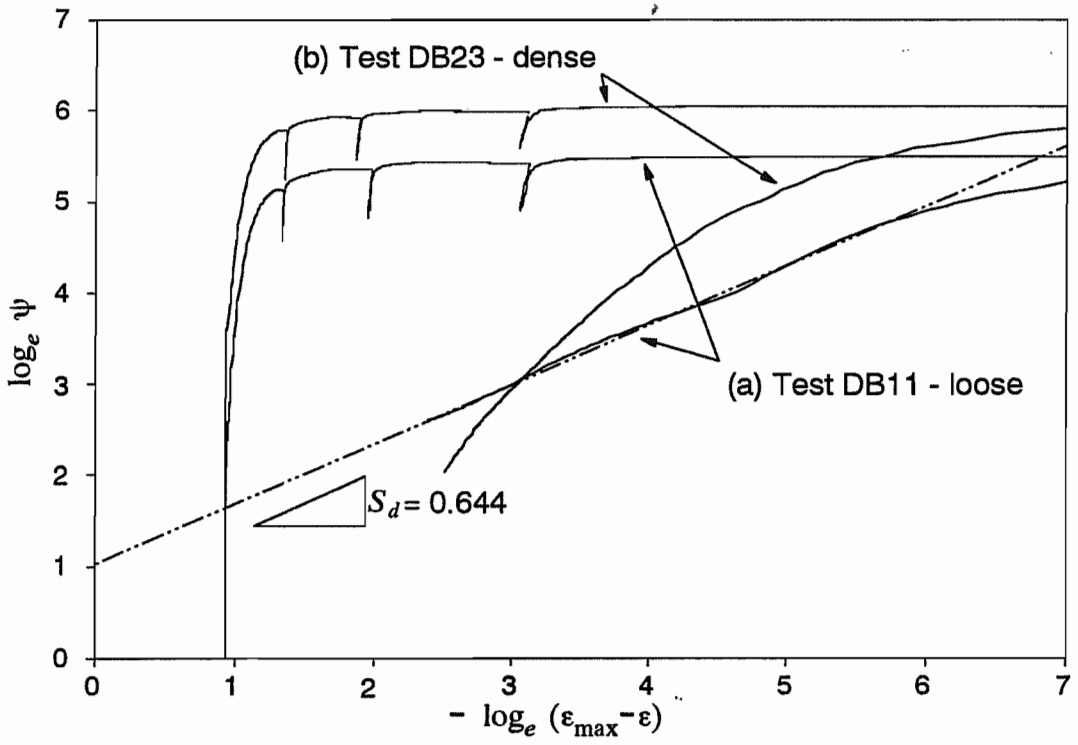

Figure 5.1 Logarithmic construction to determine the unloading slope from tests in Dogs Bay sand (a) loose (b) dense

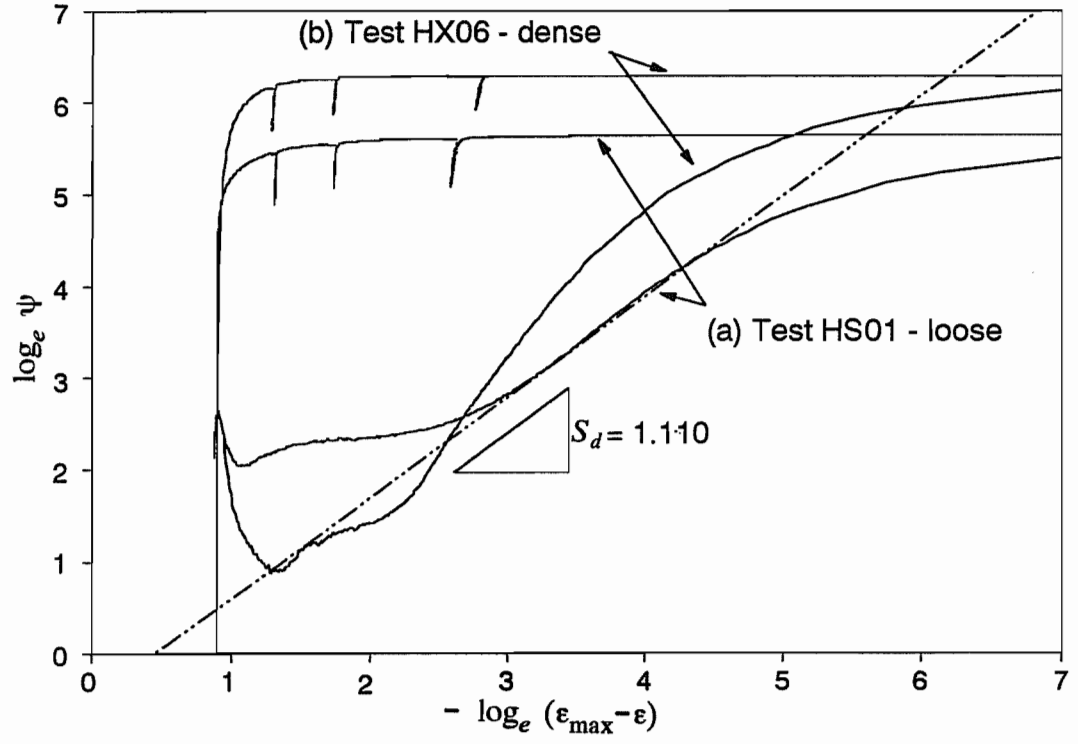

Figure 5.2 Logarithmic construction to determine the unloading slope from tests in Hokksund sand (a) loose (b) dense

This numerical analysis was refined and presented for the case of cavity expansion as a closed form solution by Yu and Houlsby (1991). From the solution it is possible to construct the complete pressure-expansion curve, with no restriction placed on the magnitude of deformation. Like the numerical analysis, the soil is modelled as linear elastic-perfectly plastic, using a Mohr-Coulomb yield criterion and assuming angles of friction and dilation that remain constant throughout the cavity expansion.

The solution has been applied to the cone pressuremeter tests in Dogs Bay sand, and the results are presented in Table 5.1. Because the analysis is applicable only to isotropic stress conditions, only those tests in Dogs Bay sand with an initial stress ratio of unity have been interpreted.

Table 5.1 Friction angles obtained from CPM tests in Dogs Bay sand using the Yu and Houlsby (1991) analysis

Test	p' (kPa)	D_r (%)	ψ_i (kPa)	$\frac{G}{p'}$	ϕ degrees
DB5	38.1	23.9	297	72	34.5
DB6	98.1	22.1	686	92	28.4
DX9	148.2	31.0	934	88	25.9
DB32	252.2	34.1	1467	93	24.1
DB17	40.8	52.1	485	95	36.9
DB10	99.2	53.8	1014	76	34.8
DB25	149.5	57.0	1332	75	30.4

Estimates of ϕ were made from measurements of ψ_i, G/p' (the average value of G obtained from CPM unload/reload loops was used, as discussed in Chapter 7) and dilation angle, ν. Dilation was assumed to be zero in the loose sands, and 10° in the dense sands. Given that

ϕ_{cv} for Dogs Bay sand is 40.3°, the Yu and Houlsby solution underpredicts friction angle, ϕ (or overpredicts limit pressure). It can be noted that at increasing mean effective stress, estimated friction angles decrease. This indicates that the initial assumption of constant ϕ and ν is not strictly valid, and this effect is more dramatic in the compressible Dogs Bay sand than in silica sands. The influence of chamber size will also contribute somewhat to the underprediction of ϕ, and this is dealt with in section 5.5.

5.2.3 Large strain critical state analysis

In both the small and large strain analyses of the previous two sections, the assumption was made that that the soil can be modelled as an elastic, perfectly plastic material with constant friction and dilation angles. In a different approach based on critical state theories, Collins *et al.* (1992) presented a large strain cavity expansion numerical analysis in which the changes in volumetric strains rather than the shear strains govern the material properties. Based on calibration chamber test data in sands, an empirical relationship was presented to provide a fit to the results of a numerical analysis, and in this section is used for comparison with the cone pressuremeter tests.

From the Collins *et al.* (1992) analysis, the angles of internal friction and dilation are assumed to vary with the mean effective stress and relative density and are thus expressed as a function of a state parameter defined as

$$\xi = \nu + \lambda \ln\left(\frac{p'}{p_1}\right) - \Gamma_1 \qquad ...(5.8)$$

where ξ is the state parameter, ν is the specific volume, p' is the mean effective stress, p_1 is a reference pressure, λ is the slope of the critical state line, and Γ_1 is the intercept on the $p' = p_1$ axis. The analysis assumes small strains in the elastic regime and large strains in the plastic regime, with expansions starting from zero initial radius. The solution for the distribution of

stresses in the elastic regime, therefore, is the same as that given by Withers *et al.* (1989). In the plastic regime, the strain is expressed in the form of a set of simultaneous partial differential equations (P.D.E) in terms of radius and time. Using the assumption that expansion occurs in a geometrically self-similar manner (which will be true as long as the problem has no characteristic length scale), the P.D.E's are reduced to ordinary differential equations and solved numerically.

Been and Jefferies (1985), cited by Collins *et al.* (1992) compared data from a diversity of sand types and reported the relationship between friction angle and state parameter.

$$\phi - \phi_{cv} = f(\xi) = A(e^{-\xi} - 1) \qquad ...(5.9)$$

where A is a parameter measured in radians in the range 0.6 to 0.95 depending on the type of sand.

Collins *et al.* (1992) fitted an empirical relationship to the results of the analysis so that estimations of limit pressure can be made from a knowledge of initial specific volume, v_0 and initial mean effective stress, p_0. The relationship takes the form

$$\frac{\psi_l}{p_0} = c_1 \, p_0^{(c_2+c_3 v_0)} \, e^{(-c_4 v_0)} \qquad ...(5.10)$$

where c_1 to c_4 are constants for a particular sand and a particular mode of cavity expansion (*i.e.* cylindrical or spherical).

The limiting cavity pressures for the six sands reported by Collins *et al.* (1992), namely Monterey, Hokksund, Kogyuk, Ottawa, Reid Bedford and Ticino sands, have been estimated using the assumption that cone resistance is best modelled as a spherical cavity expansion, and pressuremeter limit pressure is best modelled as a cylindrical cavity expansion. Expressed in the terms of the normalised factors $(q_c - \sigma_h) / \sigma_h$ and $(\psi_l - \sigma_h) / \sigma_h$, a comparison of these empirical results is made with the CPM tests in Figures 5.3 and 5.4. Of the data from six

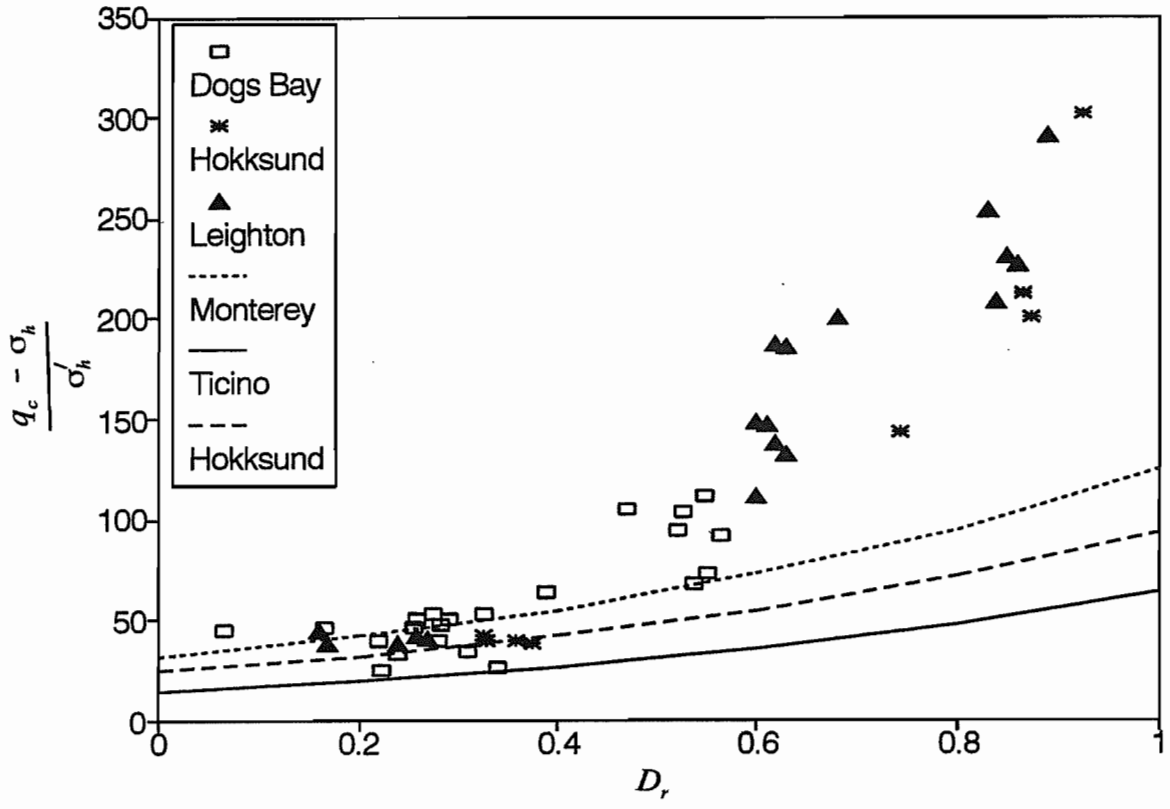

Figure 5.3 A comparison between q_c measured in the calibration chamber and the analysis of Collins *et al.* (1992)

sands, Monterey and Ticino have been plotted because they represent the upper and lower bounds respectively, while Hokksund has been plotted so that comparisons with the CPM tests in Hokksund sand can be made. In Figure 5.3, the cone resistance as estimated by equation (5.10) predicts the CPM results only for loose sands. The influence of D_r is clearly not as strong as observed in the calibration chamber. A better comparison is made in Figure 5.4 where the range of scatter of the CPM tests is comparable with the empirical predictions, and the influence of relative density is similar. The empirical estimations, however, do slightly overpredict the limit pressures obtained from CPM tests, as observed from the differences in the two sets of data for Hokksund sand.

Considering that eight different sand types are represented in Figures 5.3 and 5.4, it can be concluded that the cone resistance is not well modelled by the spherical cavity expansion analysis of Collins *et al.* (1992), and that cylindrical cavity expansion is a reasonable

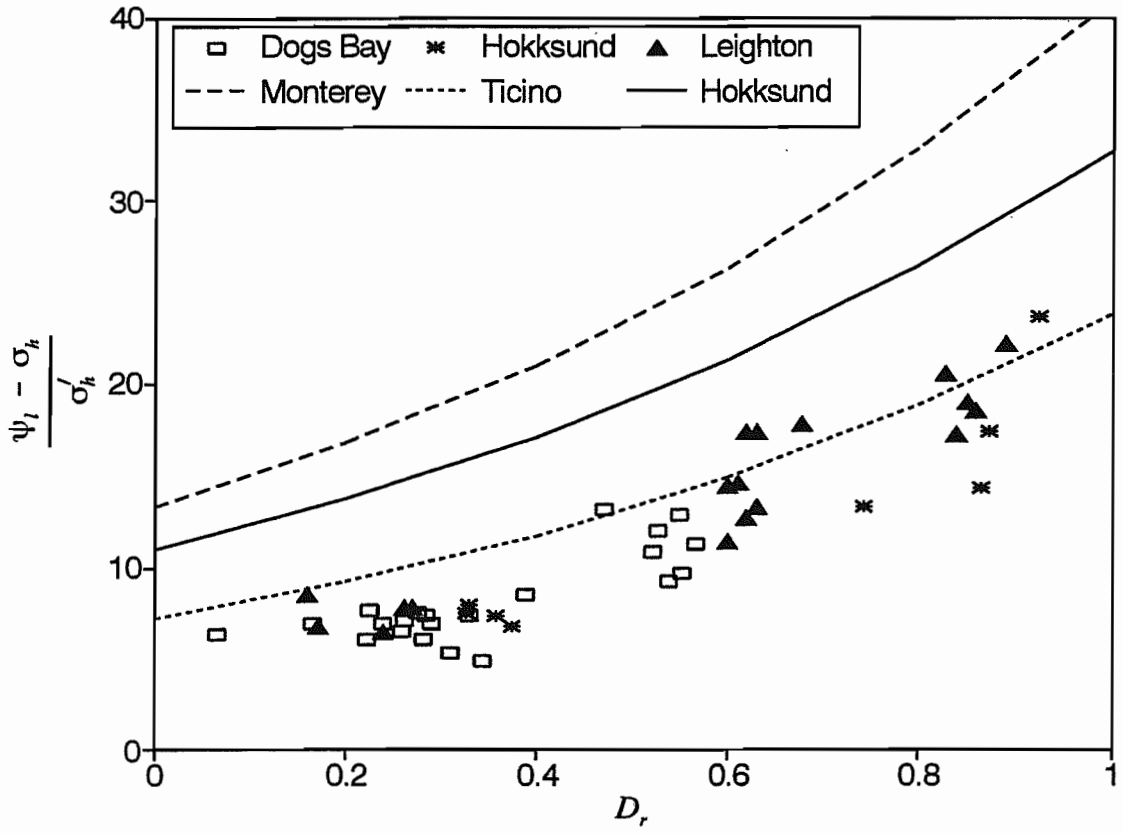

Figure 5.4 A comparison between limit pressure measured in the calibration chamber and the analysis of Collins *et al.* (1992)

assumption for the process of pressuremeter inflation.

5.2.4 General comments

Three approaches have been presented for interpretation of the cone pressuremeter in sands, which are each based upon cavity expansion theory, and they are distinguished from each other by the assumptions made about soil behaviour. Withers *et al.* (1989) have assumed that the soil can be modelled as an elastic-plastic material where elastic strains in the plastic regime have been neglected. This led to estimations of ϕ and ν which were unrealistically high for cylindrical cavity expansion and unrealistically low for cylindrical cavity contraction.

The analyses of Houlsby and Yu (1990) and Yu and Houlsby (1991) incorporate large strains more typical of cone pressuremeter behaviour, again based on the assumption that the soil can

be modelled as an elastic-perfectly plastic Mohr Coulomb material. This means that throughout an analysis, the initial estimates of ϕ and ν remain constant. Hence the limit pressures calculated from the loading analysis and the logarithmic slopes calculated for the unloading analysis are too high for rational interpretation.

The analysis of Collins *et al.* (1992) assumes that critical state theory applies, and that ϕ and ν are not constant, but vary throughout the analysis with specific volume (or relative density) and mean effective stress. While this is more fundamentally correct than the Yu and Houlsby approach, the analysis cannot be solved in closed form, requiring numerical methods for the calculation of limit pressures. For simplification, an empirical estimation of the analysis is presented, and found to underpredict significantly cone resistance as measured by the CPMT, and overpredict marginally CPM limit pressures.

The conclusion is that none of the analyses presented can accurately model the mechanism of cone penetration followed by pressuremeter inflation that is applied by the CPM in sand. This is because the stress path followed by a soil element that is initially on the axis of penetration is more complicated than is assumed by a single continuous cavity expansion. A small unloading or cavity contraction is experienced as the shoulder of the cone passes the soil element such that during pressuremeter inflation, the element will first be reloaded elastically before again yielding. Then, as pressuremeter expansion proceeds, as shown in Figure 5.5 there is a transition from a mechanism of cylindrical cavity expansion to spherical cavity expansion as the diameter of the elastic-plastic boundary approaches a dimension of similar magnitude to the length of the pressuremeter. Since neither of these features is accounted for in the above analyses, interpretation of the CPMT in sand is shown to be more successful by direct observation based upon the results of calibration chamber tests.

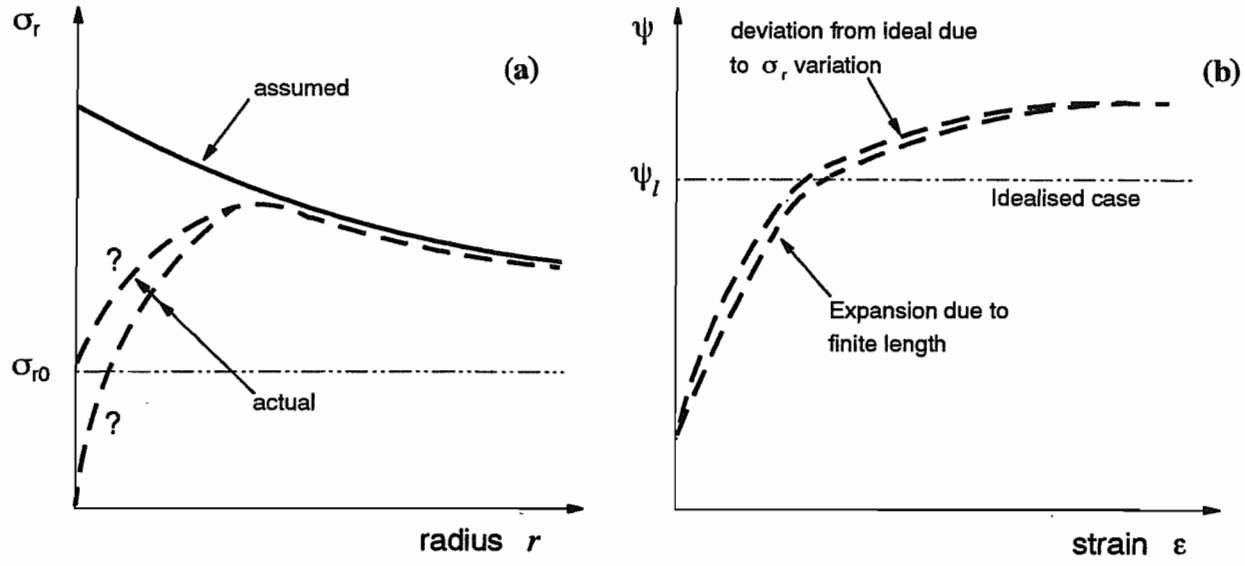

Figure 5.5 Variations of observed pressuremeter expansion from cylindrical cavity expansion theory due to (a) initial disturbance (b) finite length of the CPM

5.3 Normalising parameters

It was shown in Chapter 4 that q_c and ψ_l were best normalised by using σ_h in the ratios $(q_c-\sigma_h)/\sigma'_h$ and $(\psi_l-\sigma_h)/\sigma'_h$, as opposed to a more conventional approach using the mean effective stress, p' or the vertical stress σ'_v. Recent work by Almeida *et al.* (1991) on Quiou carbonate sand from the west coast of France has brought to question the use of relative density, D_r as the other suitable measure of soil behaviour, and proposed instead the voids ratio, e. A similar argument has been presented by Semple (1988). Almeida *et al.* (1991) carried out a series of 8 CPT tests in a large calibration chamber in Quiou sand. Cone resistance was normalised by the mean effective chamber stress, and the results were plotted against the voids ratio. Comparing with a larger database of equivalent chamber tests in Ticino sand, it was concluded that e is a better reference than D_r for comparing the behaviour of carbonate and silica sands.

In Figure 5.6, the normalised q_c values of Quiou sand and Ticino sand as reported by Almeida *et al.* (1991) are plotted against voids ratio. Added to the graph are the cone results from the

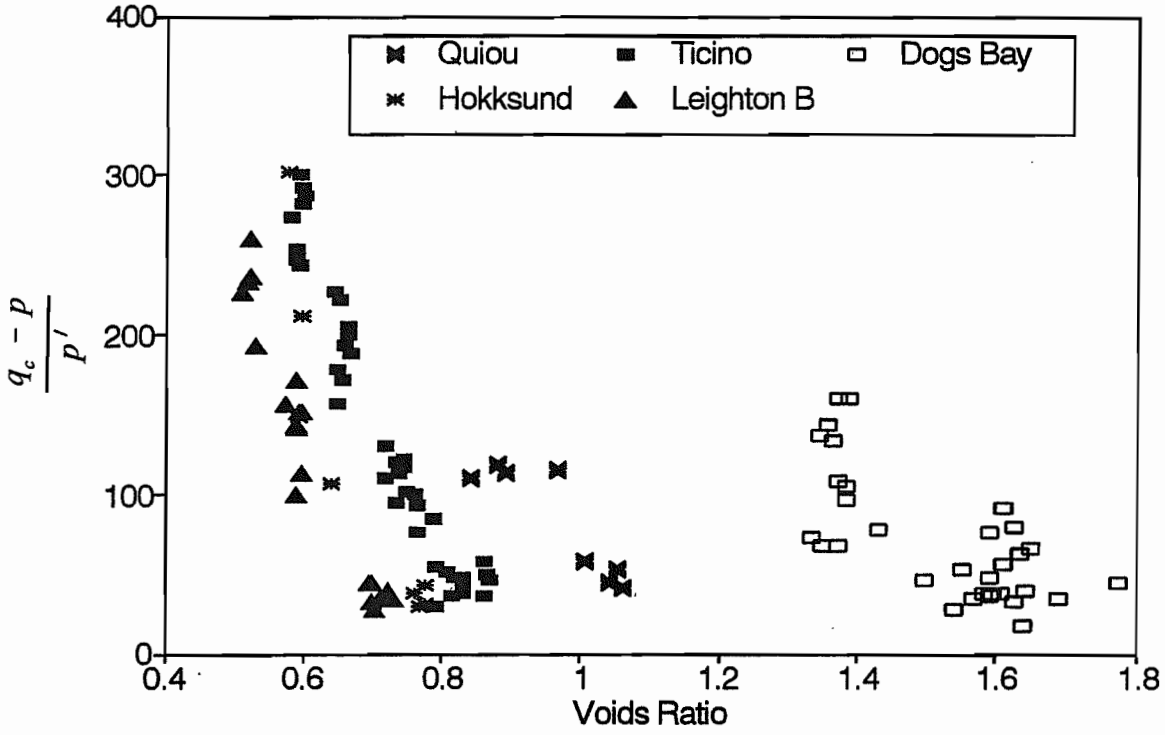

Figure 5.6 Normalised q_c against voids ratio

CPM tests in Hokksund sand, Dogs Bay sand and Leighton Buzzard sand. It is clear that no unique relationship between $(q_c - p) / p'$ and e exists, particularly when considering the high values of e shown by Dogs Bay sand. This is because the limiting voids ratios, e_{max} and e_{min} between which all the test results lie, are very different for each sand. The data are replotted in Figure 5.7 using relative density. Now all the sands lie within the same range *i.e.* $0 < D_r < 1$, where it can be seen that at a given D_r, q_c values are comparable, with the exception of Quiou sand at high D_r, where the influence of particle crushing is probably more significant.

The benefits of using relative density rather than voids ratio are clear, in that it provides a normalised measure of density which at least in part accounts for the different characteristics of different sands. The disadvantage is that it is less directly defined, depending on standard methods for measuring maximum and minimum voids ratios. The adoption of standard procedures for these density measurements which can be applied to both silica and carbonate sands, therefore, is an important priority.

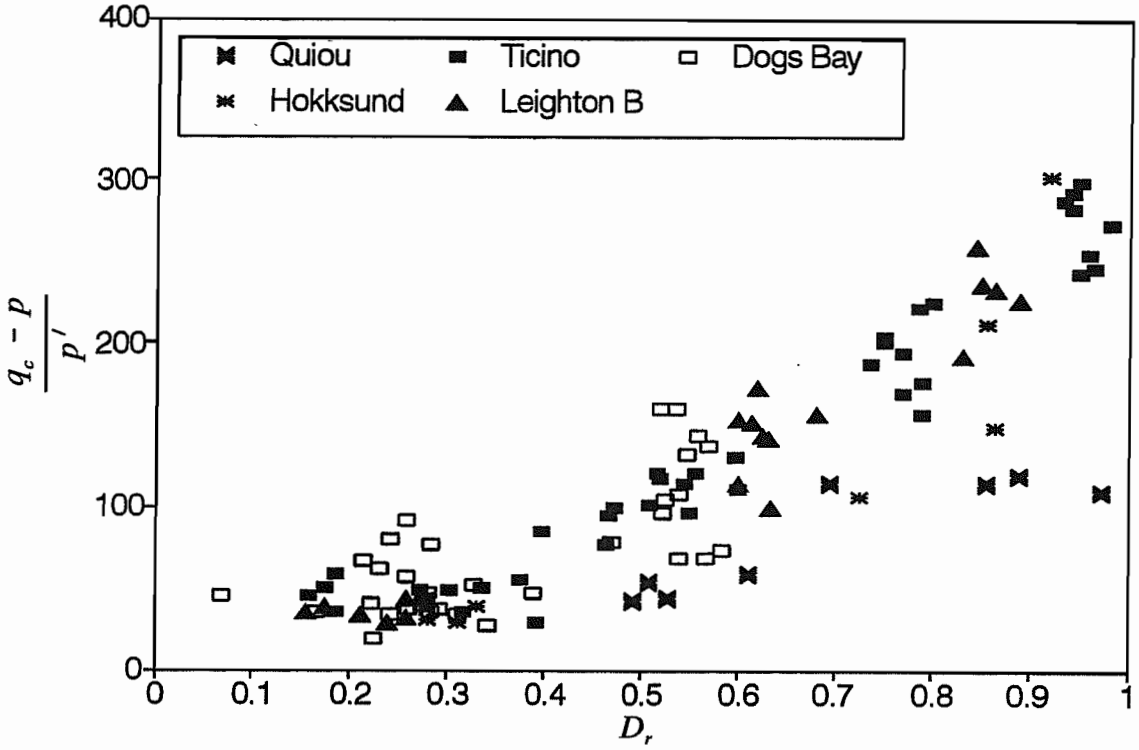

Figure 5.7 Normalised q_c against relative density

5.4 Correlations for the determination of σ_h and D_r

The results of CPM tests in Hokksund sand (Chapter 3) and Dogs Bay sand (Chapter 4) revealed that both cone resistance, q_c and the limit pressure, ψ_l were controlled by the applied horizontal stress, σ_h' and the relative density, D_r. Indeed, the influence of D_r was confirmed in the previous section. Since q_c and ψ_l represent two independent measurements obtained from the same CPM test, it follows that a combination of these measurements could be used to make estimates of the two controlling variables, σ_h' and D_r.

In Figure 5.8, the limit pressure normalised by σ_h' has been plotted against D_r for cone pressuremeter tests in the calibration chamber. Horizontal stress was taken at mid-height of the chamber, and relative density was calculated by dividing the weight of the sand sample by its volume. Tests in overconsolidated sand have been omitted, but CPM tests by Schnaid (1990) in Leighton Buzzard sand have been included. A linear relationship is evident (despite some scatter) which can be written as

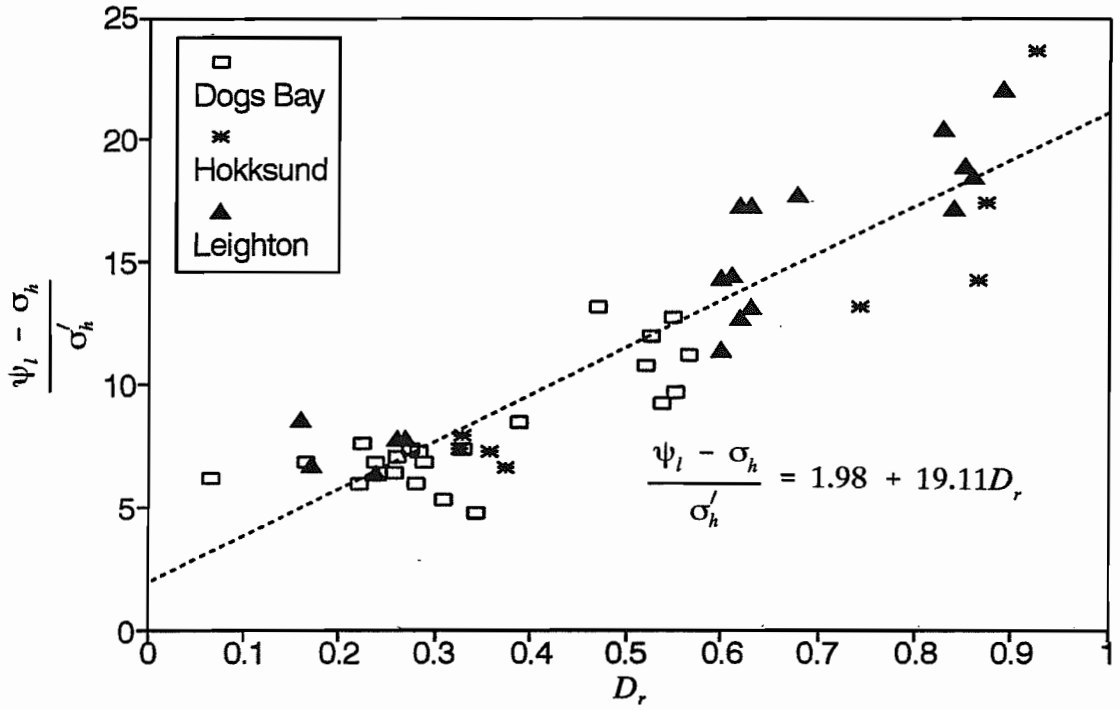

Figure 5.8 The variation of limit pressure with density from CPM tests in the calibration chamber

$$\frac{\psi_l - \sigma_h}{\sigma'_h} = 1.98 + 19.1\ D_r \qquad ...(5.11)$$

with a correlation coefficient, R^2 of 84%, and D_r is expressed as a ratio between 0 and 1. Similarly, the relationship between the CPM factor and D_r is shown in Figure 5.9 and can be approximated by the expression

$$\frac{q_c - \sigma_h}{\psi_l - \sigma_h} = 3.39 + 10.4\ D_r \qquad ...(5.12)$$

with a correlation coefficient, R^2 of 84%. Equations (5.11) and (5.12) are empirical, and applicable to calibration chamber tests within the range of stresses at which testing was carried out. Hence, the intercepts at $D_r = 0$ and the gradients of the lines for equations (5.11) and (5.12) are arbitary constants which are dependent upon the testing environment, the method of sample preparation, and proximity of the chamber walls.

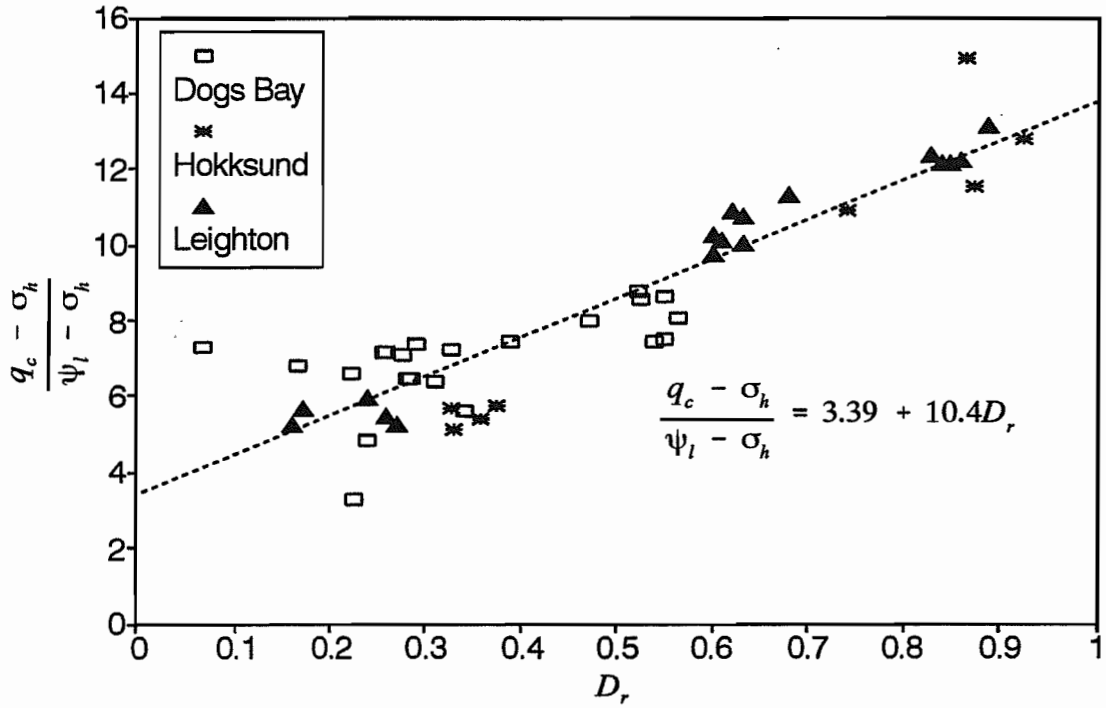

Figure 5.9 Variation of the CPM factor with relative density determined from calibration chamber tests

Since the normalised cone resistance is a product of the normalised limit pressure and the CPM factor, this implies that the variation of the normalised cone resistance with D_r should be parabolic, as equations (5.11) and (5.12) are combined to give

$$\frac{q_c - \sigma_h}{\sigma_h'} = \frac{\psi_l - \sigma_h}{\sigma_h'} \cdot \frac{q_c - \sigma_h}{\psi_l - \sigma_h} = 199\ D_r^2 + 85.4\ D_r + 6.71 \qquad ...(5.13)$$

This empirical relationship has been plotted in Figure 5.10 and provides a better fit to the results of the three sands tested than the linear relationship proposed by Schnaid (1990) based solely upon Leighton Buzzard sand. Further support for a parabolic relationship of the type expressed in equation (5.13) is evident from Figure 5.7, where D_r, based also upon tests in Ticino and Quiou sands, was clearly shown to vary with cone resistance in a non-linear manner.

Given that results for the three sands tested in the calibration chamber can be expressed by equations (5.11) to (5.13), rearrangement produces the quadratic equation

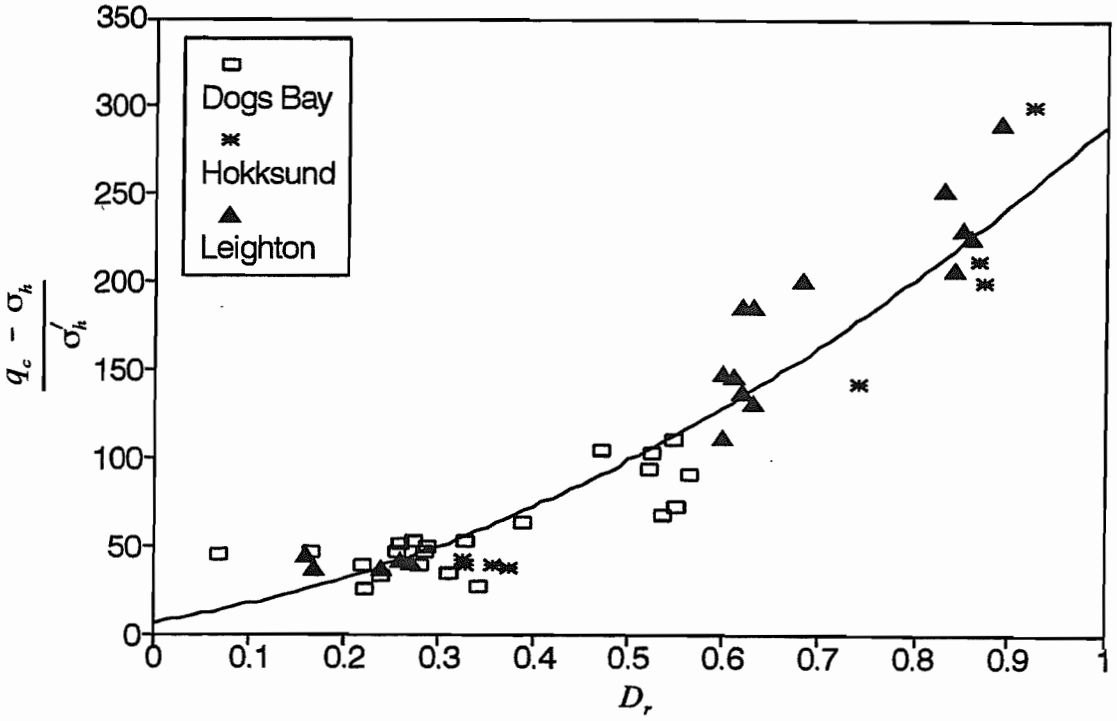

Figure 5.10 Variation of cone resistance with relative density from CPM tests in the calibration chamber

$$(\sigma_h^e)^2\ (B+AD+D-CB)\ +\ \sigma_h^e\ (\psi_1 CB-2\psi_1 AD-q_c B)\ +\ \psi_1^2 D\ =\ 0 \qquad ...(5.14)$$

where σ_h^e is an estimate of the horizontal stress determined from the positive root of equation (5.14), and the constants A & B and C & D are the intercept and gradient of the linear relationships expressed in equations (5.11) and (5.12) respectively. Here, A = 1.98, B = 19.1, C = 3.39 and D = 10.4. Similarly, an estimate of the relative density, D_r^e can be made from rearrangement of equation (5.11) to give

$$D_r^e\ =\ \left(\frac{\psi_1\ -\ \sigma_h^e}{\sigma_h^e}\ -\ A\right)\cdot\frac{1}{B} \qquad ...(5.15)$$

The success of these empirical relationships in estimating σ_h^e and D_r^e can be seen in Figures 5.11 and 5.12 respectively. In Figure 5.11, σ_h^e is plotted against the horizontal stress applied to the sample during a test, and confidence limits have been superimposed. Most estimates

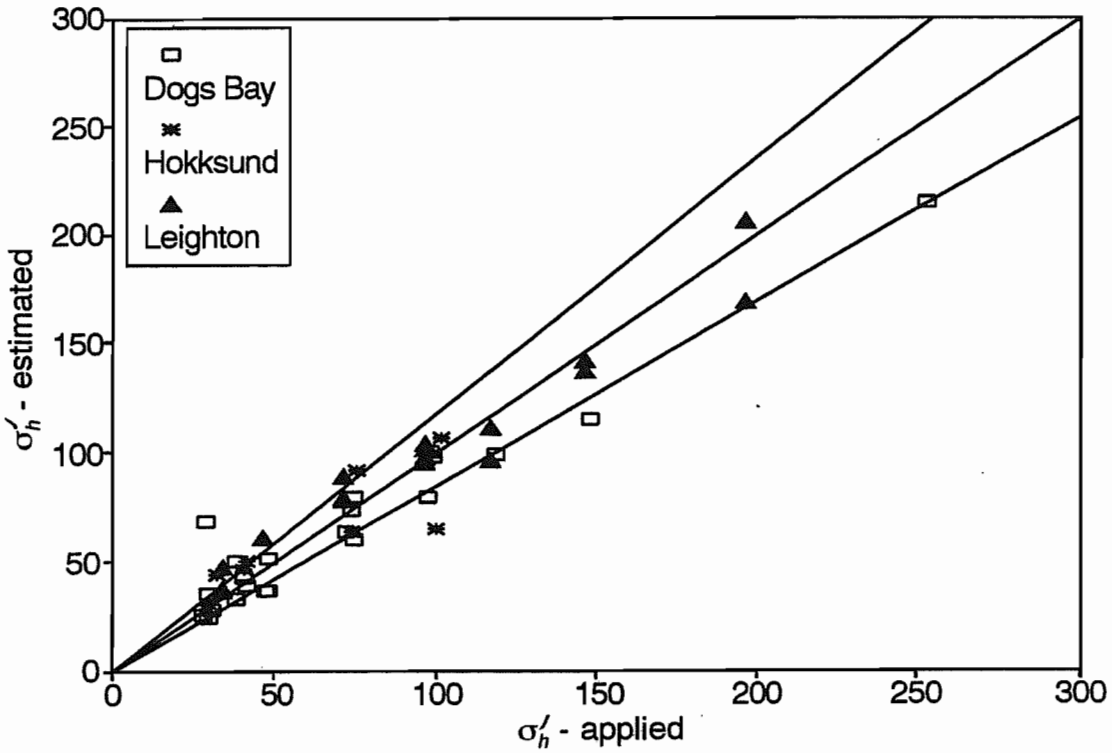

Figure 5.11 Horizontal stress estimated using empirical correlations from calibration chamber tests

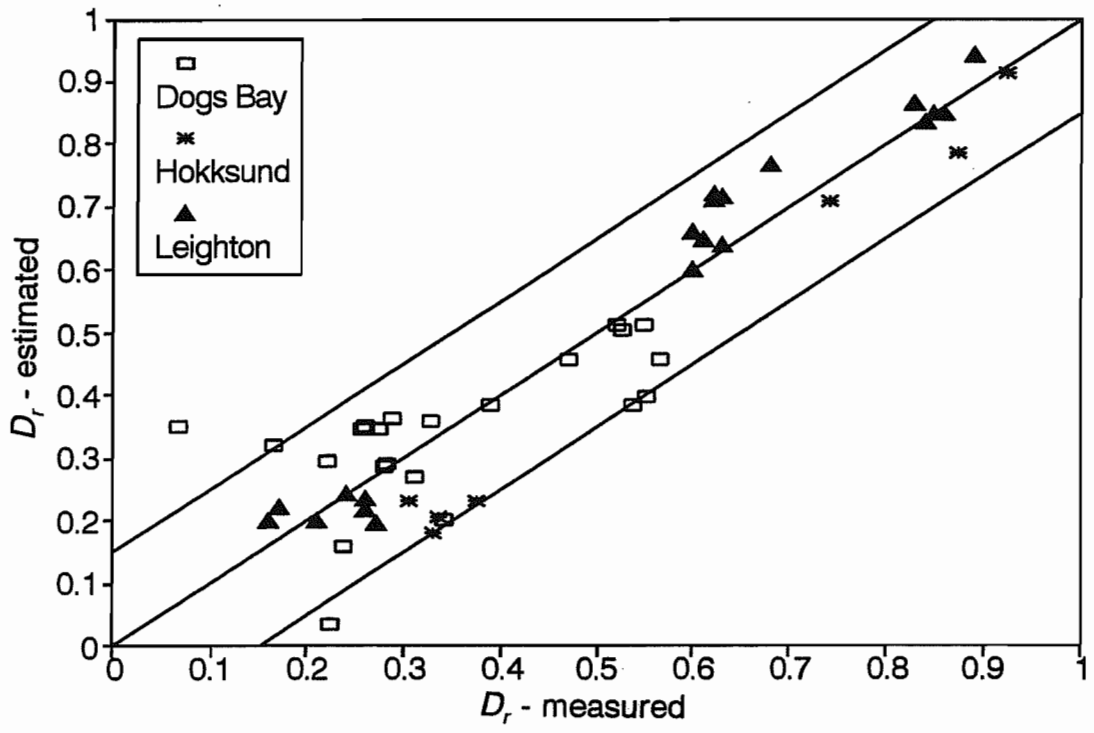

Figure 5.12 Relative density estimated using empirical correlations from calibration chamber tests

of σ'_h fall within ±15% of the applied values. It is worth noting that at higher applied stresses, values of σ'_h for Dogs Bay sand are lower, indicating the increasing significance of crushing

behaviour. This feature is difficult to detect from normalised plots of cone resistance and limit pressure with relative density. It implies that less confidence can be placed in the empirical relationships at higher stresses when testing in carbonate sands. No such deviation is evident for either the Hokksund or Leighton Buzzard sands. Estimates of D_r^e are shown in Figure 5.12. Confidence limits of ±15% have been superimposed on the plot and again, barring two tests which were carried out at the start of the programme, there is a good agreement with measured values of D_r.

As mentioned above, this empirical approach to CPM interpretation is applicable to calibration chamber tests, and care should be taken in attempting to apply it to field tests, as discussed in the following section. The results, however, are remarkably encouraging. Schnaid (1990) had found that empirical correlations could be applied to tests in one sand (Leighton Buzzard sand). The results presented here indicate that it is possible to estimate *in situ* parameters from measurements of q_c and ψ_I in sands of very different composition.

Friction angle can be estimated from relative density using, for example, the correlation proposed by Bolton (1986) given in equation (4.1). Obviously there will not be a unique relationship between ϕ_p and the CPM factor for all three sands because ϕ_{cv} and Q are different for each sand tested.

5.5 Chamber size effects

The boundary conditions of *in situ* tests cannot be reproduced in the laboratory since samples of infinite dimensions cannot be prepared. This brings to question the suitability of empirical relationships developed for the cone pressuremeter to field situations, however, if chamber size effects can be quantified, then appropriate corrections can be made. Obviously the magnitude of these effects will depend on the type of boundary conditions imposed, and the ratio of the chamber diameter, D_c to the diameter of the instrument, d_c. It has been shown in

Chapter 4 that cone resistance and limit pressure is strongly influenced by horizontal stress. Hence the lateral boundary conditions imposed by a calibration chamber are of primary importance in determining q_c and ψ_l at a given ratio of D_c / d_c compared with q_c and ψ_l obtained in a soil of infinite dimensions.

Calibration chamber tests usually represent one of 4 types of boundary condition as shown in Figure 5.13. Summarised as BC1, BC2, BC3 and BC4, conditions of constant lateral stress (BC1) and constant lateral strain (BC3) generally represent lower and upper bounds respectively to true values of q_c and ψ_l in an infinite soil. Ghionna and Jamiolkowski (1991) report developments at ISMES of a method of simulating an infinite lateral boundary in the calibration chamber. Lateral stresses are computer controlled, and corrected continuously based on measurements of lateral strain as pressuremeter inflation proceeds. At Oxford, the calibration chamber applies constant stress to the lateral boundaries (BC1), and the chamber diameter to CPM diameter ratio, D_c / d_c is about 27.

Parkin and Lunne (1982) studied the influence of boundary effects on CPT tests in Hokksund sand. They concluded that in loose sands ($D_r \approx$ 20% to 30%) for D_c / d_c ratios from 21 to 48, q_c was virtually independent of the proximity of the boundary, however, in dense sands ($D_r \approx$90%), q_c values in the chamber were found to be as low as 70% of values in an infinite soil. Belotti (1984) finds that in tests in Ticino sand, the chamber size effects are of the same order of magnitude.

In a simulation of the self-boring pressuremeter test in Leighton Buzzard sand, Fahey (1986) showed that limit pressures obtained in a cylinder of sand of finite dimensions were significantly less than the true limit pressures in an infinite soil, and dependent upon soil

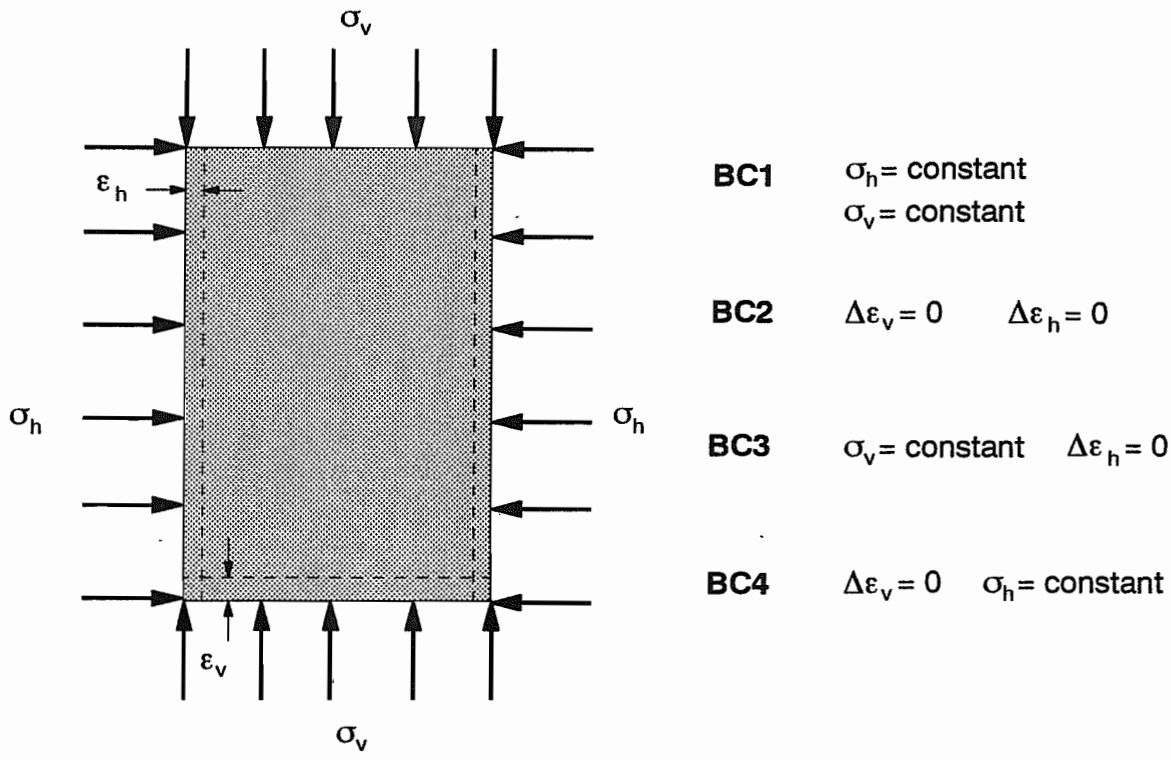

Figure 5.13 Boundary conditions commonly encountered in calibration chamber testing

strength and the ratio D_c / d_c. For D_c / d_c = 10 and values of strength and stiffness typical of dense silica sand, the ratio of ψ_l^{∞} to ψ_l^{10} was found to be around 1.9.

It appears, therefore, that chamber size effects on cone resistance and and limit pressure may be of the same order of magnitude. This implies that the CPM factor defined as $(q_c-\sigma_h)/(\psi_l-\sigma_h)$ should be less sensitive to the proximity of the chamber boundary than the individual measurements of q_c and ψ_l as the corrections would tend to cancel each other out. This has indeed found to be the case by Schnaid and Houlsby (1991) who report tests with three cone pressuremeters of different diameters (D_c / d_c ratios of 22, 27 and 38). It was found that at a particular relative density, the CPM factor remained relatively constant for the three cone pressuremeters used. They concluded that empirical correlations based upon the CPM factor could be applied directly to CPM interpretation of field tests.

Because two of the three correlations given in equations (5.11), (5.12) and (5.13) are required to make estimates of σ_h and D_r, there remains some sensitivity of either ψ_l or q_c to chamber size effects for dense, and to a lesser extent, medium dense Leighton Buzzard and Hokksund sands.

Dogs Bay sand, however is significantly less affected by chamber size effects. Using a one-dimensional finite element program developed by Yu (1990) and discussed in detail in Chapter 8, the influence of stiffness on the ratio ψ_l^{∞} / ψ_l^{27} has been assessed. The results are shown in Figure 5.14 for different values of friction and dilation angles, and the circled area represents the range of soil parameters typical of loose to dense Dogs Bay sand. Even for dense sand, chamber size corrections are less than 9%, which is within the range of scatter exhibited in the estimations of σ_h and D_r shown in Figures 5.11 and 5.12.

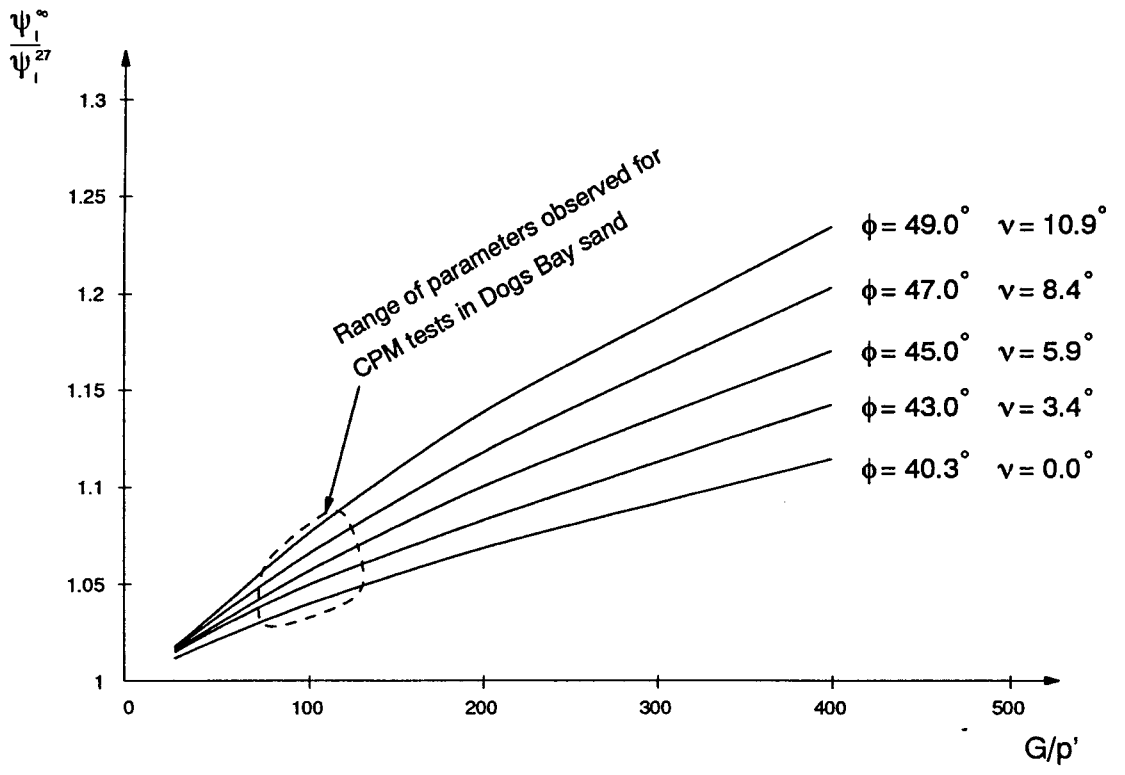

Figure 5.14 Results from a numerical analysis to determine the influence of chamber size effects on tests in Dogs Bay sand

It can be concluded, therefore, that correlations developed in the calibration chamber are applicable to field conditions for sands of sufficiently low stiffness and/or density. For the dense silica based sands, some caution should be used in applying these correlations directly. Without allowing for such corrections, field estimates of limit pressure could be under estimated leading to overestimates of friction angle.

5.6 Conclusions

In a review of the recent methods of interpretation of cone pressuremeter tests in sand, it has been found that cavity expansion theories have only limited success in predicting q_c and ψ_l values. This is thought to be due to mechanisms of deformation induced in the sand during CPM insertion and subsequent inflation that are not consistent with the continuous expansion of a single cylindrical or spherical cavity.

A better approach has been to use correlations developed in the Oxford calibration chamber based on tests in three very different sands. The independent measurement of q_c and ψ_l allows estimates of σ_h and D_r to be made, and these estimates show a good agreement with applied and measured values of σ_h and D_r. When applied to field conditions, the correlations must be used with care. At sufficiently high lateral stresses, carbonate sands have been shown to be influenced by particle crushing, resulting in underestimates of σ_h^e, although silica sands appear to be relatively unaffected by crushing. However, for the fixed ratio of chamber diameter to CPM diameter of 27, tests in dense silica based sands can underestimate ψ_l and q_c field measurements by up to 40%, while tests in carbonate sands are generally insensitive to chamber size effects and hence applicable to field interpretations.

Considering the high voids ratios of Dogs Bay sand, it has been shown that relative density is a better parameter for assessing the behaviour of different sands than initial voids ratio.

CHAPTER 6

TESTS IN SOFT CLAY AT BOTHKENNAR

6.1 Introduction

The calibration of new *in situ* devices requires tests in conditions where *in situ* stresses and soil properties are either controlled or measured, and where a high turn-around of tests is possible so that a database of experience can be developed. In sands, calibration chamber tests meet these demands successfully: *in situ* stresses and relative density can be specified, and samples can be prepared in a matter of hours. Considering the difficulty of obtaining undisturbed sand samples from the field, calibration chamber testing has become a well established technique.

In clays, the philosophy is different, and more emphasis is placed on the calibration of *in situ* devices in the field. This is because of the increasing confidence in soil properties measured from laboratory tests on undisturbed samples, and the impracticalities of creating large scale samples for calibration chamber testing. For example, preparation of a clay sample of height 1m and diameter 0.8m by one-dimensional consolidation of a slurry can require some 6 to 7 weeks (Anderson and Pyrah, 1991). In this case the device tested was a self-boring pressuremeter. For research on *in situ* devices that have already been well established in the field, calibration chamber tests in clay can prove worthwhile, as shown for tests carried out with the dilatometer (Smith, 1990) and the cone penetrometer (Huang *et al.*, 1991; Voyiadjis *et al.*, 1991). Because the time required to complete a chamber test in clay is so great, it is more practical to calibrate relatively new *in situ* devices in the field. Such tests should logically be located at sites where the ground conditions are relatively uniform and well

documented.

At present the database of cone pressuremeter tests in clays comprises tests by Houlsby and Withers (1988) and Campanella *et al.* (1990). From a set of seven CPM tests at a stiff clay site near Cambridge, U.K., Houlsby and Withers (1988) developed an analysis for the cone pressuremeter test based on cavity contraction theory. Estimates of the undrained shear strength, s_u, *in situ* horizontal stress, σ_{h0}, and elastic shear modulus, G were made and compared with results from SBPM tests, triaxial tests and screw plate tests. Campanella *et al.* (1990) compared results between some SBPM tests, seismic CPM tests and CPM tests at three soft clay sites in the lower mainland area of British Columbia, Canada. Methods of analysis developed for the SBPM were applied to the CPM with some success. This appears to be the extent of reported use of the cone pressuremeter in clay. It is clear that further CPM testing is required, particularly in soft clays in order to validate the analysis of Houlsby and Withers (1988).

In this chapter, results are presented from a set of 12 cone pressuremeter tests in a soft clay site at Bothkennar in Scotland. A description of the site and summary of the soil conditions is given, followed by a description of the 15cm^2 cone pressuremeter. The test procedure is discussed, with particular reference made to relevant corrections and calibrations. From the test results, estimates of s_u, σ_{h0} and G are made using the analysis of Houlsby and Withers (1988) and compared with the results from a wide range of tests which make up the initial investigation at Bothkennar reported by Nash *et al.* (1992). Conclusions are then drawn about the potential of the CPM in measuring undrained properties of the soil.

6.2 The test site at Bothkennar

The cone pressuremeter tests reported in this chapter were carried out at the SERC National soft clay site in Scotland. The site was purchased in 1987 specifically for experimental geotechnical research at large or full scale. A detailed characterization of the soil properties

was undertaken which included *in situ* tests and laboratory tests on undisturbed and reconstituted samples. The papers arising from the investigations are published in Géotechnique, Vol. 42, No. 2 (1992).

The site lies in the parish of Bothkennar about halfway between Edinburgh and Glasgow. It is located at OS NS 921861, and covers an area of 11 hectares of low lying field. The site is bounded by flood embankments on three sides, as shown in the site plan of Figure 6.1. There is a gentle gradient of about 1 in 70 running from south to north. Location of the CPM soundings is shown in the figure. Three soundings were completed 6 metres apart on a triangular grid.

From the investigations reported by Nash *et al.* (1992), a brief review of the soil strata and relevant properties is discussed here. A summary of the strata that exist beneath the test site is presented in Table 6.1.

Table 6.1 Summary of strata beneath the test bed site (after Nash *et al.*, 1992)

Thickness (m)	Stratum	Stratigraphy
1.5	Firm, dark brown clayey **silt** with rootlets and layers of shell	Crust
16.0	Soft, becoming firm, dark grey/black micaceous silty **clay**/clayey **silt**, partly thinly laminated and mottled	Grangemouth, Claret beds
1.5	Fine to coarse grey/brown **sand** with shell fragments	Letham beds

The stratum of interest to this research is the 16m layer of soft, silty clay which forms part of the Grangemouth/Claret beds. The water table lies at a depth of about 0.8m. The moisture contents of the soft clay layer range from approximately 40% just below the surface crust and

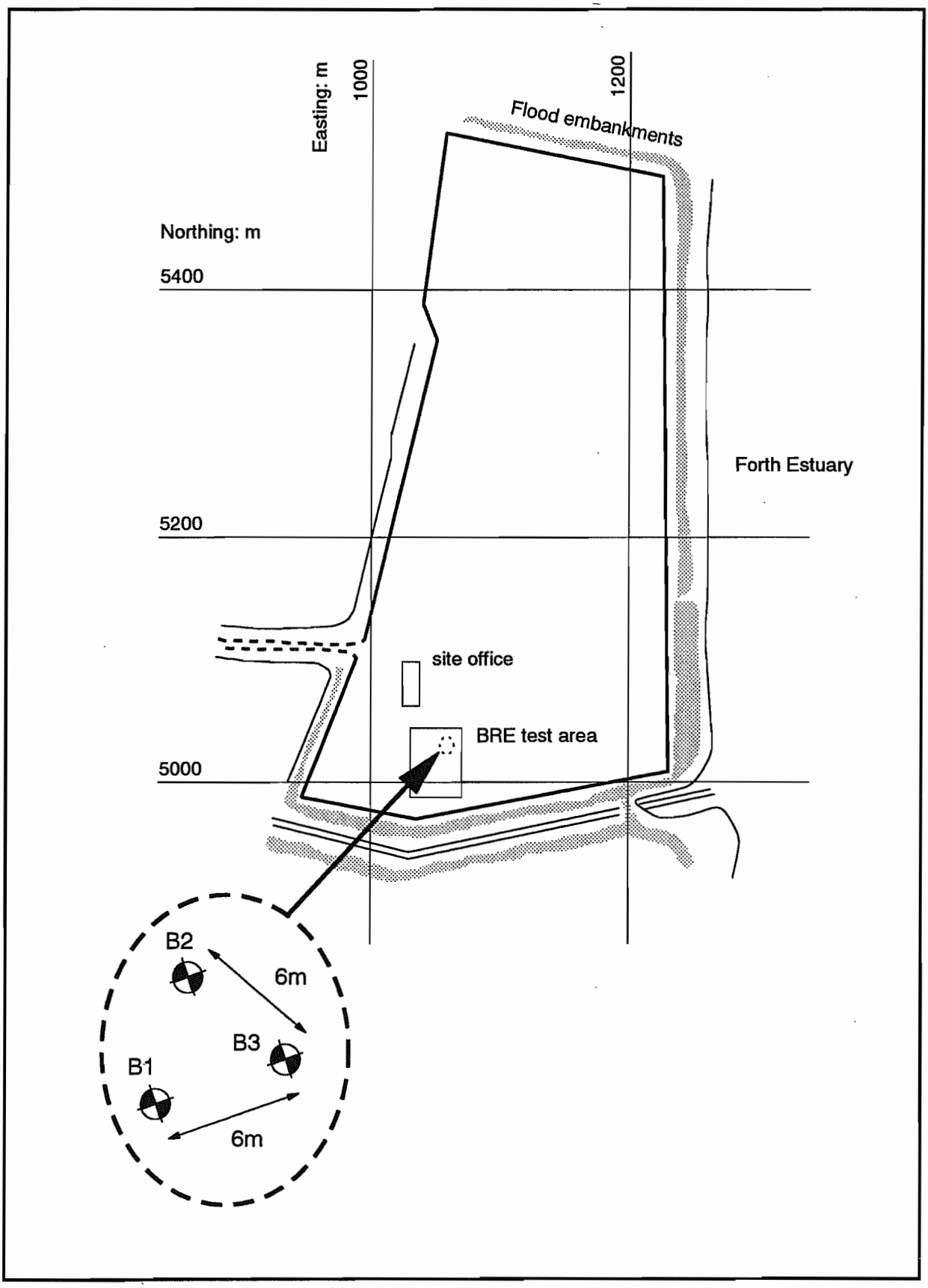

Figure 6.1 Approximate location of CPM soundings at the Bothkennar soft clay site

at the base of the layer to approximately 65% at around 8m depth. The liquid limit is generally 65% to 80% to a depth of about 12m and then decreases to about 50% just above the underlying sand layers, with a typical plastic limit of about 25% throughout. The clay is lightly overconsolidated with an OCR which drops to about 1.5 by 6m depth.

The results of *in situ* and laboratory tests which characterize the site further are discussed in more detail in section 6.5 as they are used for direct comparison with results from the cone pressuremeter tests.

6.3 15cm² cone pressuremeter

6.3.1 Cone pressuremeter details

The 15cm² cone pressuremeter was designed and built by Cambridge In Situ and is owned by Fugro McClelland. It formed the basic design for the smaller 10cm² cone pressuremeter detailed in Chapter 2, although there are some fundamental differences between the two devices which are discussed here.

The basic components of the 15cm² cone pressuremeter have already been shown in Figure 1.2, and are discussed fully by Withers *et al.* (1986). The device comprises a 15cm² instrumented cone behind which is mounted a pressuremeter module of the same diameter (43.7mm). Distance between the cone and the pressuremeter module is set by a cone spacer. Onshore, the CPM is jacked into the ground by a cone truck, where headroom limitations restrict the overall length of the device, and hence the length of the cone spacer can be adjusted depending on the requirements of the test programme. With a piezocone attached, the CPM is 2.5m long. The tests reported in this chapter, however, utilised only the instrumented cone and friction sleeve measurements and the overall length of the CPM in this configuration was 2.08m.

The pressuremeter membrane has a length of 450mm and thus the length to diameter ratio of

the device is 10.3. As with the 10cm² CPM, the radial expansion of the membrane is measured by three instrumented strain arms located at mid-height of the pressuremeter module. Unlike the 10cm² CPM, however, amplification of the signals from the strain arms takes place "downhole" within a housing immediately behind the pressuremeter module (the cone signals are passed independently through the pressuremeter modules to the surface on separate wires). Inflation of the membrane is achieved by nitrogen gas. The pressuremeter has a differential capacity of 10MPa and a radial expansion limit of 50% which is about 11mm of travel of the strain arms. The CPM is attached to standard cone rods by a cone rod adaptor, as in a cone penetration test.

Cone pressuremeter tests were controlled from the cone truck using a strain control unit, to which was attached a portable computer with appropriate software for data logging. In addition to the cone signals, readings of total pressure and radial displacement for each strain arm were recorded.

6.3.2 Test procedure

Before inserting the cone pressuremeter into the ground, it was necessary to push a slightly oversized "dummy cone" through a firm crust of soil at the top 1.5m of each probe location. This was required to minimise the amount of friction and abrasion experienced by the Chinese lantern during insertion.

The cone pressuremeter was then jacked into the ground at the standard rate of 2cm/sec, with continuous readings of cone resistance and friction ratio recorded by an automatic plotter. An example of one of the soil profiles recorded in this way is presented in Figure 6.2.

The centre of the pressuremeter was located one metre behind the cone tip, and so cone tip penetration was stopped one metre deeper than the test location. The time between the end

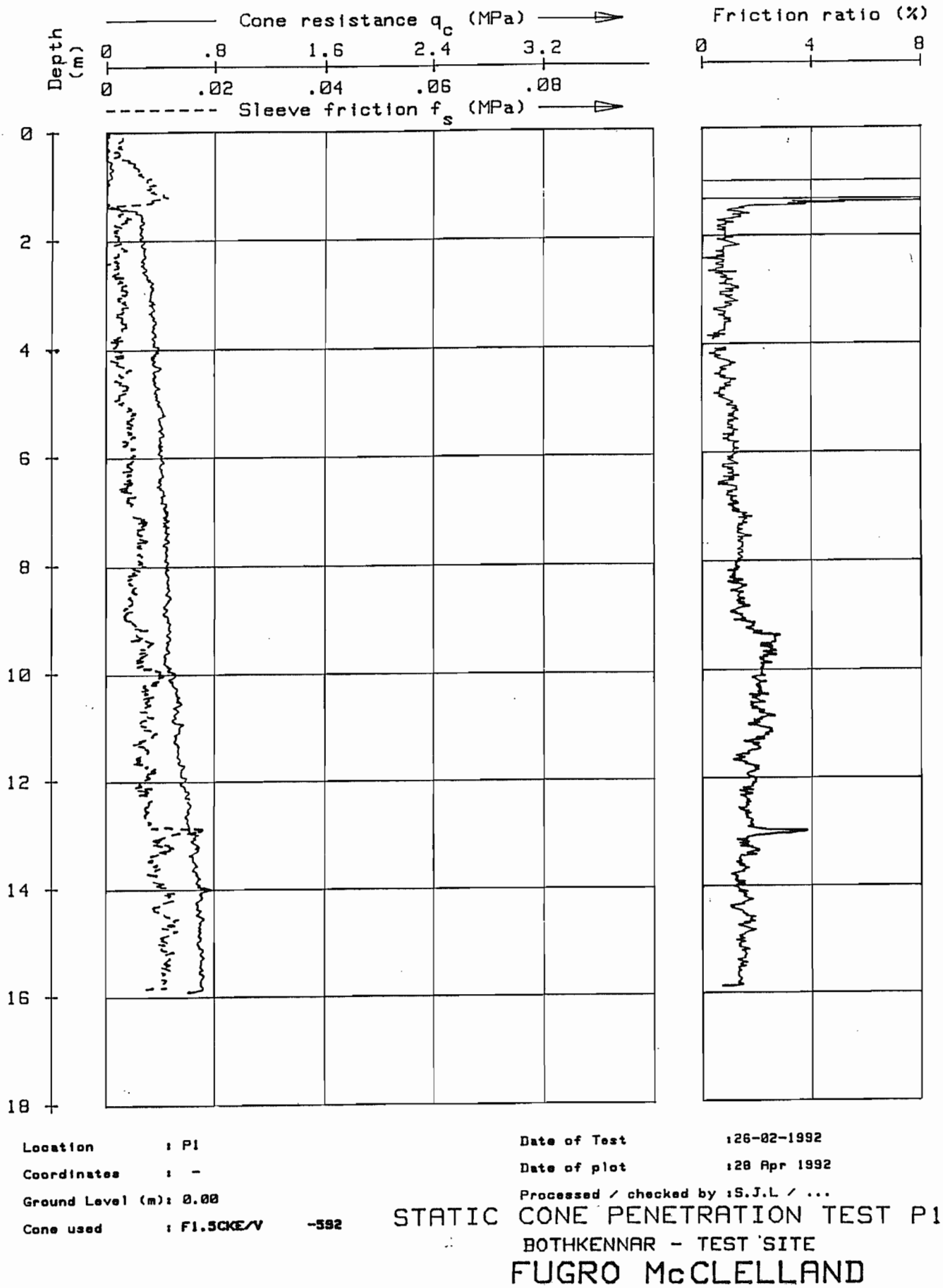

Figure 6.2 Cone penetrometer profile recorded on site at Bothkennar

of the cone penetration and the start of the pressuremeter inflation varied between 4 and 8 minutes while the operators prepared the strain control unit and data logging software for a pressuremeter test.

The membrane was inflated at a rate of 2% per minute until one of the strain arms registered a radial expansion of 50% (about 11mm travel). At three intervals during the test, inflation was stopped and the strain held for one to two minutes followed by a rapid unload-reload loop. This procedure was undertaken to minimise the hysteresis from soil creep in the unload-reload loops. If the process was performed too slowly, however, dissipation of pore pressures could have occurred, resulting in partial drainage (and hence consolidation) of the surrounding soil. This phenomenon has been identified in self-boring pressuremeter tests (Anderson and Pyrah, 1989; Fukagawa *et al.*, 1990) and the cone pressuremeter tests of Houlsby and Withers (1988), although it is difficult to separate the influence of creep and consolidation.

At no stage was the cavity pressure during an unload-reload loop allowed to fall below $\psi_m - 2s_u$ where ψ_m was the maximum cavity pressure prior to unloading. This ensured that changes in the pressuremeter strain were due solely to the elastic response of the soil.

Upon reaching maximum expansion, the pressuremeter was unloaded at a rate of 2% per minute until the unloading slope became close to horizontal, at which point the pressuremeter was vented. A typical pressuremeter test carried out in this manner has been plotted in Figure 6.3. The individual measurements of radial expansion and pressure from each strain arm location reveal in the figure that membrane expansion was not completely symmetrical about the axis of the pressuremeter. This was also observed for the expansion of the 10cm² cone pressuremeter as discussed in Chapter 2, and is attributed to the additional stiffness of the single spot welded strip along the join of the Chinese lantern. While the absolute position of the strain arms was found to vary in this way for all of the tests, differences in the results obtained between the arms after data reduction was found to be minimal.

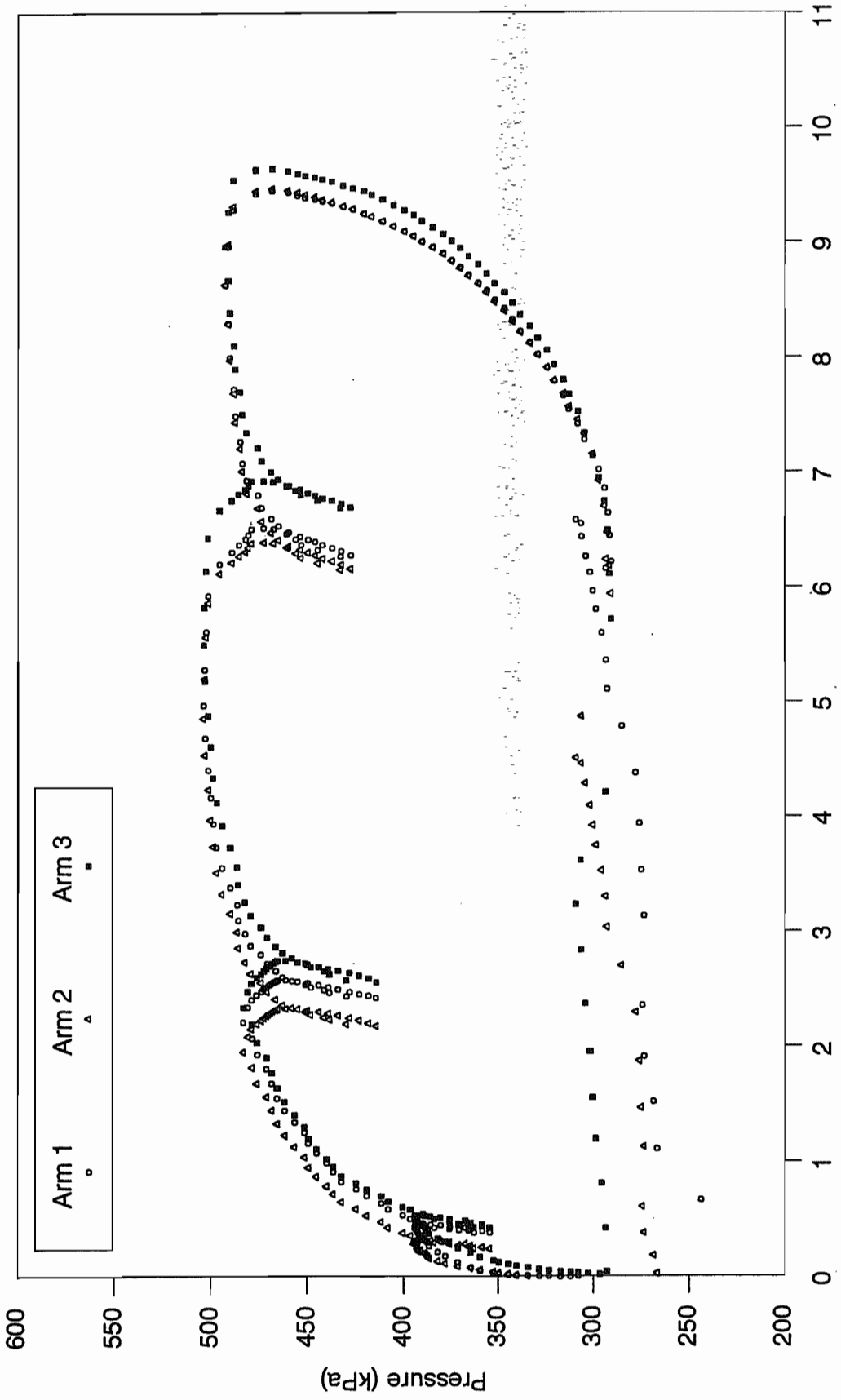

Figure 6.3 Field measurements for test B1T4, depth 12m

The minimum depth interval between subsequent pressuremeter tests was set at 3m to ensure that there was no influence from previous tests on the pressuremeter measurements.

6.3.3 Corrections and calibrations

Conversion of the pressuremeter data from recorded voltages to engineering units was carried out on site during each test by the data logging software, resulting in three separate readings of pressure in kPa and arm extension in mm. To obtain a single pressure-expansion curve, the pressure readings were averaged, and the arm readings were fitted by a circle using the program VTOENG as described in Chapter 3.

Membrane stiffness was found to be a particularly important correction to the measured pressure-expansion curve. The data logging software used in the field approximated membrane stiffness by a linear increase of pressure with strain, specified by an intercept and pressure-expansion gradient for each arm, as shown in Figure 6.4. Based on a 15cm^2 CPM pressure expansion carried out in air and with experience from the 10cm^2 CPM programme, it was considered more consistent to apply a closer approximation of membrane stiffness to the field data. In Figure 6.4, the pressure-expansion curve of a CPM inflation in air is also shown. Superimposed on the figure is a fitted curve using the three parameter hyperbola of equation (3.2). The maximum correction is approximately 150kPa. At the shallowest depth of the tests at Bothkennar, this correction was found to be around 35% of the limit pressure obtained in the soil.

The compliance of the pressuremeter was also measured in the laboratory. In soft soils, the stiffness of the instrument is high compared to the stiffness of the soil, and so compliance corrections are usually extremely small. Nevertheless, corrections to the measured unload-reload moduli were made, and this will be discussed in more detail in Chapter 7.

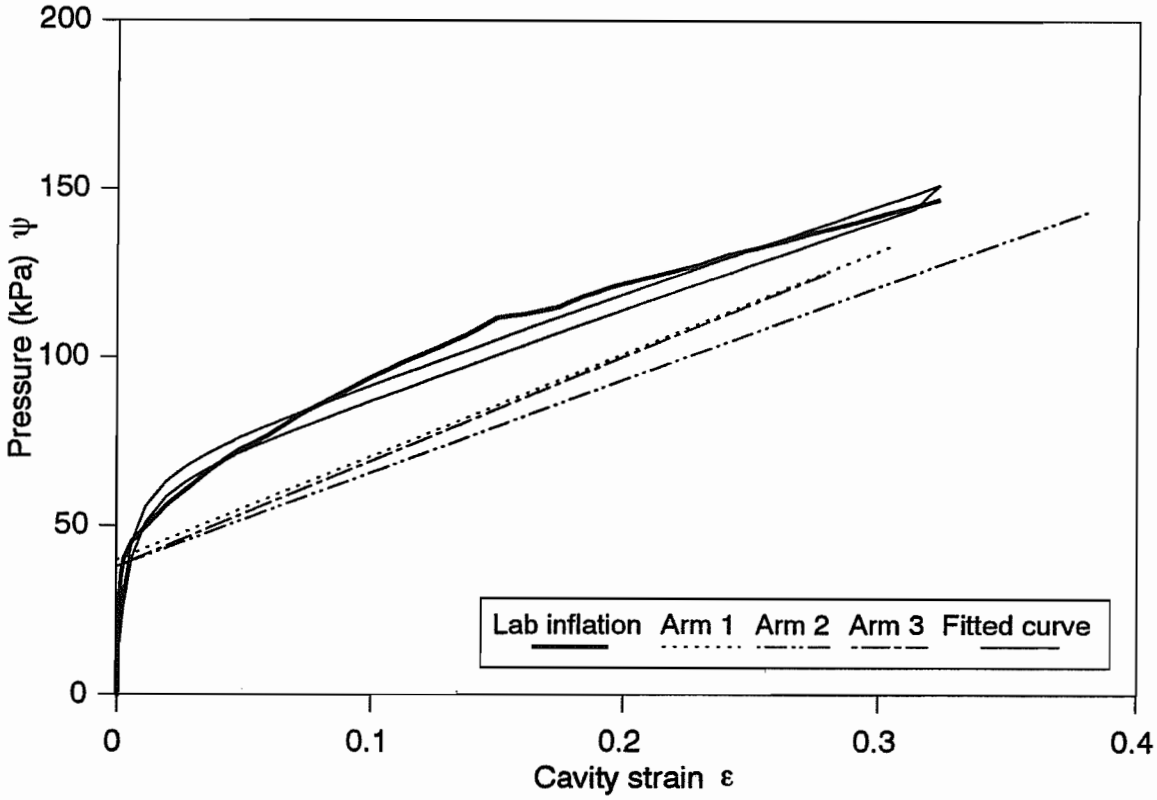

Figure 6.4 Air calibration curve for 15cm² cone pressuremeter

6.4 Test results

6.4.1 Pressuremeter testing

A set of 12 pressure-strain curves was obtained from the CPM tests carried out at Bothkennar using the procedures described above. In Figure 6.5, three such curves are shown, obtained from test depths of 3m, 9m and 15m. Even on initial observation, prior to the analysis which follows, it is evident that the slopes of the unload-reload loops and the unloading curve increase with depth and that limit pressure appears to increase uniformly with depth. The first unload-reload loop of test B1T1 at a strain of about 0.01 was not carried out using the correct procedure and has not been used in any of the analyses. At the point where the cavity contraction curve was considered sufficiently well defined, the pressuremeter was vented, and this is indicated in the figure by the arrows.

The pressuremeter inflations were taken to cavity strains in excess of 30%, by which time a limit pressure was well defined. The maximum pressure obtained in any particular test was

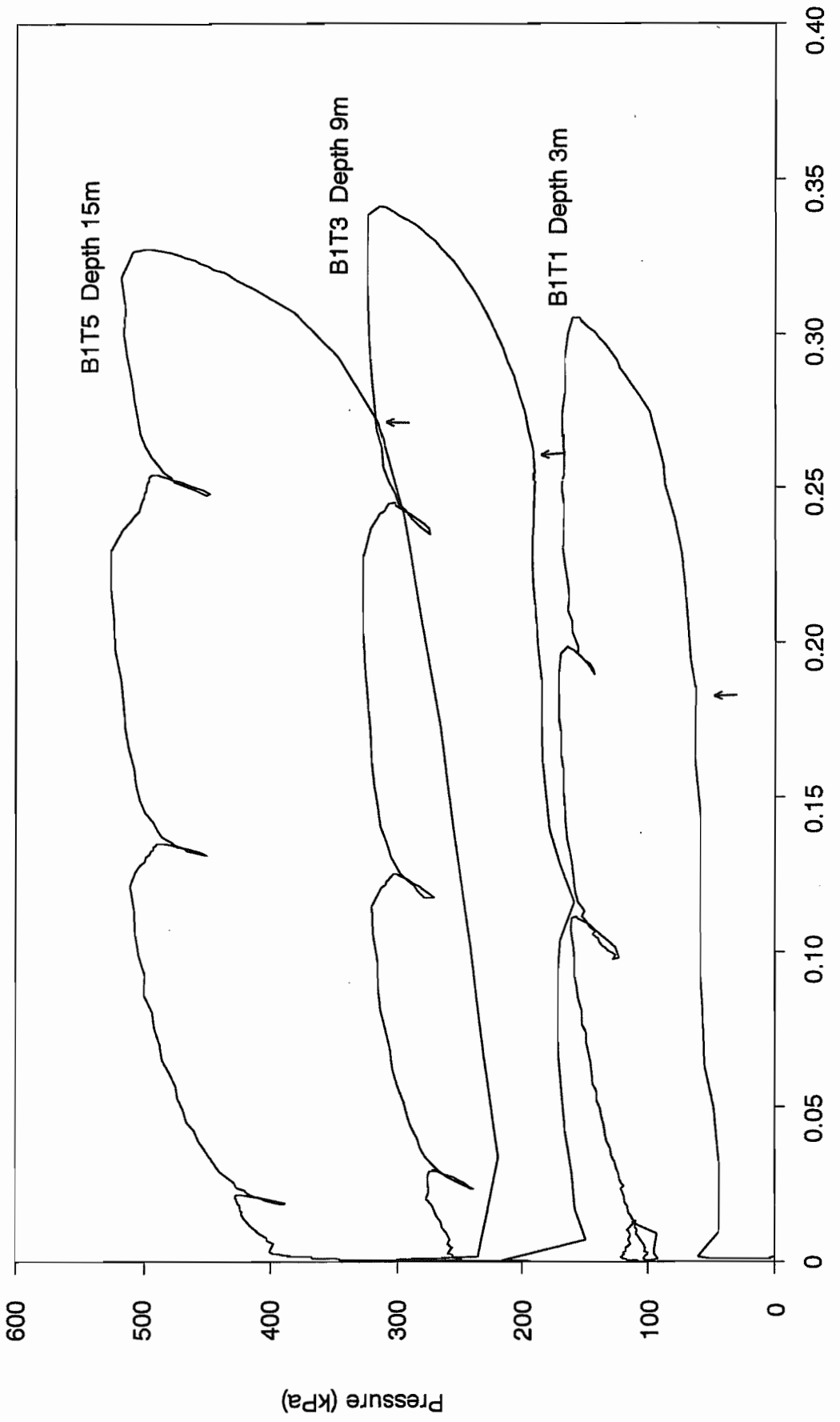

Figure 6.5 Pressure-strain curves for CPM tests at Bothkennar

not, in fact, at the maximum strain but usually found at strains of between 15% and 25%. This is probably an indication of the sensitivity of the pressuremeter test to the membrane stiffness response. Limit pressure was taken as the maximum pressure achieved after 25% cavity strain, although the difference between maximum pressure and limit pressure was never greater than 2.5% in any of the tests.

The Houlsby and Withers (1988) analysis was reviewed in Chapter 1. It was shown that from a measurement of limit pressure and the slope of the linear portion in unloading of the plot of cavity pressure, ψ against $-\log_e(\varepsilon_{max}-\varepsilon)$, estimates of undrained shear strength, s_u, shear modulus from cavity contraction, G_{cc} and *in situ* horizontal stress, σ_{h0} could be made, as shown in Figure 1.7. When plotted in the form of Figure 1.7, the cone pressuremeter tests were indeed found to exhibit clear limit pressures and clear linear sections in unloading. Two such tests, which represent the worst and best examples of unloading curves have been plotted in this way in Figures 6.6 and 6.7 respectively. The limit pressure and the unloading slope are represented in the figures by the chain-dotted lines, and have been fitted graphically.

The test results are summarised in Table 6.2. Limit pressures for each test are given, as are the graphical estimates of s_u, G_{cc} and σ_{h0}. The rigidity index, I_r is expressed by the ratio G_{cc}/s_u.

6.4.2 Cone penetration

All the pressuremeter tests were carried out in three soundings, where continuous measurements of cone resistance, q_c with depth were recorded. These cone penetration tests presented the opportunity for further independent measurement of soil properties. Agreement between the CPT tests as shown in Figure 6.8 provides good evidence for the uniformity of the soil conditions at Bothkennar. In the figure, values of cone resistance have been averaged over depth intervals of 1 metre. Due to equipment problems on site, test B3 was terminated at 12m.

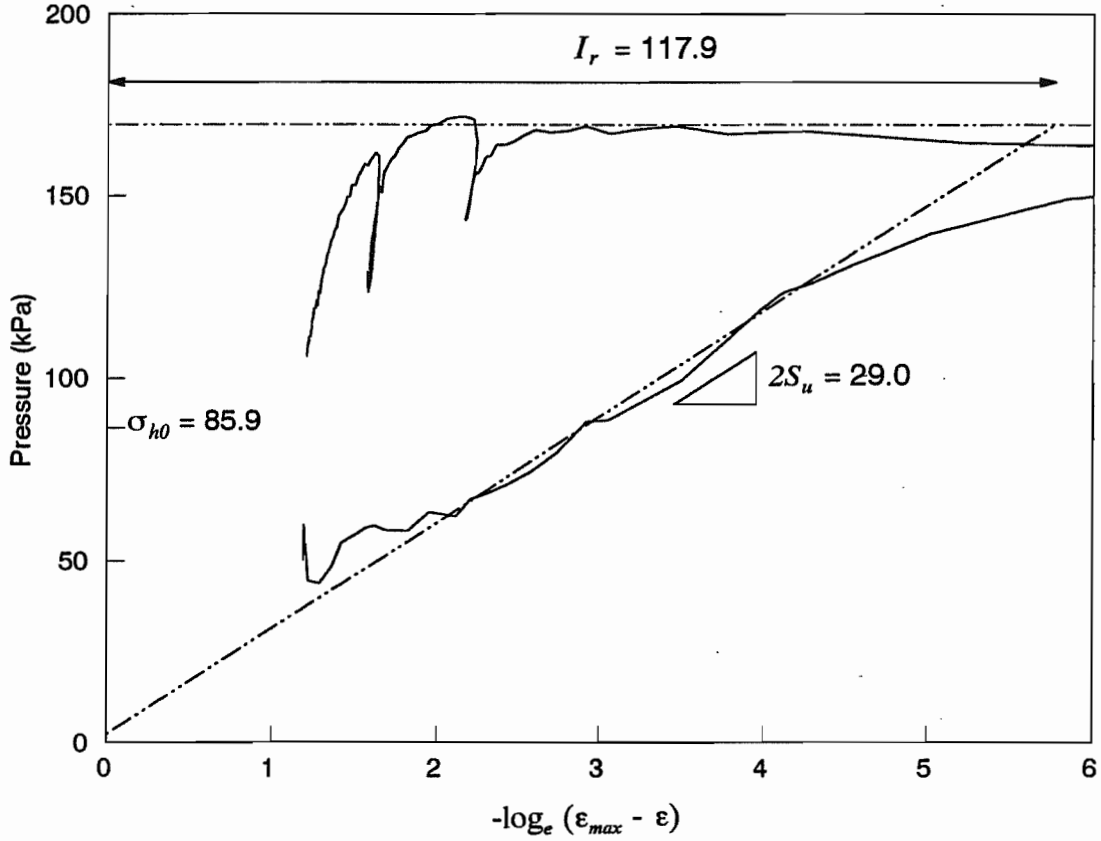

Figure 6.6 Logarithmic construction for Test B1T1, depth 3m

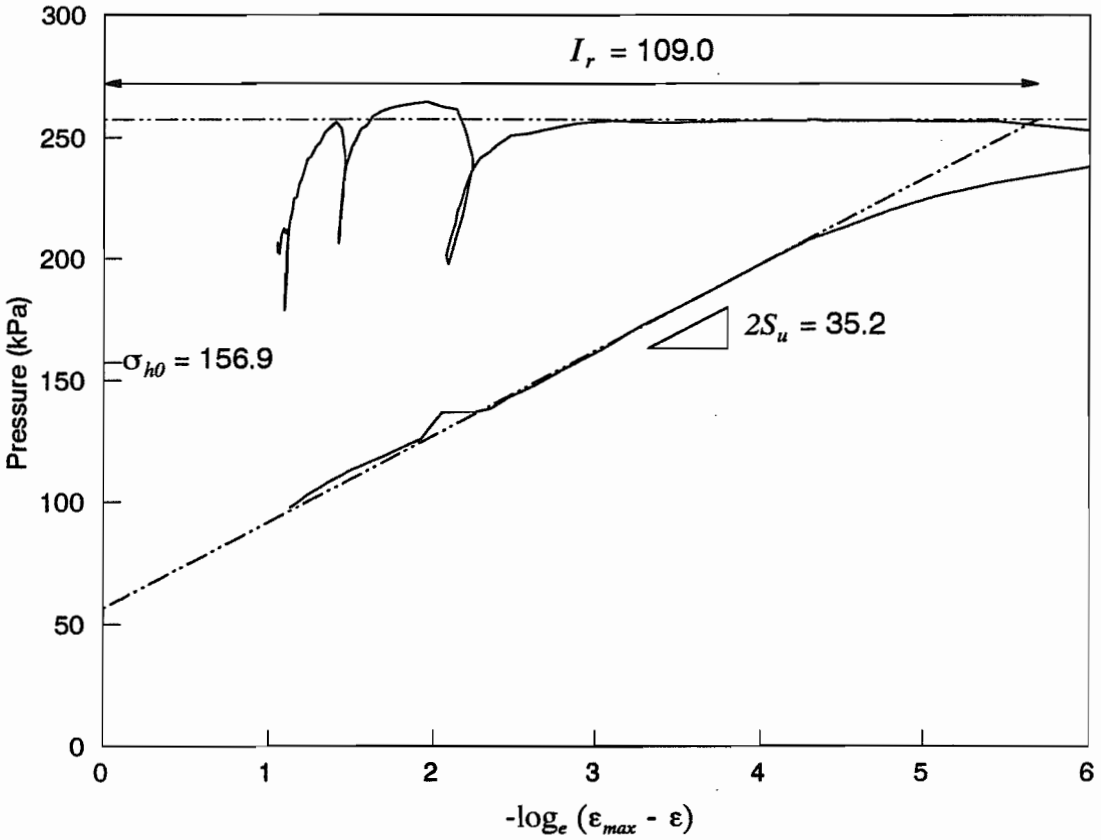

Figure 6.7 Logarithmic construction for Test B2T2, depth 7m

Table 6.2 Results of cone pressuremeter tests at Bothkennar

Test	Depth m	ψ_l (kPa)	s_u (kPa)	G_{cc} (MPa)	σ_{ho} (kPa)	I_r
B1T1	3	169.6	14.5	1.71	85.9	117.8
B2T1	4	174.1	14.2	1.38	95.0	97.3
B3T1	5	197.0	16.9	1.56	103.4	92.1
B1T2	6	244.3	19.3	1.43	141.7	73.9
B2T2	7	257.1	17.6	1.92	156.8	109.0
B3T3	8	287.2	21.2	1.73	172.5	81.5
B1T3	9	325.8	21.5	2.27	204.2	105.7
B2T3	10	347.2	23.6	2.64	212.4	112.0
B1T4	12	436.2	27.1	4.22	272.4	155.9
B2T4	13	449.0	26.3	3.91	291.0	148.4
B1T5	15	518.9	32.9	4.46	324.4	135.5
B2T5	16	544.9	34.8	6.12	330.2	175.9

Conversion of q_c to undrained shear strength, s_u depends upon an empirical cone factor, N_k in the relationship

$$s_u = \frac{q_c - \sigma_{v0}}{N_k} \qquad ...(6.1)$$

where σ_{v0} is the *in situ* total vertical stress. Evidence for this was presented by Lunne *et al.* (1976). N_k for a soil is usually back calculated using field vane strengths, and generally varies between 14 and 21 for most clays of low overconsolidation ratio, dependent upon the plasticity index, I_p. Correlations between N_k and I_p are given by Aas *et al.* (1986) and Powell and Quarterman (1988). Assuming an average I_p of 40% for the Bothkennar clay, as suggested by Nash *et al.* (1992), N_k was found to be 17.5. This leads to the estimation of s_u from the cone resistance profiles, as summarised in Table 6.3. Note that numbers in **bold type** represent estimates of s_u made at the same locations as the pressuremeter tests.

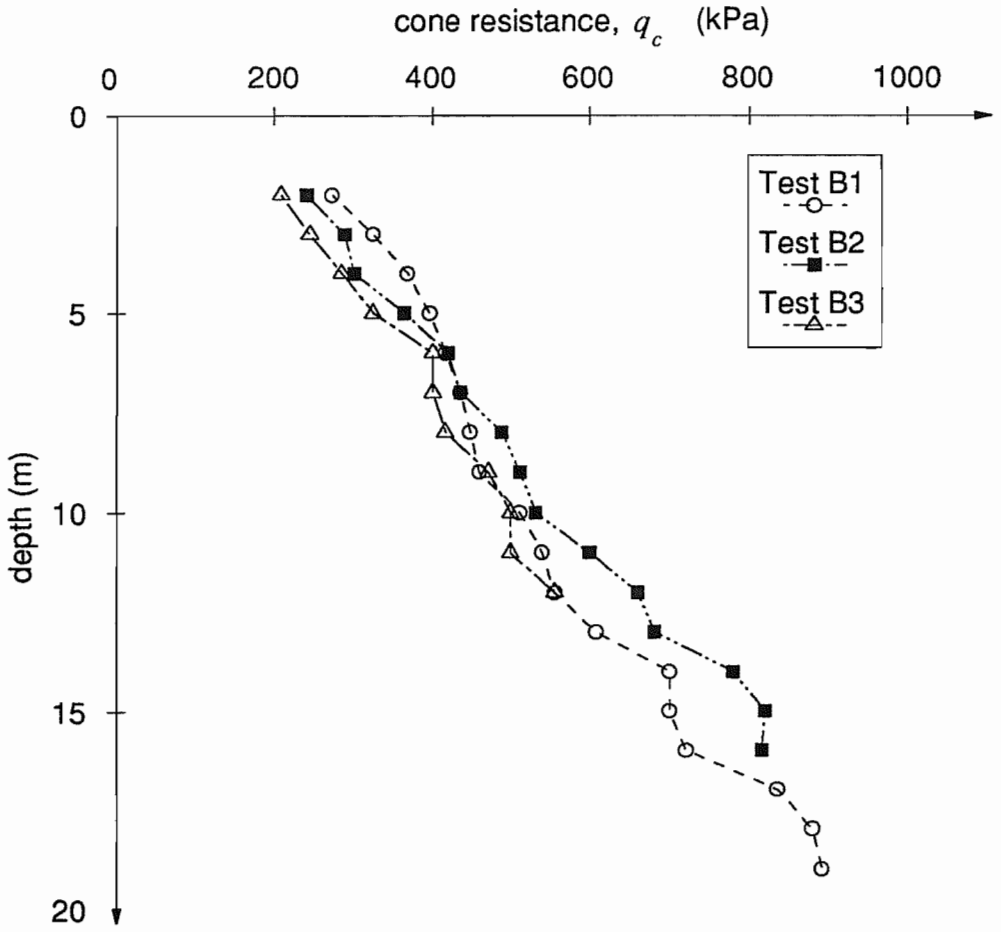

Figure 6.8 Cone resistance profiles from CPM tests at Bothkennar

Table 6.3 Undrained shear strength estimated from CPMT cone resistances

Depth (m)	σ_{v0} (kPa)	B1 (kPa)		B2 (kPa)		B3 (kPa)		$s_{u\,av}$
		q_c	s_u	q_c	s_u	q_c	s_u	
3	49.1	324	**15.7**	288	13.7	244	11.1	13.5
4	65.2	368	17.3	300	**13.4**	284	12.5	14.4
5	81.3	396	18.0	364	16.2	324	**13.9**	16.0
6	97.4	416	**18.2**	420	18.4	400	17.3	18.0
7	113.5	436	18.4	436	**18.4**	400	16.4	17.7
8	129.6	448	18.2	488	20.5	416	**16.4**	18.3
9	145.7	460	**18.0**	512	20.9	472	18.6	19.2
10	161.8	512	20.0	532	**21.2**	500	19.3	20.2
11	177.9	540	20.7	600	24.1	500	18.4	21.1
12	194.0	556	**20.7**	660	26.6	556	20.7	22.7
13	210.1	608	22.7	680	**26.9**			24.8
14	226.2	700	27.1	780	31.6			29.4
15	242.3	700	**26.2**	820	33.0			29.6
16	258.4	720	26.4	816	**31.9**			29.1

Without the additional information provided by piezocone testing, however, these estimates of s_u will be somewhat in error. Aas *et al.* (1986) show that a corrected cone resistance, q_t given by

$$q_t = q_c + u(1 - a) \qquad ...(6.2)$$

where u = pore pressure behind the cone during penetration

a = area ratio which is constant for a specific cone

results in far more consistent estimates of s_u from the relationship

$$s_u = \frac{q_t - \sigma_{v0}}{N_{kt}} \qquad ...(6.3)$$

where N_{kt} is the empirical cone factor related to q_t. The area ratio, a depends upon the location of the piezocone filter. It can be concluded from the cone penetration tests that without a pore pressure correction to q_c, estimates of q_c given in Table 6.3 are lower bound values. This is indeed confirmed by the estimates of s_u from the pressuremeter tests in Table 6.2, and will be discussed in the following section in the light of other *in situ* and laboratory tests carried out at Bothkennar.

6.5 Analysis

6.5.1 Undrained shear strength

The estimates of undrained shear strength, s_u made from the cavity contraction curve of the cone pressuremeter tests have been plotted in Figure 6.9. Clearly a linear increase with depth is evident. The values of s_u obtained from the cone penetration tests are also plotted, and as expected, fall below the pressuremeter values, as no correction to q_c was possible without pore pressure measurements.

Nash *et al.* (1992) report estimates of s_u made from self-boring pressuremeter tests, field vane (VANE) tests and unconsolidated undrained triaxial (UUT) tests, and these have all been plotted in Figure 6.9 for comparison with CPM values. The vane tests and triaxial tests both

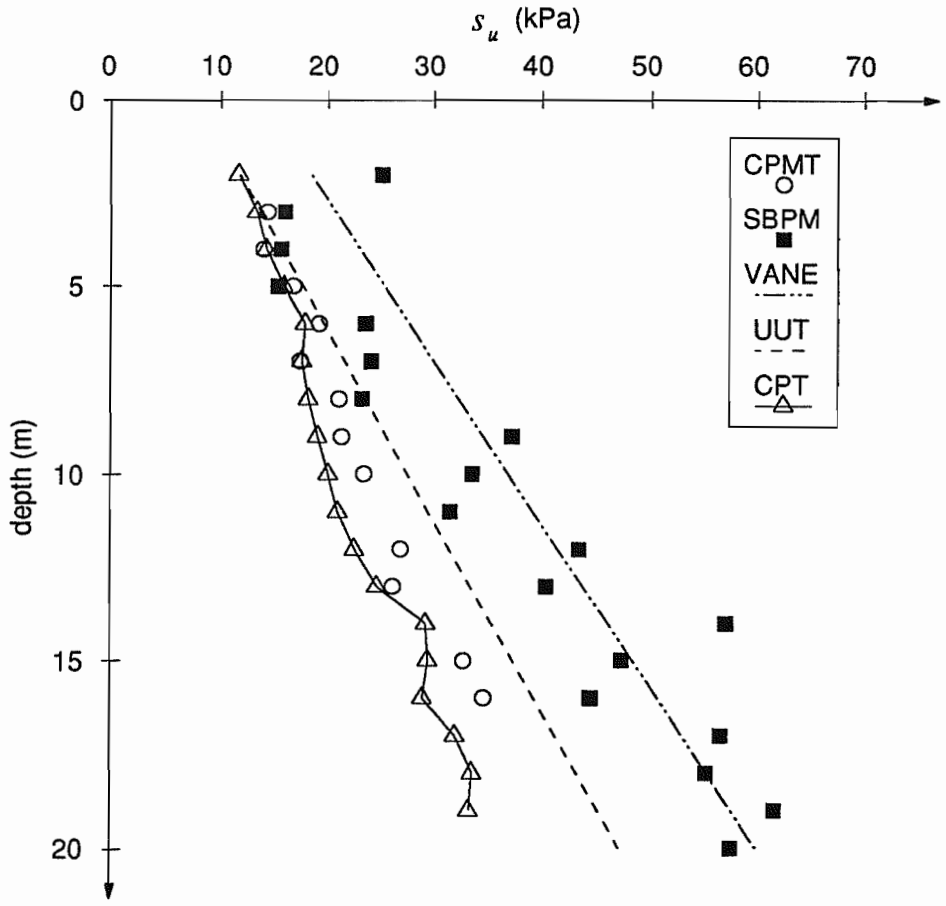

Figure 6.9 Estimates of s_u from *in situ* and laboratory tests

showed a very consistent linear increase of s_u with depth, and hence, have been plotted in the figure as single lines. While all the data show the trend of linearly increasing s_u with depth, there is a quantitative disagreement between the tests. There are several possible reasons for the observed discrepancies in measured values of s_u between various tests, and they are discussed here.

Firstly, since different soil tests subject the soil to different modes of failure, it follows that the relative values of principal stresses at failure are different, and hence different strength measurements are expected. This is illustrated in Figure 6.10, which shows the deformation modes and associated strain conditions of the triaxial compression test, field vane test and pressuremeter test. Triaxial compression as a mode of deformation is shown in Figure 6.10(a). In such conditions, the principal stress directions are fixed throughout the test. The mode of failure of the field vane is one of direct simple shear as shown in Figure 6.10(b), albeit not

the same as a conventional direct shear test because of the different orientation of the specimen. In a pressuremeter test, membrane expansion is theoretically a plane strain deformation problem, as shown in Figure 6.10(c). This applies, of course, to an infinitely long pressuremeter. With a length to diameter ratio of 6, the SBPM does not cause true plane strain soil deformations. The shorter the expanding length of pressuremeter, the more closely a deformation will approximate an expanding sphere rather than an expanding cylinder and the greater the overestimate of strength. This has been verified numerically by Borsetto *et al.* (1983) and Yu (1990). General experience from a large number of sites indicates that s_u obtained from SBPM tests is consistently greater than other *in situ* methods (Windle and Wroth, 1977; Ghionna *et al.*, 1983; Lacasse *et al.*, 1990) and this is attributed also to initial disturbance during installation.

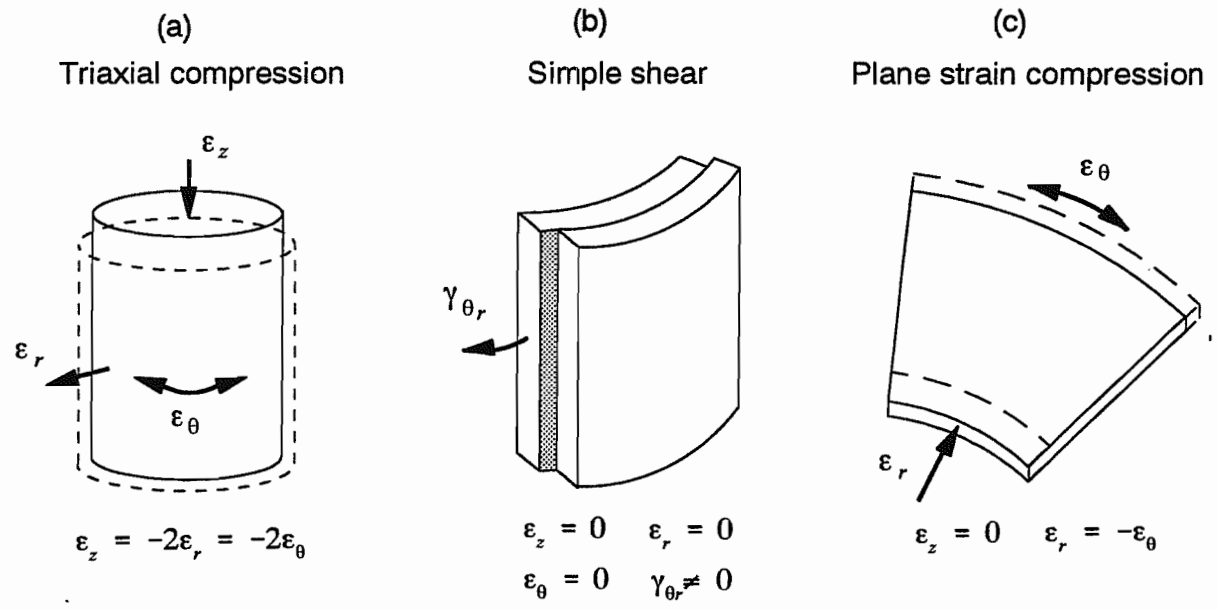

Figure 6.10 Modes of deformation

Secondly, differences in strain rates between test procedures can influence undrained strength. The vane test is carried out in the field at a speed of rotation such that the strain rates applied to the failing soil are considerably higher than in triaxial tests. This inevitably leads to higher undrained strengths. Such differences between pressuremeter tests and triaxial tests are notably less pronounced.

Thirdly, the deviatoric stress at large strains of a clay subjected to shearing is usually less than observed peak values, as shown in Figure 6.11. Undrained strengths determined from the triaxial tests reported by Nash *et al.* (1992) are peak values. The cone pressuremeter test, however, is capable of large strains before a limit pressure is determined, and is probably more closely related to residual triaxial strengths.

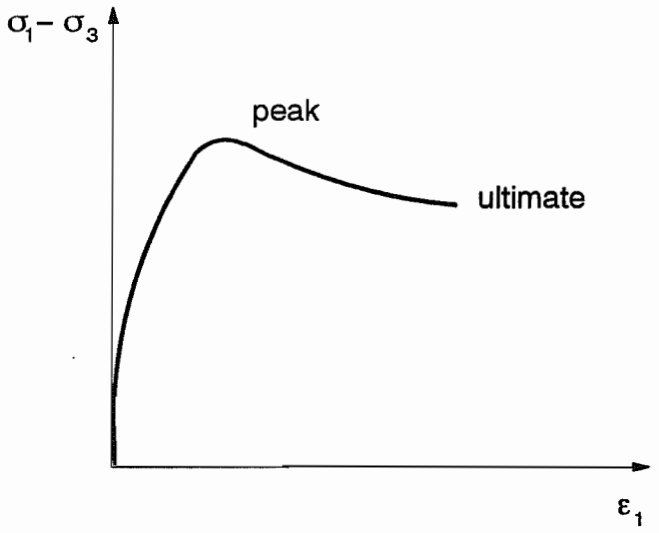

Figure 6.11 Generalised behaviour of cohesive soils in triaxial compression

In short, it is evident that the shear strengths measured by the various test methods are different. The undrained triaxial test commonly forms the reference to which other tests are related, and is used here for this purpose. Field vane values of s_u are probably overestimated because of the high rate of strain during the test. Self-boring pressuremeter tests frequently overestimate s_u, and this is attributed in part to the relatively low length to diameter ratio of the device. The cone pressuremeter tests marginally underpredict values of s_u probably because s_u has been determined at large strains. With these differences accounted for, it can be concluded that the cone pressuremeter can provide reliable measurements of undrained strength using the analysis of Houlsby and Withers (1988).

6.5.2 Elastic shear modulus

Undrained shear strength discussed in the previous section was related back to a laboratory reference test: the triaxial test. Shear modulus, however, is very sensitive to disturbance, and without the availability of high quality sampling and testing techniques, is difficult to measure in the laboratory. Because most soils show highly non-linear stress strain behaviour at low strains (Jardine *et al.*, 1986), it is more applicable to relate shear modulus to a strain amplitude for comparison with other tests.

The cone pressuremeter can provide estimates of shear modulus from unload-reload loops and from cavity contraction analysis. Unlike the self-boring pressuremeter, no attempts are made to measure initial tangent, G_t or secant, G_s moduli because of the large amount of disturbance experienced by the soil after CPM insertion. The advantage of measuring shear modulus from unload-reload loops (given by G_{ur}) is that the strain amplitude is easily measured. The advantage of measuring shear modulus from cavity contraction analysis (given by G_{cc}) is that the influence of initial disturbance is expected to be minimised. G_{cc}, however, is not associated with a measured strain amplitude because it is derived from a geometrical construction. This issue is covered in more detail in Chapter 7, where differences between G_{ur} and G_{cc} from the same pressuremeter test are discussed.

At this stage it is worthwhile comparing G_{cc} obtained from the Houlsby and Withers (1988) analysis with moduli measured from other tests at Bothkennar. This is done in Figure 6.12 where values of G_{cc} from the CPM test are plotted with G_{ur} from SBPM tests and G_{sc} from seismic cone penetrometer tests (SCPT). Clearly the trend of increasing G with depth is evident from all the tests, and differences in magnitude of G are attributed to the fact that the tests measure the stiffness by imposing very different strain amplitudes on the soil. When normalised by the values from the SCPT as shown in Figure 6.13, it can be seen that both the CPM and SBPM tests show a similar magnitude of variation. Small unload-reload loops from the SBPM give a shear modulus about one quarter of the value measured at very small

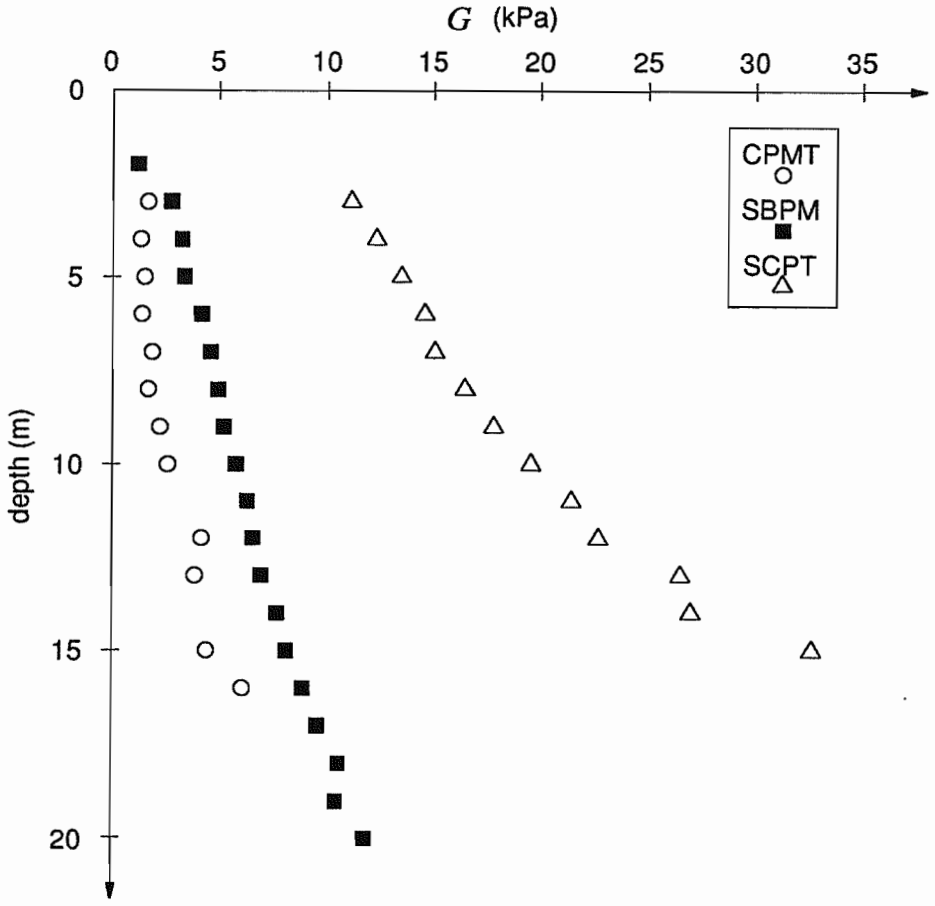

Figure 6.12 Shear moduli measurements at Bothkennar

strain by seismic cone, and the interpretation of the unloading curve of the CPM gives a modulus about half as small again.

6.5.3 *In situ* horizontal stress

The *in situ* horizontal stress, σ_{h0} measured from the CPM has been plotted in Figure 6.14 in the form of K_0, with SBPM and dilatometer, DMT results included. The SBPM measures σ_{h0} directly from inspection of the lift-off pressures of the individual strain arms, as outlined by Mair and Wood (1987). The interpretation of lift-off pressures, however, can be quite subjective, and Nash *et al.* (1992) report higher estimates of K_0 than suggested by the test contractors. Both sets of data have been presented in Figure 6.14. The DMT uses empirical correlation for estimation of σ_{h0} (Marchetti, 1980). The horizontal stress measured by the CPM has been corrected to account for the finite length of the instrument according to the

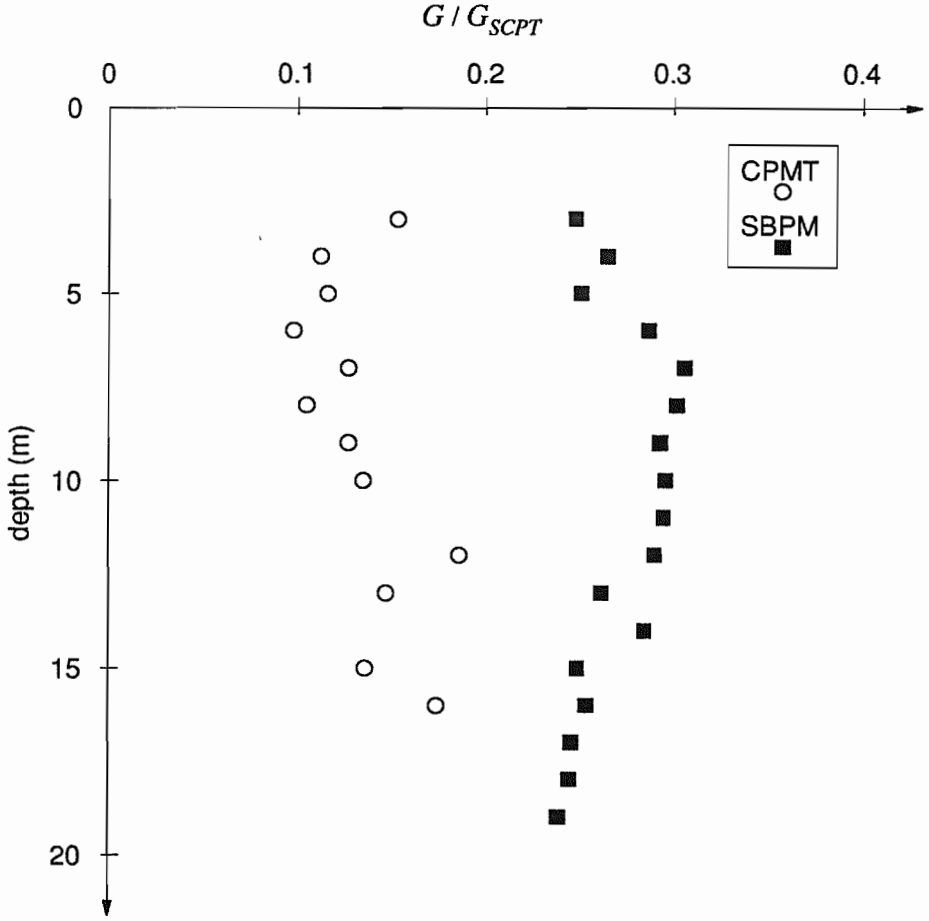

Figure 6.13 Shear moduli normalised by seismic cone measurements

relationship suggested by Yu (1990)

$$\frac{\sigma_{h0}^{10} - \sigma_{h0}^{\infty}}{s_u} = 0.630 + 0.0733 \log_e I_r \qquad ...(6.4)$$

based on finite element studies with an assumed soil model. Even with the correction of equation (6.4), the CPM is found to overestimate σ_{h0} by an average factor of about 2.5 compared with SBPM or DMT estimates. This, in fact, confirms the findings of Houlsby and Withers (1988) on application of the analysis to their own tests. It was postulated that for interpretation of σ_{h0}, a mode of deformation somewhere between cylindrical and spherical cavity contraction was more appropriate. At the end of pressuremeter inflation, the elastic-plastic boundary has a radius of about $1.5R_i(I_r)^{0.5}$ for a 50% increase in radius. The clay at Bothkennar has a rigidity index, I_r of about 120, averaged from Table 6.2, compared with

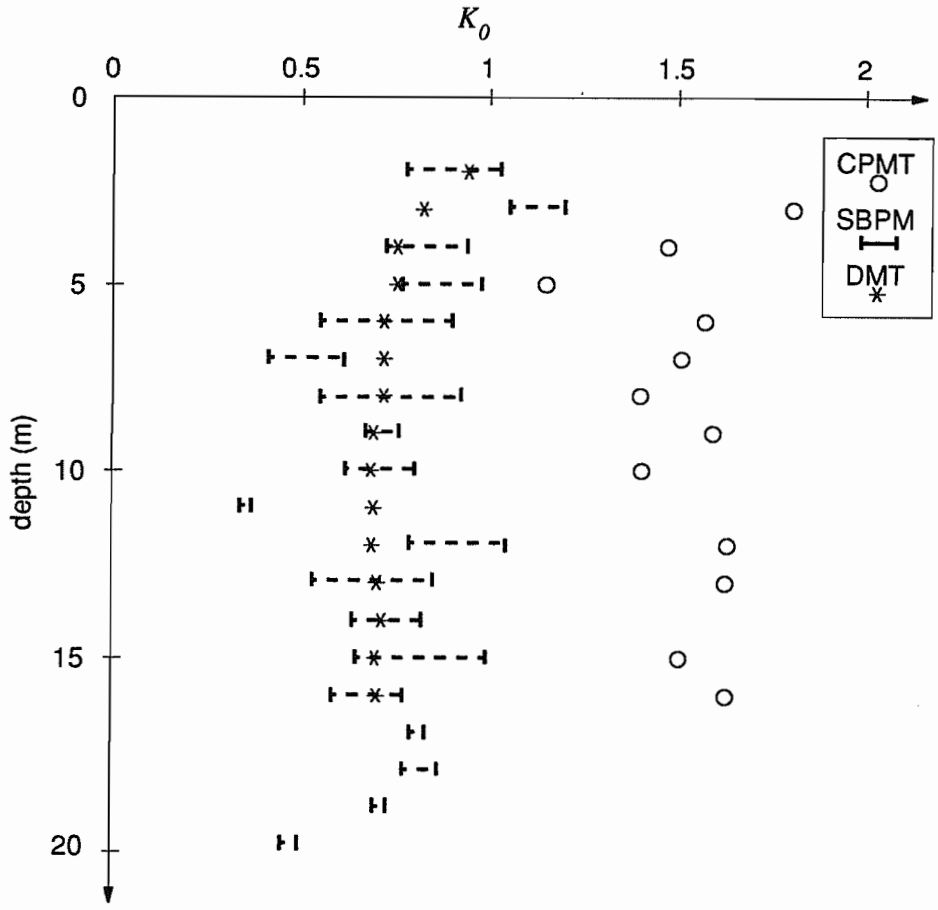

Figure 6.14 Estimates of the stress ratio made from *in situ* tests at Bothkennar

about 250 for the clay at the Madingley site reported by Houlsby and Withers (1988). Hence any correction to K_0 to account for the transition from cylindrical to spherical conditions at Bothkennar should be smaller than at Madingley. The observed overestimate from Figure 6.14 is, however, slightly greater than at Madingley. Based on the limited amount of data available, it is concluded that the Houlsby and Withers analysis is not suitable for interpretation of σ_{h0}.

6.6 Conclusions

Extending the limited amount of data available on cone pressuremeter testing in clay, a programme of 12 CPM tests has been carried out at the SERC National soft clay test site at Bothkennar, Scotland. The site at Bothkennar has remarkably uniform ground conditions, comprising a layer up to 16m thick of lightly overconsolidated silty clay with properties that increase linearly with depth. Much recent effort has been spent in characterization of the soil

conditions at this site and a large amount of field and laboratory testing is reported in the literature which has been referred to for reliable calibration of the cone pressuremeter.

A CPM test procedure was adopted which incorporated three unload-reload loops, identification of a limit pressure and a well defined contraction curve. The magnitude of the membrane stiffness correction was shown to be significant to tests in soft clay.

Based on the large strain cavity contraction analysis of Houlsby and Withers (1988), estimates of undrained shear strength, shear modulus and *in situ* horizontal stress were made from the CPM. Measurements taken from cone resistance profiles were also made to provide independent values of undrained shear strength, although it was found that without the benefits of piezocone readings, only lower bound estimates of strength could be made. Considering this, there was good agreement between undrained shear strength estimates from cone resistance and from CPM cavity contraction.

The cone pressuremeter was found to give as consistent a measure of undrained shear strength as SBPM tests, VANE tests and UUT tests. Observed strength variations between the tests were attributed to different deformation modes, rate effects and disturbance effects.

Shear modulus data obtained from cavity contraction showed very consistent trends. The strong influence of strain amplitude on stiffness measured by different tests was identified. Shear modulus from the cone pressuremeter test, however, is not measured at a defined strain amplitude. The implication of this feature of cavity contraction analysis will be discussed further in Chapter 7.

Estimates of the *in situ* horizontal stress were found to be significantly higher than other *in situ* tests, which confirms the results from reported tests in stiff clay.

CHAPTER 7

SHEAR MODULUS

7.1 Introduction

Pressuremeters are among the few *in situ* devices capable of measuring both strength and stiffness properties of a soil. Interpretation of cone pressuremeter tests to determine strength (*i.e.* D_r and hence ϕ) has been dealt with in Chapter 5, and for clays, the undrained shear strength, s_u has been measured with confidence in Chapter 6. In this chapter, estimates of shear modulus, G are made from cone pressuremeter tests in sands and clays with particular reference to the use of unload-reload loops in the test procedure.

Experience has shown that shear modulus measured from the unload-reload loop, G_{ur} of a self-boring pressuremeter test is almost completely independent from disturbance (Hughes, 1982; Wroth, 1982; Robertson and Hughes, 1986). Early work with the cone pressuremeter has indeed confirmed the insensitivity of G_{ur} in both sands and clays, despite the large amounts of soil disturbance caused to the soil by CPM insertion (Houlsby and Withers, 1988; Withers *et al.*, 1989).

For application to geotechnical problems, however, it is necessary to reference G_{ur} to both a stress and a strain level. Contrary to the assumption of linear elastic-perfectly plastic material behaviour used in the interpretation of pressuremeter tests, soils exhibit non-linear stress-strain behaviour; a feature which is evident at strain levels starting well below those measured by the pressuremeter.

Non-linear stress-strain behaviour has been recognised by many researchers: Seed and Idriss (1970); Hardin and Drnevich (1972), Iwasaki *et al.* (1976); Seed *et al.* (1986); Jardine *et al.* (1986) among others, and is illustrated by the dotted line in Figure 7.1. Two features of non-linear soil behaviour are evident from the figure. With increasing strain amplitudes

(1) the hysteresis of the unload-reload cycle increases

(2) the gradient of the unload-reload cycle decreases.

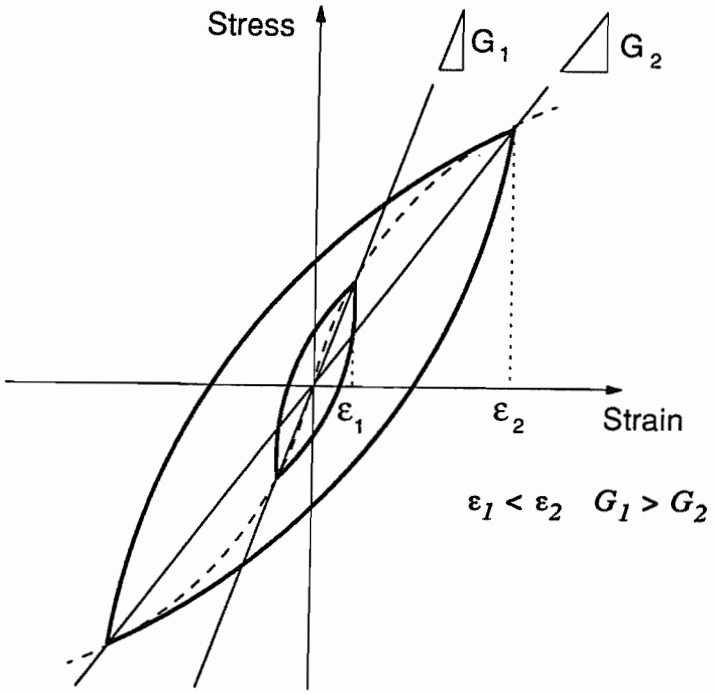

Figure 7.1 Non-linear stress-strain behaviour at different strain amplitudes

From elastic theory, G is a secant modulus connecting the apices of the unload-reload cycle. The variation of G with shear strain for sands has been quantified by Seed *et al.* (1986), as shown in Figure 7.2, with the range of strain amplitudes typically measured from unload-reload loops of pressuremeter tests included. Furthermore, Seed *et al.* (1986) cite the work of Iwasaki *et al.* (1976) and show that the normalised shear modulus increases with mean effective stress as shown in the figure.

After making corrections for instrument stiffness and geometry, values of shear modulus obtained from the unload-reload loops of CPM tests in sand are presented in this chapter. G_{ur} obtained from strain arm measurements and volume change measurements with the 10cm²

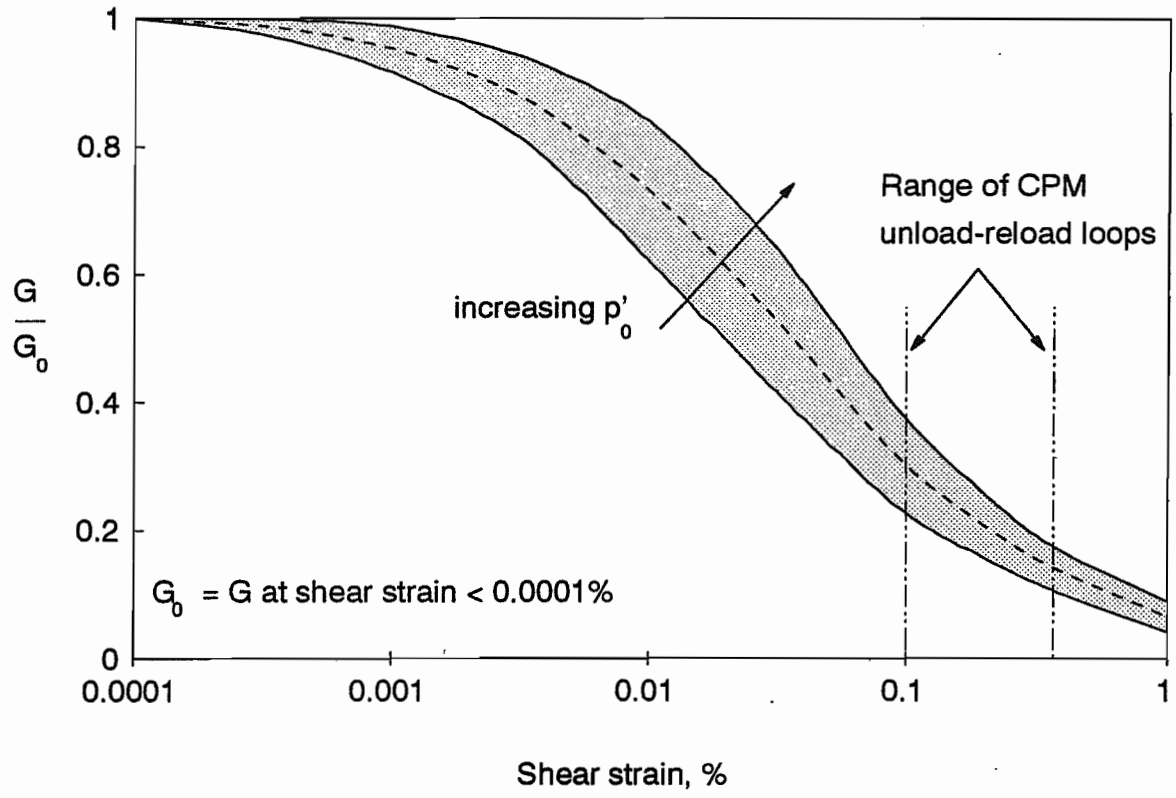

Figure 7.2 Variation of normalised shear modulus with strain amplitude (after Seed *et al.* (1986)

CPM are compared and discussed. Non-linearity of the loops is seen to be slightly greater in reloading than unloading, and is attributed to microplasticity and some creep straining. The influence of stress level on G_{ur} is identified and a normalising procedure is applied so that G_{ur} can be extrapolated to stress levels outside the range at which testing was carried out. Scatter observed in the results is attributed to strain amplitude.

For the soft clay tests at Bothkennar, shear modulus values obtained from unload-reload loops are presented and compared to estimates from the cavity contraction analysis, G_{cc} presented in Chapter 6. The same has been done for G_{ur} from tests in stiff clay at the Madingley site (Houlsby and Withers, 1988), as no interpretation of unload-reload loops from these field tests has been made before. Recent approaches for interpreting non-linear stiffness data from undrained pressuremeter tests are discussed and applied to the data.

7.2 Measurement of shear modulus

7.2.1 10cm² cone pressuremeter

Application of cavity expansion theory to pressuremeter interpretation requires the assumption of isotropic, linear elastic-perfectly plastic material behaviour. The pressure and the cavity strain are related to the elastic shear modulus by the equation

$$G = \frac{1}{2} \cdot \frac{d\psi}{d\varepsilon_c} \qquad ...(7.1)$$

as shown by Gibson and Anderson (1961) for an undrained analysis of the pressuremeter test. Since it is shear stress and not compressive stress that causes soil deformation, equation (7.1) also holds for a drained analysis, as long as the decrease in cavity pressure, $\Delta\psi$ is not sufficient to cause reverse plasticity of the sand which takes place when

$$\Delta\psi = \psi \cdot \frac{2\sin\phi_{ps}}{1 + \sin\phi_{ps}} \qquad ...(7.2)$$

where ϕ_{ps} is the plane strain friction angle of the sand (Wroth, 1982).

Cavity strain of the 10cm² CPM in the calibration chamber was measured directly from a set of three strain gauged arms at mid-height of the pressuremeter and indirectly from the volume of oil required to inflate the membrane. Volume readings were indirect because cavity strain was calculated from the measured travel of a piston in the pressurisation system as described in Chapter 2, and the assumption that the pressuremeter membrane expanded as a right cylinder, but with corrections applied (based on finite element analyses) to make these comparable to the arms measurements.

The pressure-strain curve for a typical unload-reload loop in Dogs Bay sand using arm

measurements is shown in Figure 7.3. For comparison, the same loop is also shown using volume change measurements of strain. Both curves exhibit non-linear behaviour, even though the change in cavity pressure was not sufficient to cause reverse plasticity of the soil.

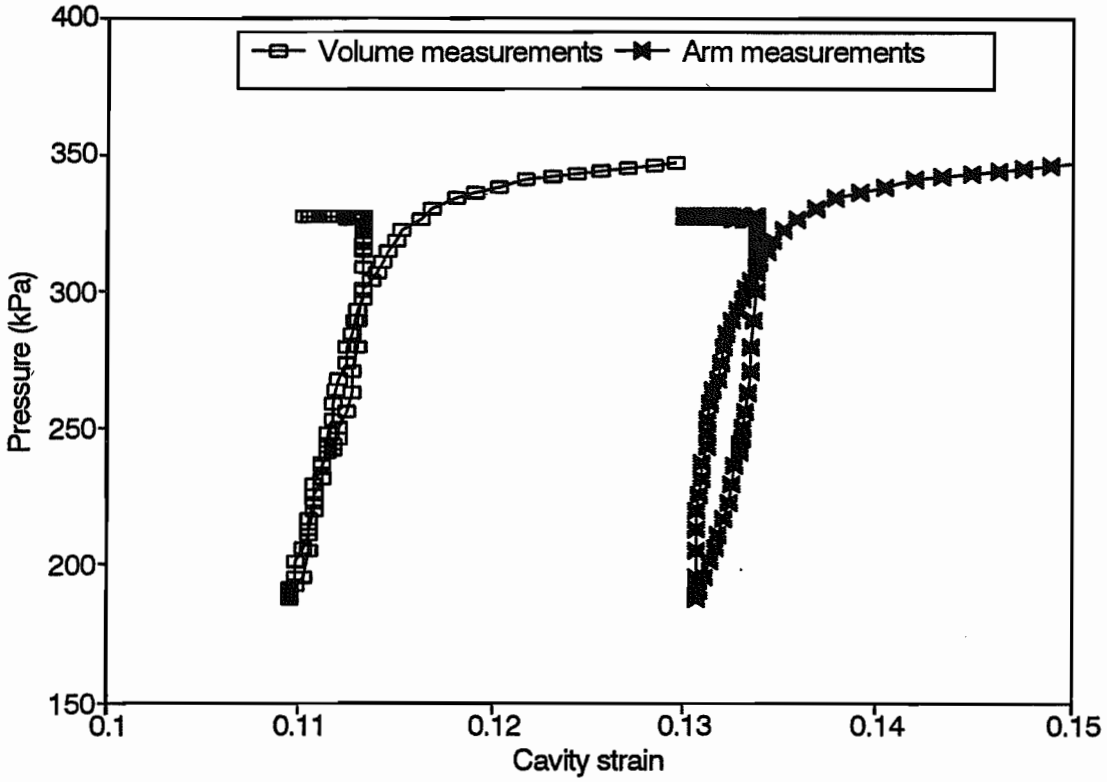

Figure 7.3 A typical unload-reload loop in Dogs Bay sand

Two approaches for computing G from an unload-reload loop have been adopted (Schnaid, 1990). In the first approach, G is obtained from the gradient of a chord connecting the apices of the loop. In the second approach, G is obtained from the gradient of the line of best fit determined from a linear regression analysis on the unload-reload data. These approaches are applicable to both arm and volume change measurements and have been labelled G_{ch}^{a} , G_{ls}^{a} , G_{ch}^{v} , G_{ls}^{v} respectively. A summary of corrected results of shear moduli obtained from these approaches is given in section 7.4.

7.2.2 15cm² cone pressuremeter

The calibration chamber tests in sand were carried out at relatively slow strain rates so that an optimum number of data points was generated. In clay, however, the possibility of causing partial drainage of the soil surrounding the pressuremeter meant that it was necessary to carry out expansions (and particularly unload-reload loops) at relatively high strain rates. As a result, there were fewer data points generated for each loop with the 15cm² CPM in the field than with the 10cm² CPM in the laboratory. In Figure 7.4, typical unload-reload loops are shown from a test at Bothkennar based upon arm measurements. Because inflation was achieved by nitrogen gas, no volume change measurements were made. Shear modulus was obtained both from the gradient of the chord connecting the apices of the loop, G_{ch} and from the gradient of the line of best fit to the unload-reload data, G_{ls}.

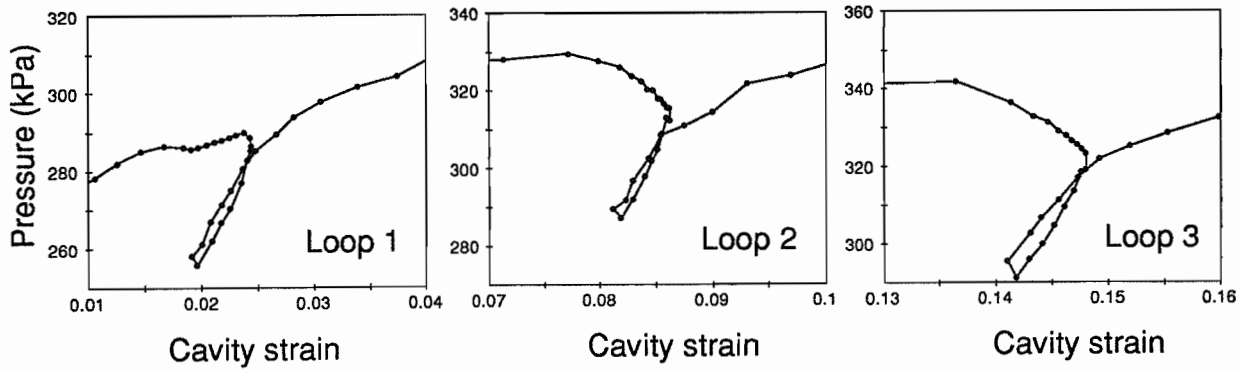

Figure 7.4 Unload-reload loops from test B2T3 at Bothkennar

7.3 Corrections to pressuremeter data

7.3.1 Compliance

Pressuremeters exhibit an inherent stiffness in response to applied cavity pressures which can influence measured soil stiffness. In soft soils, the pressure required to achieve a particular strain amplitude during an unload-reload loop is low and results in negligible deformation of the mechanical components of the pressuremeter. In stiff soils, however, cavity pressures are significantly higher and can result in instrument deformations of a similar order of magnitude as soil deformations. This phenomenon is termed compliance and has been identified by Mair and Wood (1987) and Fahey and Jewell (1990). Correct interpretation of soil stiffness

obtained from an unload-reload loop should account for instrument compliance in the form of a correction to measured values of shear modulus. Fahey and Jewell (1990) recommend a correction procedure which requires inflation of the pressuremeter module in a thick walled, effectively rigid steel tube. From the pressure-strain curve, an estimate of the instrument stiffness can be made, G_{system} at any level of cavity pressure.

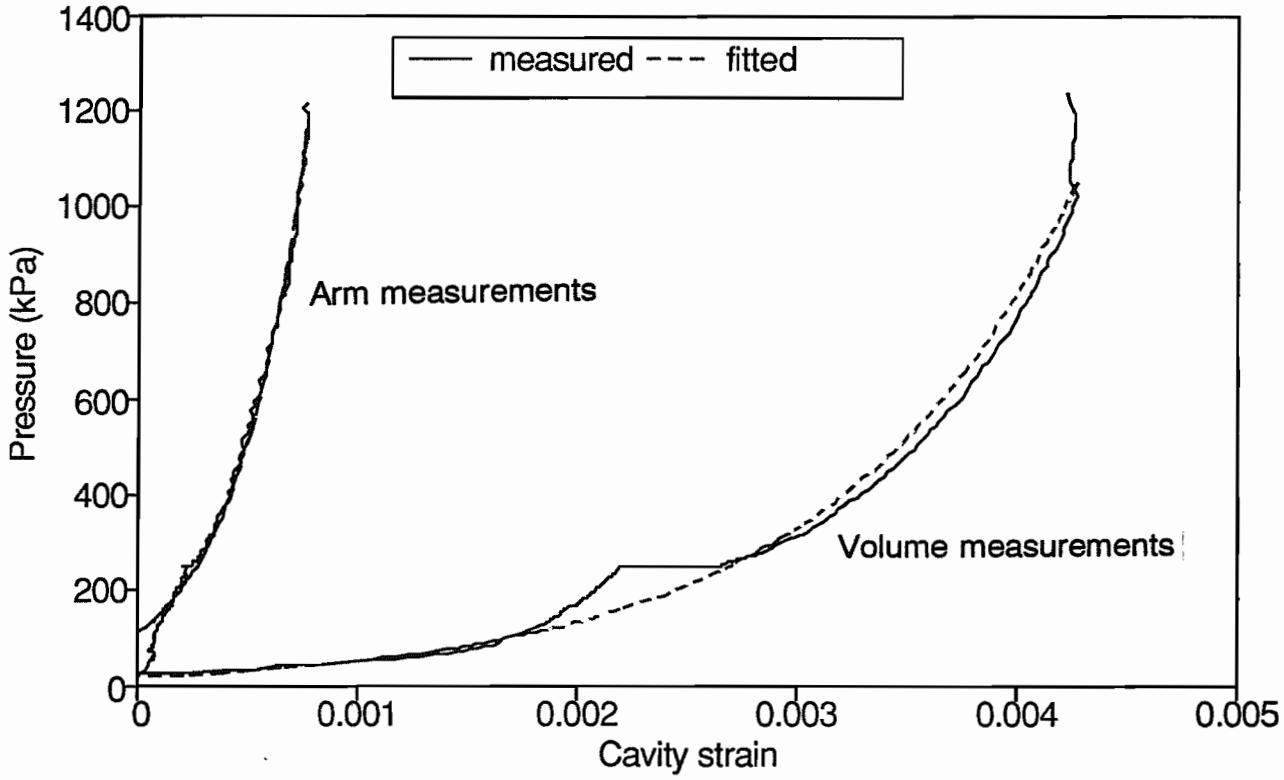

Figure 7.5 10cm² cone pressuremeter inflation in a "rigid" tube

In Figure 7.5, the results of a 10cm² CPM inflation in a "rigid" tube are presented for both arm and volume measurements. Zero strain has been taken as the point at which the membrane came into contact with the tube. It is apparent that instrument stiffness is significantly greater when computed from the strain arm readings than when computed from volume change readings. This is because the latter are also subject to line and control unit flexibility. The pressure-strain curves of Figure 7.5 have been fitted by an exponential function of the form

$$\psi = Ae^{B\varepsilon} \qquad ...(7.3)$$

For the arm measurements, the constants A and B were found to be 111.8 and 3074.7 respectively, and for the volume change measurements, A and B were found to be 21.8 and 907.4 respectively. G_{system} was then obtained from the tangential slope of the pressure-strain curve at the required pressure, using equation (7.1). The compliance curve for the 15cm² CPM was of a similar form to that of the 10cm² CPM, and a similar procedure was used to determine G_{system}.

As suggested by Fahey and Jewell (1990), the measured shear modulus of the soil is then corrected to account for compliance by the relationship

$$\frac{1}{G_{corrected}} = \frac{1}{G_{measured}} - \frac{1}{G_{system}} \qquad ...(7.4)$$

This correction was applied to all unload-reload loops of both the 10cm² CPM and the 15cm² CPM. The largest arm correction factor to measured values of G in sand was 1.05 and the largest volume change correction factor was 1.16. In the soft clay at Bothkennar, the largest correction factor was 1.06.

7.3.2 Pressuremeter length correction

Elastic cavity expansion theory is used is used to compute shear modulus from an unload-reload loop. The theory assumes that deformations occur under conditions of plane strain, *i.e.* zero strains in the vertical direction. This assumption only holds if the pressuremeter is infinitely long. In reality, the cone pressuremeters have a finite length to diameter ratio of 10. End constraints on the pressuremeter membrane have an influence on the measured cavity strain and, therefore, a correction to the measured shear modulus is required. Houlsby and Carter (1990) carried out a two-dimensional numerical study to investigate geometry effects on the results of pressuremeter tests. For a length to diameter ratio of 10, it was found that a correction to G_{ur} computed from arm measurements of 0.997 was required. A correction to G_{ur} computed from volume change measurements of 0.907 was also required.

7.4 Stiffness measurements in sand

7.4.1 Summary of results

After making the corrections for compliance and pressuremeter geometry, estimates of G_{ch} and G_{ls} from arm measurements and volume change measurements were made from every unload-reload loop and the results are presented in Tables 7.1 and 7.2 for Dogs Bay sand and Hokksund sand respectively. In the tables, p_c' is the mean effective stress in the soil adjacent to the pressuremeter prior to unloading. A procedure for determining p_c' is presented in section 7.4.4. $\Delta\varepsilon$ is the strain amplitude of the unload-reload loop measured between the apices.

7.4.2 Comparison between arm and volume change strain measurements

A comparison of shear moduli estimated in Dogs Bay sand from arm measurements is made with shear moduli estimated from volume change measurements in Figure 7.6. In the figure, G has been calculated from both chord and least square measurements. There is a tendency for G_{ch}^{a} and G_{ls}^{a} to be greater than G_{ch}^{v} and G_{ls}^{v}. This slight overestimation is consistent with the magnitude of the strain amplitudes over which shear moduli were calculated. As shown in Table 7.1, the average strain amplitude from arm measurements was 0.00303 and from volume change measurements was 0.00346. Following the discussion on the non-linear stress-strain behaviour in section 7.1, larger strain amplitudes result in lower estimates of shear modulus, as has been observed. Considering this behaviour, it is evident that the two approaches of measuring shear modulus are in good agreement.

Table 7.1 Corrected shear moduli from unload-reload loops in Dogs Bay sand

Test	p_c'	Arms			Volume change		
		G_{ch}	G_{ls}	$\Delta\varepsilon$	G_{ch}	G_{ls}	$\Delta\varepsilon$
DX1 UR1	126.6	16.6	11.9	0.00238	9.1	8.3	0.00392
DX1 UR2	135.0	11.5	11.0	0.00287	9.5	9.1	0.00355
DB11 UR1	95.0	11.0	8.5	0.00308	7.7	7.4	0.00430
DB11 UR2	120.1	11.3	10.0	0.00279	8.1	8.7	0.00357
DB11 UR3	127.2	12.4	11.3	0.00261	7.9	8.5	0.00427
DB30 UR1	106.7	12.3	9.5	0.00311	12.6	10.6	0.00289
DB30 UR2	121.5	12.3	10.8	0.00296	11.1	10.7	0.00322
DB30 UR3	129.2	12.9	10.9	0.00294	10.1	9.7	0.00393
DB3 UR1	206.7	17.4	15.0	0.00279	13.2	13.6	0.00303
DB3 UR2	217.6	19.5	18.4	0.00251	13.9	14.2	0.00381
DB2 UR1	293.1	21.7	18.1	0.00432	18.7	18.3	0.00420
DB2 UR2	313.3	16.3	16.5	0.00299	20.7	19.7	0.00308
DB12 UR1	253.1	29.3	24.8	0.00291	19.2	18.8	0.00415
DB12 UR2	307.3	31.7	27.9	0.00244	18.8	19.2	0.00377
DB12 UR3	332.7	32.9	30.4	0.00236	20.6	20.4	0.00406
DB5 UR1	139.4	11.4	9.9	0.00409	8.0	8.4	0.00515
DB5 UR2	156.8	11.2	10.1	0.00364	9.3	9.8	0.00385
DB5 UR3	166.4	10.5	10.3	0.00338	9.7	10.4	0.00343
DB21 UR1	183.5	20.8	13.8	0.00298	14.6	14.1	0.00372
DB21 UR2	204.9	18.2	14.4	0.00377	12.7	12.9	0.00470
DB21 UR3	214.6	18.8	15.9	0.00298	14.1	14.5	0.00353
DB22 UR1	170.7	21.9	17.5	0.00280	15.5	14.8	0.00359
DB22 UR2	217.0	18.8	16.7	0.00337	13.2	11.6	0.00342
DB0 UR1	174.2	21.5	17.7	0.00213	11.7	9.9	0.00319
DB0 UR2	188.3	18.2	16.1	0.00278	12.7	13.3	0.00399
DB6 UR1	341.9	31.9	27.5	0.00306	22.5	21.5	0.00405
DB6 UR2	369.2	36.5	33.5	0.00273	21.5	21.4	0.00429
DB6 UR3	383.9	32.0	30.8	0.00311	22.0	21.5	0.00454
DX9 UR1	459.7	42.1	37.4	0.00291	41.2	37.3	0.00287
DX9 UR2	498.2	44.5	40.4	0.00278	36.3	34.9	0.00333
DX9 UR3	518.5	42.0	40.9	0.00260	41.8	39.2	0.00264
DB32 UR1	698.5	61.8	50.6	0.00331	56.5	53.8	0.00344
DB32 UR2	760.9	60.6	51.1	0.00323	50.3	49.7	0.00369
DB32 UR3	800.1	66.7	61.6	0.00313	59.5	54.6	0.00325
DB7 UR1	176.9	17.5	13.8	0.00312	11.2	11.1	0.00437
DB7 UR2	191.8	18.3	14.8	0.00284	11.1	11.5	0.00436
DB7 UR3	197.6	16.1	12.9	0.00319	10.9	11.2	0.00457
DB20 UR1	237.6	28.2	21.0	0.00256	21.7	20.5	0.00313
DB20 UR2	271.4	30.4	23.0	0.00237	22.9	22.1	0.00290
DB20 UR3	288.5	21.6	20.1	0.00349	20.4	19.4	0.00353
DB4 UR1	184.2	16.5	14.1	0.00346	11.9	11.5	0.00425
DB4 UR2	204.8	19.5	16.6	0.00274	12.3	12.7	0.00405
DB4 UR3	215.5	16.6	15.7	0.00311	11.5	11.9	0.00494
DB8 UR1	416.4	37.2	32.8	0.00301	34.9	32.7	0.00310
DB8 UR2	448.1	38.0	36.2	0.00286	33.4	31.0	0.00312
DB8 UR3	465.8	36.9	36.4	0.00286	34.6	31.3	0.00314

Table 7.1 (continued)

Test	p_c'	Arms			Volume change		
		G_{ch}	G_{ls}	$\Delta\varepsilon$	G_{ch}	G_{ls}	$\Delta\varepsilon$
DB15 UR1	120.1	15.2	11.4	0.00312	9.6	9.1	0.00428
DB15 UR2	144.0	15.4	14.2	0.00276	10.6	10.5	0.00354
DB15 UR3	152.9	15.4	13.6	0.00287	11.9	12.2	0.00359
DB23 UR1	167.7	15.8	13.8	0.00376	15.4	14.9	0.00354
DB23 UR2	193.7	14.7	14.7	0.00328	14.6	14.3	0.00356
DB23 UR3	206.6	19.1	18.4	0.00181	14.3	13.8	0.00321
DB26 UR1	197.9	18.6	14.9	0.00338	17.7	17.7	0.00340
DB26 UR2	224.3	21.0	17.2	0.00233	18.2	17.0	0.00277
DB26 UR3	237.1	19.2	18.3	0.00243	17.8	16.7	0.00284
DB16 UR1	365.9	39.5	31.9	0.00285	31.9	31.5	0.00315
DB16 UR2	424.6	38.8	32.8	0.00317	30.4	30.5	0.00334
DB16 UR3	451.9	35.5	31.2	0.00386	32.7	29.6	0.00346
DB17 UR1	201.0	22.0	15.4	0.00335	17.1	15.6	0.00382
DB17 UR2	233.3	22.1	20.1	0.00304	16.6	15.6	0.00392
DB17 UR3	244.6	24.6	24.9	0.00284	15.6	16.0	0.00451
DB27 UR1	257.4	25.7	23.8	0.00308	29.9	29.3	0.00259
DB27 UR2	293.2	22.8	20.8	0.00327	26.0	24.0	0.00265
DB27 UR3	305.7	24.5	23.2	0.00249	25.0	22.4	0.00280
DB24 UR1	294.4	27.9	23.7	0.00309	29.1	26.5	0.00283
DB24 UR2	324.4	26.2	24.5	0.00281	28.9	26.2	0.00262
DB24 UR3	336.8	26.0	26.8	0.00235	27.2	25.2	0.00275
DB10 UR1	435.2	36.6	28.7	0.00372	40.2	37.8	0.00318
DB10 UR2	494.2	34.2	29.3	0.00424	33.8	32.1	0.00406
DB10 UR3	528.6	41.5	33.0	0.00339	38.5	34.7	0.00339
DX18 UR1	437.6	41.8	31.9	0.00278	-	-	-
DX18 UR2	481.4	35.8	31.4	0.00352	-	-	-
DX18 UR3	509.7	37.6	36.1	0.00337	45.3	40.7	0.00196
DB25 UR1	574.3	51.2	43.4	0.00320	54.4	46.5	0.00289
DB25 UR2	632.2	48.2	42.6	0.00302	50.9	46.0	0.00275
DB25 UR3	670.7	50.4	51.3	0.00272	56.9	55.8	0.00247
DB19 UR1	267.7	24.1	20.0	0.00373	27.7	26.0	0.00298
DB19 UR2	307.2	29.3	20.9	0.00324	24.1	23.0	0.00347
DB19 UR3	328.8	26.5	22.5	0.00342	23.4	22.4	0.00329
DB28 UR1	345.7	33.2	26.9	0.00285	39.8	31.7	0.00229
DB28 UR2	393.8	33.1	27.9	0.00289	31.2	28.5	0.00278
DB28 UR3	415.4	32.7	34.6	0.00244	32.8	30.1	0.00252
DY29 UR1	287.4	24.6	21.5	0.00363	28.1	25.6	0.00293
DY29 UR2	327.1	26.1	23.9	0.00304	29.0	25.3	0.00248
DY29 UR3	346.1	26.4	24.6	0.00287	29.2	24.6	0.00251
		maximum $\Delta\varepsilon$		0.00432	maximum $\Delta\varepsilon$		0.00515
		minimum $\Delta\varepsilon$		0.00181	minimum $\Delta\varepsilon$		0.00196
		average $\Delta\varepsilon$		0.00303	average $\Delta\varepsilon$		0.00346

Table 7.2 Corrected shear moduli from unload-reload loops in Hokksund sand

Test	p_c'	Arms			Volume change		
		G_{ch}	G_{ls}	$\Delta\varepsilon$	G_{ch}	G_{ls}	$\Delta\varepsilon$
HS01 UR1	142.6	14.4	11.6	0.00313	12.5	12.9	0.00342
HS01 UR2	157.8	14.4	13.5	0.00281	12.5	12.9	0.00309
HS01 UR3	167.4	15.3	13.7	0.00286	11.6	12.0	0.00369
HS02 UR1	327.3	50.6	38.5	0.00094	27.0	24.8	0.00165
HS02 UR2	357.2	35.8	31.3	0.00188	25.7	25.2	0.00229
HS02 UR3	377.1	27.4	24.1	0.00375	19.3	37.7	0.00021
HS03 UR1	179.0	28.2	17.7	0.00115	17.8	15.7	0.00162
HS03 UR2	199.6	20.5	18.0	0.00193	17.9	18.7	0.00209
HS03 UR3	207.4	15.3	14.3	0.00371	15.3	15.7	0.00354
HS04 UR1	405.0	29.7	22.5	0.00413	28.0	27.7	0.00408
HS04 UR2	450.3	42.1	30.8	0.00202	30.9	30.4	0.00265
HS04 UR3	471.7	47.5	37.8	0.00106	35.0	32.4	0.00141
HS05 UR1	155.9	17.0	13.1	0.00276	13.3	13.1	0.00341
HS05 UR2	175.8	18.9	16.6	0.00186	14.4	14.6	0.00255
HS05 UR3	185.0	27.3	17.5	0.00090	17.3	15.0	0.00146
HS06 UR1	208.5	22.2	17.4	0.00303	17.8	17.3	0.00370
HS06 UR2	231.4	20.9	18.4	0.00289	17.4	17.2	0.00335
HS06 UR3	241.3	21.1	17.8	0.00289	17.7	17.0	0.00328
HX06 UR1	260.4	25.4	19.7	0.00312	19.7	20.4	0.00385
HX06 UR2	288.6	24.6	21.4	0.00292	19.9	20.5	0.00342
HX06 UR3	295.8	24.4	22.6	0.00296	20.4	21.3	0.00330
HS07 UR1	424.4	56.1	44.6	0.00111	46.5	44.2	0.00125
HS07 UR2	463.5	41.7	40.7	0.00201	34.2	33.9	0.00228
HS07 UR3	488.8	35.0	30.7	0.00394	30.7	30.2	0.00409
HX07 UR1	474.7	40.1	33.2	0.00311	34.0	33.5	0.00340
HX07 UR2	528.7	40.7	36.5	0.00307	34.0	33.6	0.00328
HX07 UR3	561.2	42.3	42.7	0.00294	37.6	38.2	0.00307
HS09 UR1	754.0	63.8	45.3	0.00320	57.7	52.4	0.00326
HS09 UR2	816.8	58.9	48.4	0.00323	56.5	53.4	0.00325
HS09 UR3	839.0	69.0	50.1	0.00318	48.5	48.3	0.00422
HS10 UR1	452.6	36.8	28.4	0.00322	30.3	30.0	0.00365
HS10 UR2	467.5	36.8	31.9	0.00296	29.0	28.9	0.00356
HS10 UR3	483.0	38.0	31.8	0.00290	29.9	29.8	0.00366
		maximum $\Delta\varepsilon$		0.00413	maximum $\Delta\varepsilon$		0.00422
		minimum $\Delta\varepsilon$		0.00090	minimum $\Delta\varepsilon$		0.00021
		average $\Delta\varepsilon$		0.00265	average $\Delta\varepsilon$		0.00294

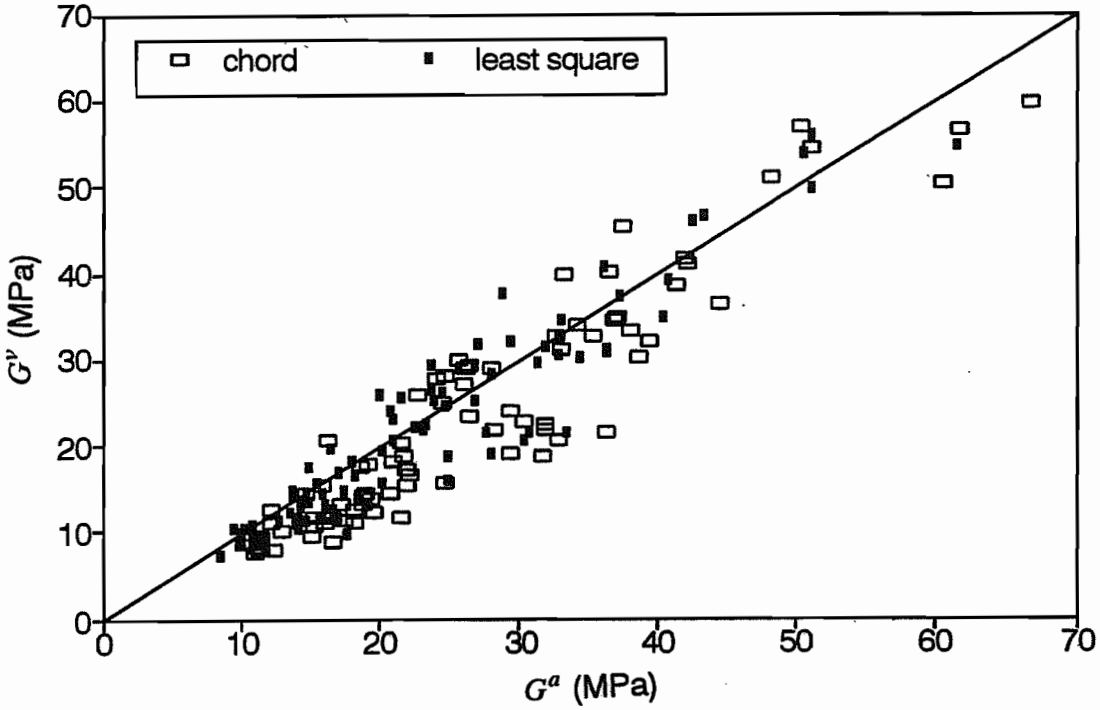

Figure 7.6 A comparison between arm and volumetric measurements of shear modulus made from CPM unload-reload loops in Dogs Bay sand

7.4.3 Comparison between *G* measured by chord and least square methods

In Figure 7.7, a comparison has been made between shear modulus measured by the chord method, G_{ch} and shear modulus measured by the least square method, G_{ls} for arm and volume change measurements. If sand behaves as an elastic-perfectly plastic material, then cavity expansion theory shows that an unload-reload loop takes the form of a single straight line of gradient $2G$, and G_{ch} and G_{ls} are equal. What is observed is a hysteresis in the loop as a result of either non-linear behaviour or the decay of creep strains with time, or a combination of the two. Most creep strains, however, were allowed to decay during a pressure holding test prior to unloading. The ratio of G_{ch}/G_{ls} gives an indication of the symmetry of the loop about its apices, but no indication of the magnitude of the hysteresis, defined as the area of the loop. In Figure 7.7, G^a_{ch} is about 5% greater than G^a_{ls}. This implies that the unloading section of a loop is slightly more linear than the loading section. It is also evident that G^v_{ch} is almost identical to G^v_{ls} for a significant range of G, and at higher moduli, a similar trend to that shown by the arm measurements is exhibited. Bellotti *et al.* (1989) suggest that soil behaviour

is influenced by microplasticity when the strain amplitude exceeds twice an elastic threshold strain, *i.e.* $\Delta\varepsilon > 2\varepsilon_t^e$. Below $2\varepsilon_t^e$, Bellotti *et al.* show evidence from resonant column tests that $G_{ur} \approx G_0$. It is difficult to determine for carbonate sands whether microplasticity would be dominated by particle crushing or particle rotation and rearrangement or by a combination of these effects.

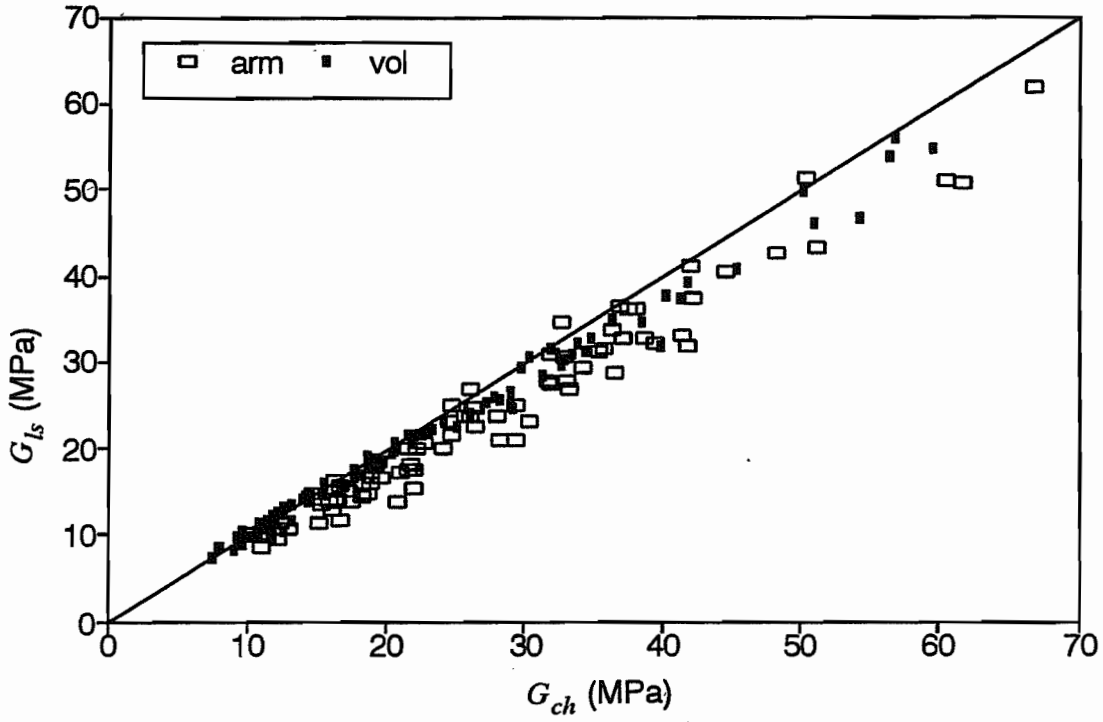

Figure 7.7 A comparison between least square and chord measurements of shear modulus made from CPM unload-reload loops in Dogs Bay sand

7.4.4 Influence of stress level

Having established the reasons for differences between G_{ch}^a , G_{ls}^a , G_{ch}^v , G_{ls}^v, further discussion will concentrate upon only one of these measurements, G_{ch}^a so that the influence of stress and strain level can be investigated.

It is assumed that elastic cavity expansion theory can be used to interpret unload-reload behaviour. Immediately prior to unloading, the mean effective stress acting on the soil around the pressuremeter probe, p_c' can be calculated from the cavity pressure, ψ_c.

For plane strain soil deformations, the radial stress acting on the pressuremeter-soil interface is given by $\sigma_r' = \psi_c$.

From a series of plane strain tests performed in the simple shear apparatus, Stroud (1971) showed that sand fails with a constant ratio of effective stresses. The hoop stress, σ_θ can then be related to σ_r' by the equation

$$\sigma_\theta' = \sigma_r' \left(\frac{1 - S}{1 + S} \right) \qquad ...(7.5)$$

where $S = \sin\phi_{ps}$. The intermediate stress, σ_z', is harder to estimate. One possible procedure is to assume a fully associated flow rule from the Matsuoka plasticity model (Matsuoka, 1976), where the dilation angle, ν is equal to the friction angle ϕ_{ps}. Burd (1986) then shows that σ_z can be related to the in-plane stresses by the relationship

$$\sigma_z' = \sqrt{\sigma_r' \sigma_\theta'} \qquad ...(7.6)$$

The consequences of assuming an associated dilation angle are thought to be minor. Any error in estimation of σ_z' results in only a third of that error in estimation of p_c', and since shear modulus is shown to be related to the logarithm of p_c', the affect on the variation of G as a result of such an assumption is negligible. Furthermore, the relationship of equation (7.6) agrees closely with experimental work reported by Stroud (1971) and Bishop (1971).

The mean effective stress at the start of an unload-reload loop, p_c' defined by

$$p_c' = \frac{\sigma_r' + \sigma_\theta' + \sigma_z'}{3} \qquad ...(7.7)$$

can be expressed in terms of equations (7.5) and (7.6) to give

$$p_c' = \frac{\sigma_r'}{3}\left(1 + \frac{1-S}{1+S} + \sqrt{\frac{1-S}{1+S}}\right) \qquad ...(7.8)$$

Values of p_c' for unload-reload loops in Dogs Bay sand and Hokksund sand are given in Tables 7.1 and 7.2 respectively.

The variation of shear modulus with p_c' (both normalised with respect to atmospheric pressure) is shown in the logarithmic plot of Figure 7.8 for tests in Dogs Bay sand. Moduli calculated from tests in dense and loose sands have been plotted together because they exhibit a similar trend. A single relationship can be used to fit the data as first suggested by Janbu (1963), and takes the form

$$\frac{G}{p_a} = K_G \left(\frac{p_c'}{p_a}\right)^n \qquad ...(7.9)$$

where K_G = a modulus number and n = a modulus exponent. Relationships between G and p' of this form have been reported by Wroth *et al.* (1979), Robertson and Hughes (1986), Bruzzi *et al.* (1986), Bellotti *et al.* (1989), Schnaid (1990) and others. For most silica sands, n is usually between 0.4 and 0.8. For the Dogs Bay carbonate sand, n was found to be 0.877 and K_G was found to be 103. Both n and K_G were generally insensitive to density as is evident in Figure 7.8. Although it was ensured during testing that all unload-reload loops were carried out at approximately the same strain amplitude, scatter observed in the measured moduli is attributed largely to variations in $\Delta\varepsilon$.

Wroth *et al.* (1979) proposed the relationship

$$\frac{G}{p_a} = \frac{710}{1+1600\gamma}\left[\frac{p}{p_a}\right]^{(0.765-0.33\exp(-3000\gamma))} \cdot 1.23 \cdot \left[0.9+\frac{D_r}{500}\right] \qquad ...(7.10)$$

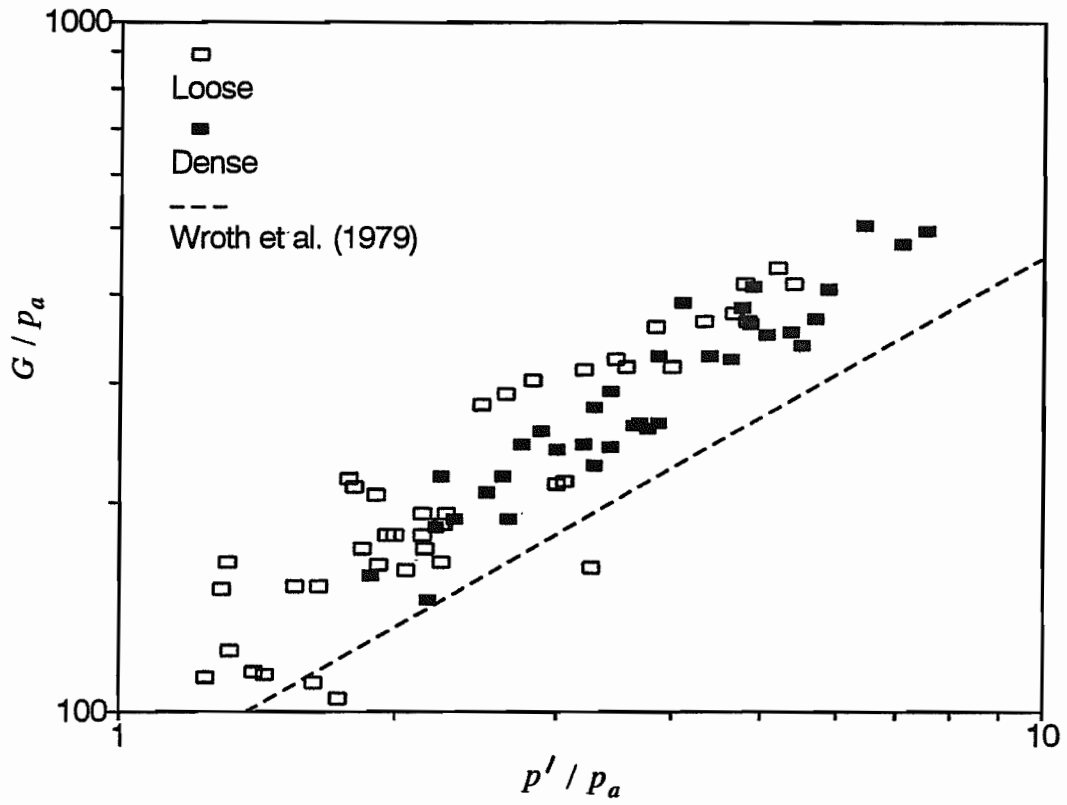

Figure 7.8 The influence of stress level on shear modulus measured from CPM unload-reload loops in Dogs Bay sand

based on an extensive database of soil types. The variation of G with p' is shown to depend on the strain amplitude, and in equation (7.10) this is expressed in terms of a shear strain $\gamma = 2\Delta\varepsilon$ for measurements taken from unload-reload loops. The Wroth *et al.* (1979) relationship is very similar to the relationship of Seed *et al.* (1986) which was shown in Figure 7.2. It has been applied to the data obtained from unload-reload loops in Dogs Bay sand, for an average γ of 0.006 and D_r of 25% (loose sand). The influence of density on G estimated from equation (4.10) is, in fact, minor. Estimates of G made in this way are plotted in Figure 7.8 as a dashed line. There is a slight underprediction of the CPM moduli, but considering the broad range of sand types that the Wroth *et al.* (1979) relationship is based upon, a very good agreement exists with the Dogs Bay sand data.

7.4.5 Influence of strain amplitude

The degree of scatter exhibited in Figure 7.8 between the measured shear modulus, G_{ur}^{m} and

the shear modulus calculated from equation (7.9), G_{ur}^{c} is expressed by the ratio G_{ur}^{m} / G_{ur}^{c} for a p' corresponding to G_{ur}^{m} as specified in Table 7.1. The variation of this ratio with strain amplitude is presented in Figure 7.9, where $\Delta\varepsilon^{m}$ / $\Delta\varepsilon^{av}$ is the ratio of the measured strain amplitude to the average value of $\Delta\varepsilon$ for all Dogs Bay sand unload-reload loops. The figure shows broadly that as strain amplitude is increased, shear modulus decreases. Tests in both loose and dense Dogs Bay sand exhibit this behaviour. Because all the tests were carried out at approximately the same strain amplitude, the ratio $\Delta\varepsilon^{m}$ / $\Delta\varepsilon^{av}$ remains very close to unity, and a more precise relationship between G_{ur}^{m} / G_{ur}^{c} and $\Delta\varepsilon^{m}$ / $\Delta\varepsilon^{av}$ is difficult to ascertain.

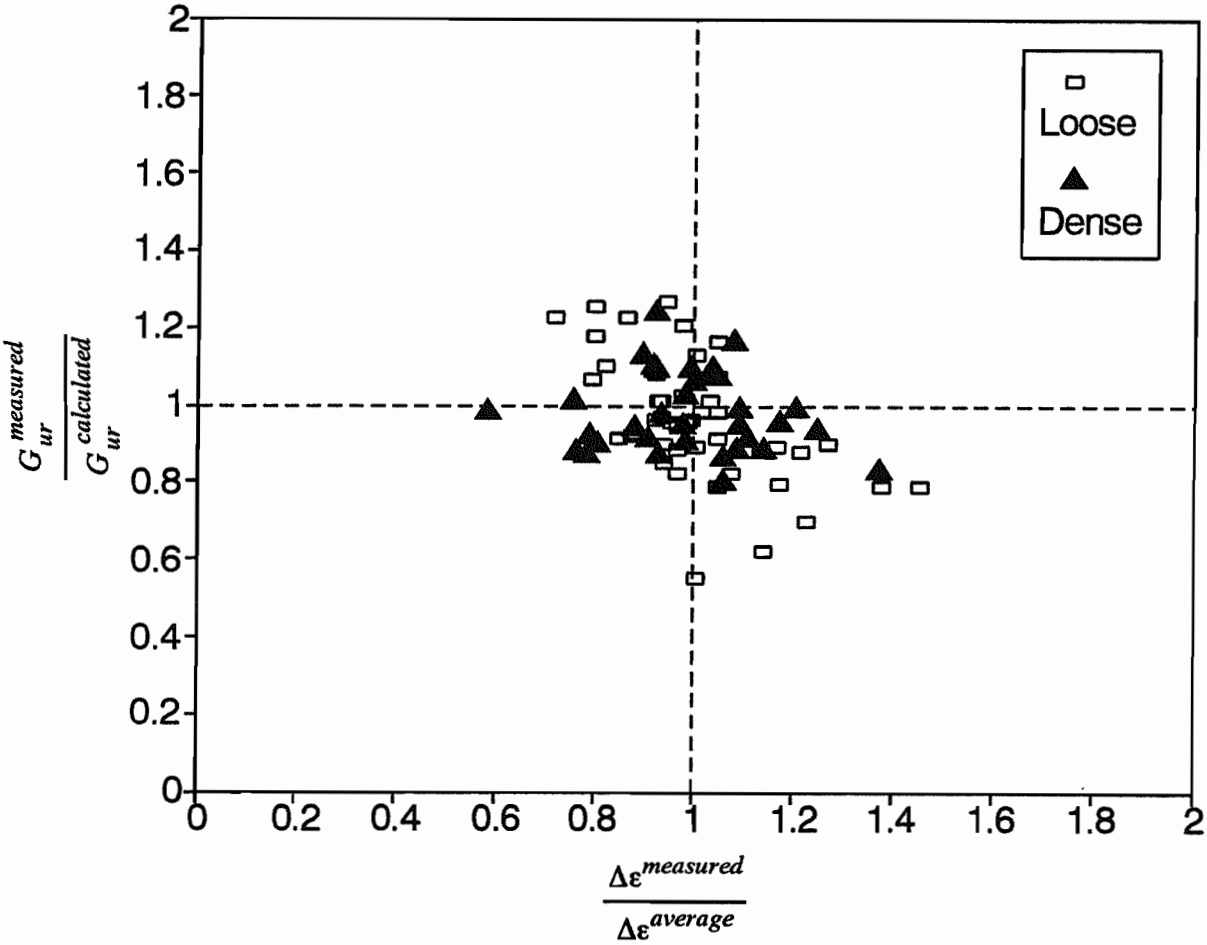

Figure 7.9 The influence of strain amplitude on shear modulus measured in Dogs Bay sand

The trend shown in Figure 7.9 has been clarified by a group of tests in Hokksund sand, where the strain amplitude was deliberately varied. In tests HS02 and HS03, the first, second and third unload-reload loops were carried out with strain amplitudes of 0.001, 0.002 and 0.004 respectively. In tests HS04 and HS05, the first, second and third unload-reload loops were carried out with strain amplitudes of 0.004, 0.002 and 0.001 respectively. The nature and position of these loops are shown in relation to the overall pressuremeter curve for test HS02 in Figure 7.10 and test HS04 in Figure 7.11. Corrected values of G^a_{ch} and $\Delta\varepsilon$ are also presented in the figure for each loop. It is clear from a comparison between the figures that the magnitude of the shear modulus is controlled by the strain amplitude of the loop. There is no evidence to suggest that the cavity strain level at the start of each loop had any influence on the measured shear modulus.

In a similar procedure to that used for Dogs Bay sand, the shear modulus for Hokksund sand was related to mean effective stress by equation (7.9). The modulus number, K_G was found to be 112 and the modulus exponent, n was found to be 0.831, and neither value showed sensitivity to the density. Because of the deliberate variation of strain amplitude and the relatively small number of loops carried out in Hokksund sand, much scatter was observed between log G/p_a and log p'/p_a. Hence only a limited confidence can be placed in the values of K_G and n. Qualitatively, the relationship between G^m_{ur} / G^c_{ur} and $\Delta\varepsilon^m$ / $\Delta\varepsilon^{av}$ as shown in Figure 7.12 is well defined. A dashed line appears in the figure which highlights this trend.

Using the relationships of Janbu (1963) in equation (7.9) and Wroth *et al.* (1979) in equation (7.10), it is postulated that an estimate of G_0 could be made from the cone pressuremeter. This procedure would require sufficient confidence being placed in the parameters K_G and n (which requires a large number of unload-reload loops at a constant strain amplitude), and in the variation of G with $\Delta\varepsilon$ (which requires a large number of unload-reload loops at varying strain amplitudes). No published G_0 data was available for comparison, and so the accuracy of this predictive method remains unclear.

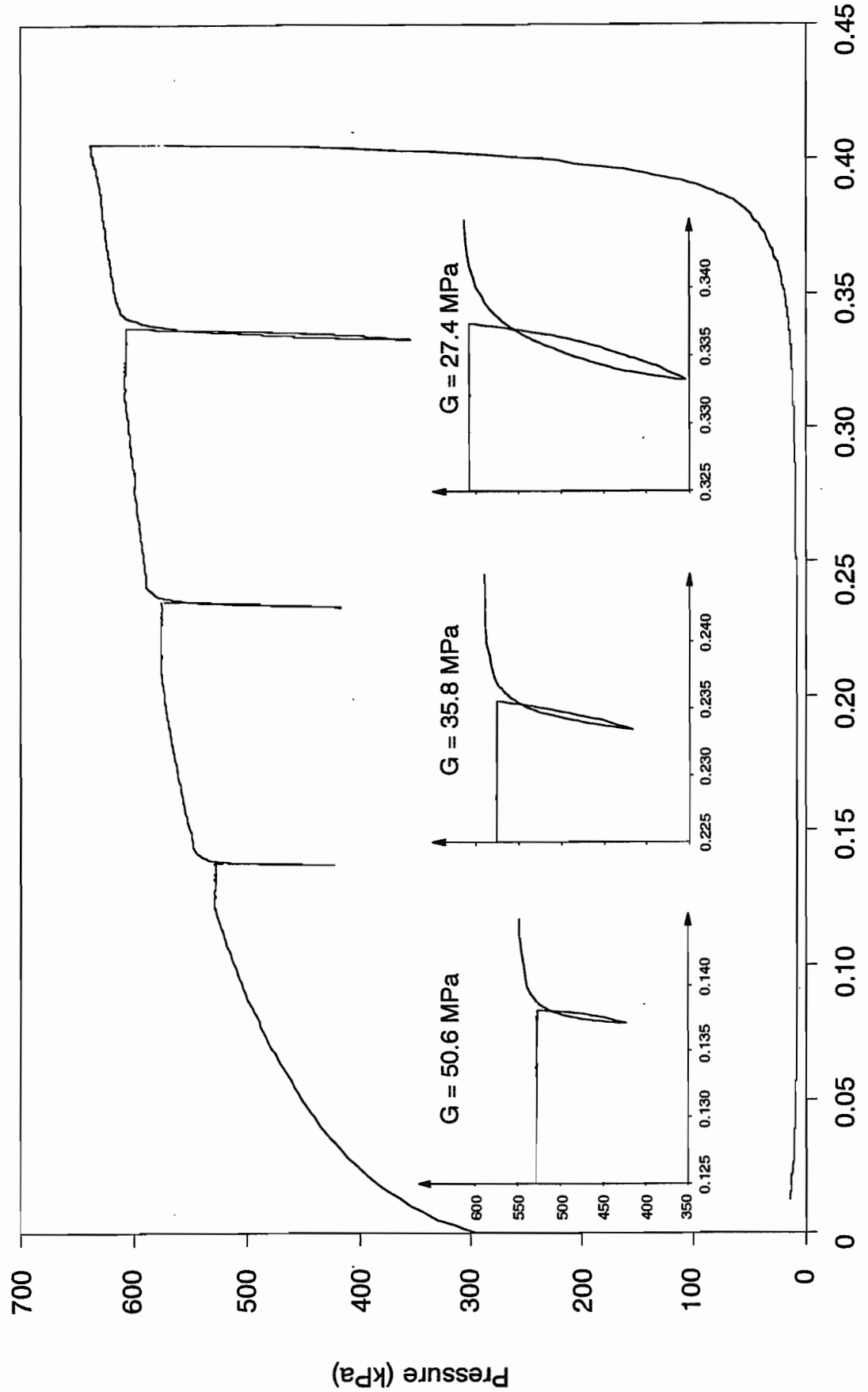

Figure 7.10 Unload-reload loops for test HS02

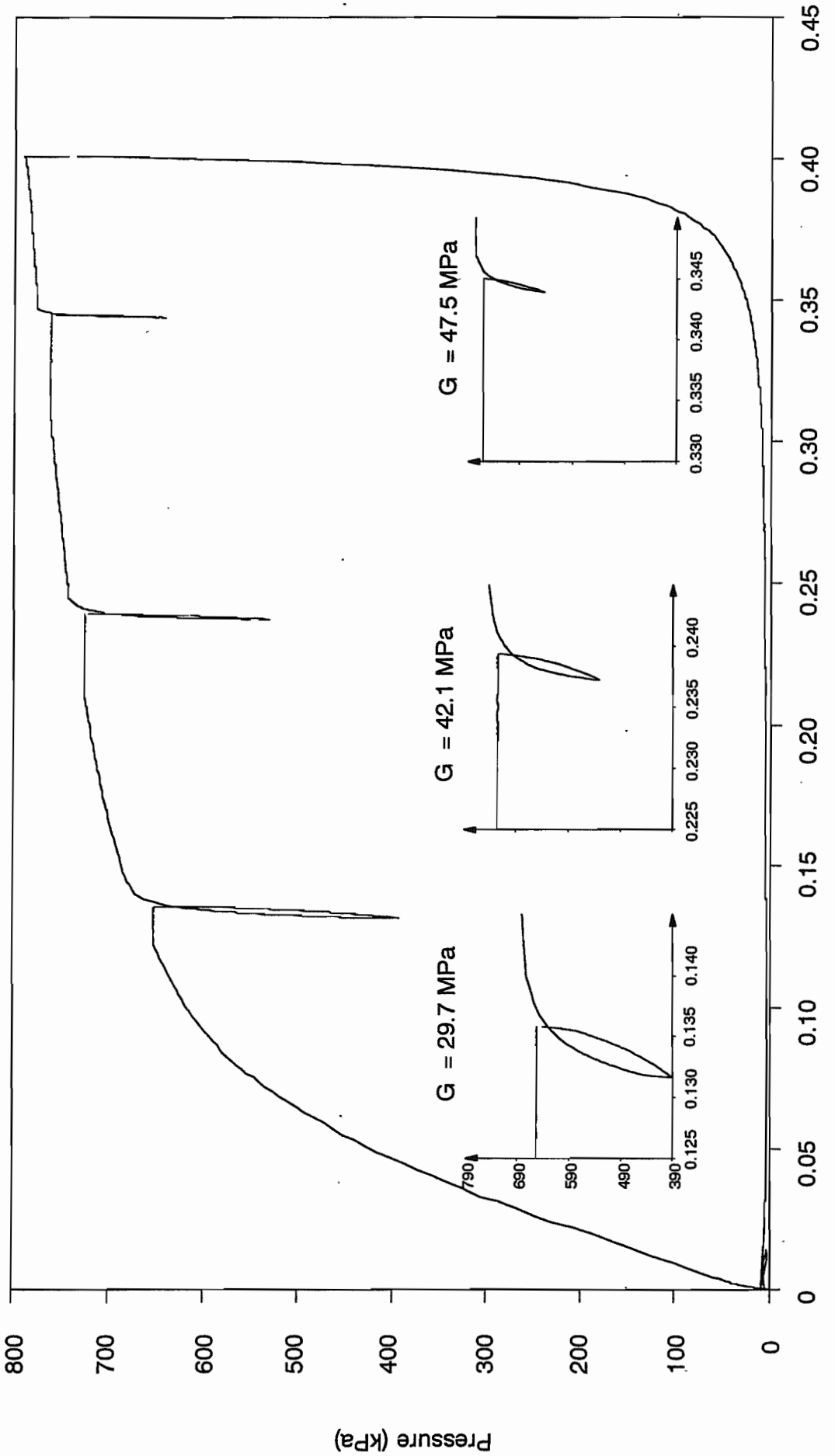

Figure 7.11 Unload-reload loops for test HS04

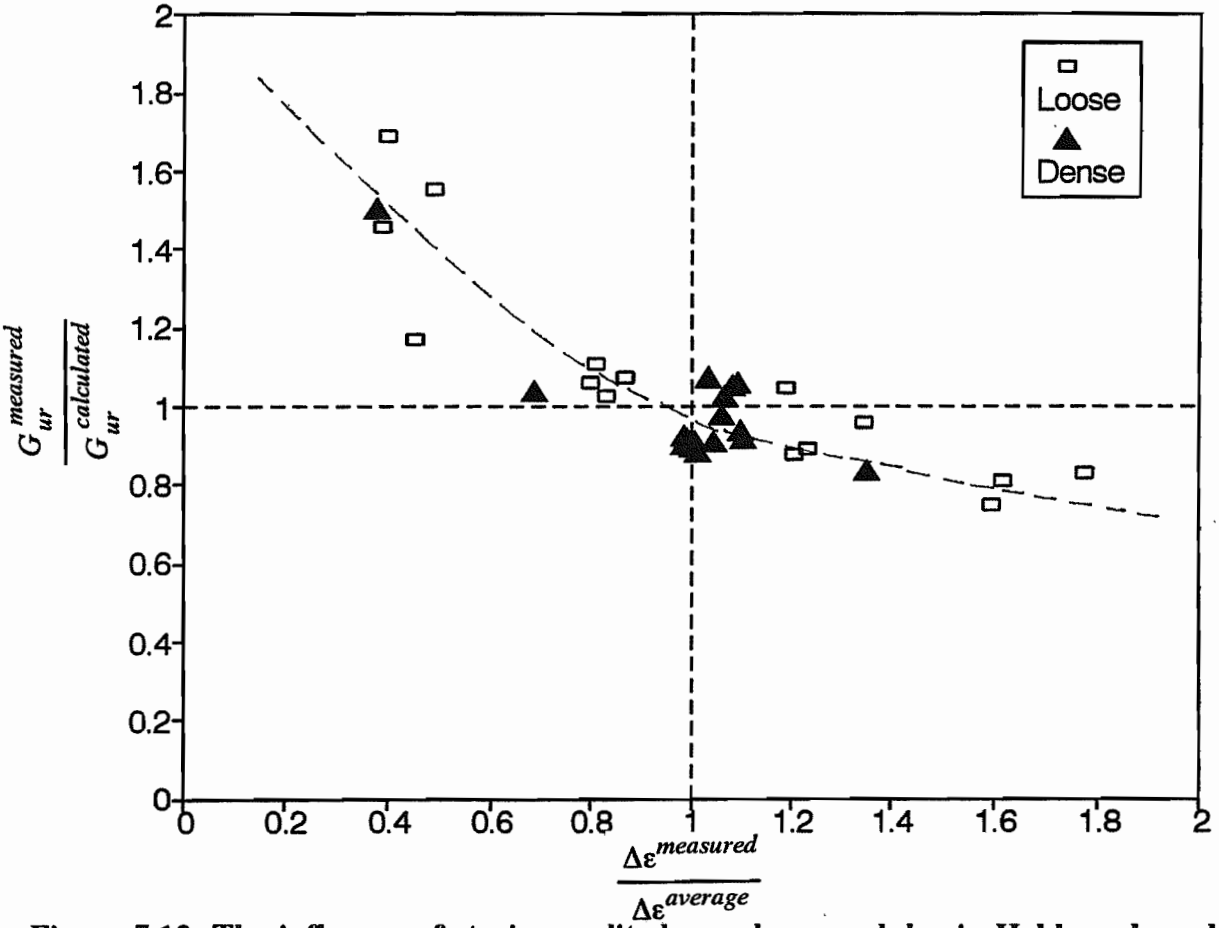

Figure 7.12 The influence of strain amplitude on shear modulus in Hokksund sand

7.5 Stiffness measurements in clay

7.5.1 Summary of results

A total of 12 cone pressuremeter tests were completed at Bothkennar, and during each test, three unload-reload loops were carried out. Estimates of shear modulus, corrected for pressuremeter compliance and geometry, are summarised in Table 7.3.

As an indication of the consistency of the methods of measuring shear modulus, values of G_{ch} have been plotted against values of G_{ls} in Figure 7.13. The two methods agree closely, with G_{ls} found to be lower than G_{ch} by a constant ratio of 0.86. Hence, it was only necessary to use G_{ch} values in the analysis of shear modulus.

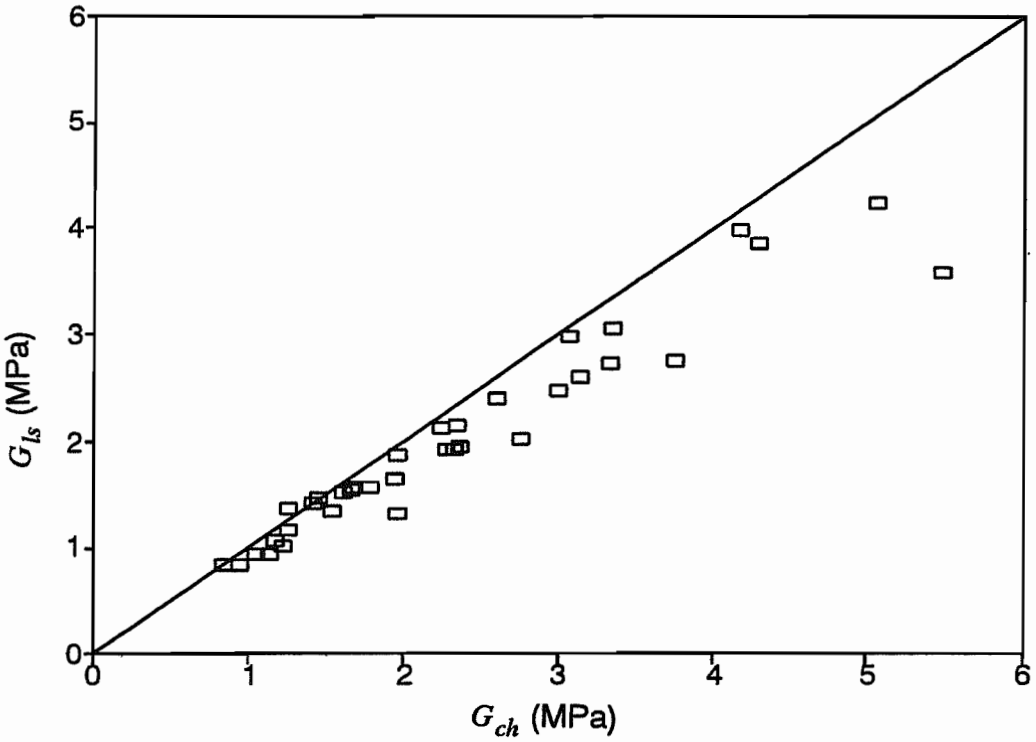

Figure 7.13 Comparison between least square and chord measurements of shear modulus made from CPM unload-reload loops at Bothkennar

Table 7.3 Unload-reload moduli at Bothkennar

Test	Depth (m)	p_0' (kPa)	Loop 1		Loop 2		Loop 3	
			G_{ur} (MPa)	Δε	G_{ur} (MPa)	Δε	G_{ur} (MPa)	Δε
B1T1	3	24.5	-	-	1.1	0.0102	0.9	0.0046
B2T1	4	28.3	1.3	0.0048	1.0	0.0104	0.8	0.0161
B3T1	5	33.4	1.7	0.0059	1.2	0.0093	1.2	0.0075
B1T2	6	37.5	2.1	0.0037	1.7	0.0090	1.1	0.0145
B2T2	7	42.5	2.1	0.0070	1.6	0.0091	1.2	0.0163
B3T3	8	47.5	1.6	0.0070	1.9	0.0078	1.5	0.0106
B1T3	9	51.3	2.5	0.0054	1.9	0.0061	1.4	0.0075
B2T3	10	55.8	3.0	0.0044	2.9	0.0036	2.3	0.0056
B1T4	12	65.7	4.1	0.0034	3.0	0.0053	2.3	0.0055
B2T4	13	71.4	2.7	0.0113	2.3	0.0188	1.6	0.0236
B1T5	15	80.9	4.9	0.0023	4.1	0.0023	3.3	0.0044
B2T5	16	86.1	5.3	0.0071	3.7	0.0103	3.3	0.0121

A summary of corrected shear moduli calculated from the unload-reload loops of CPM tests carried out at Madingley is presented in Table 7.4.

Table 7.4 Unload-reload moduli at Madingley

Test	Depth (m)	p_0' (kPa)	Loop 1		Loop 2	
			G_{ur} (MPa)	Δε	G_{ur} (MPa)	Δε
MG3	4.0	120	15.98	0.00633	11.55	0.00892
MG15	4.0	120	15.51	0.00617	11.56	0.01106
MG19	4.0	120	11.89	0.00519	9.79	0.00817
MG5	9.0	214	33.31	0.00392	27.10	0.00482
MG7	13.98	308	45.81	0.00394	40.16	0.00408
MG17	14.48	318	40.14	0.00653	34.02	0.00833
MG9	18.0	384	35.25	0.00522	30.41	0.00563

7.5.2 G_{ur} and G_{cc}

The analysis of Houlsby and Withers (1988) resulted in estimates of shear modulus made from the pressuremeter unloading curve, G_{cc} as discussed in Chapter 6. Because G_{cc} is not associated directly with a strain amplitude, it has been related to G_{ur} by the ratio G_{ur} / G_{cc} as shown in Figure 7.14 for tests at Bothkennar and Madingley. The figure shows scatter because of the variation of stress level between unload-reload loops within a pressuremeter test, and to a lesser extent, some instrument error. From the figure it is evident that the ratio G_{ur} / G_{cc} reaches unity at a strain amplitudes of around 0.006 both for tests in soft clay and for tests in stiff clay. Further CPM tests are required in clays of various degrees of overconsolidation to understand whether a single strain amplitude can indeed be used for interpreting stiffness values from unloading data.

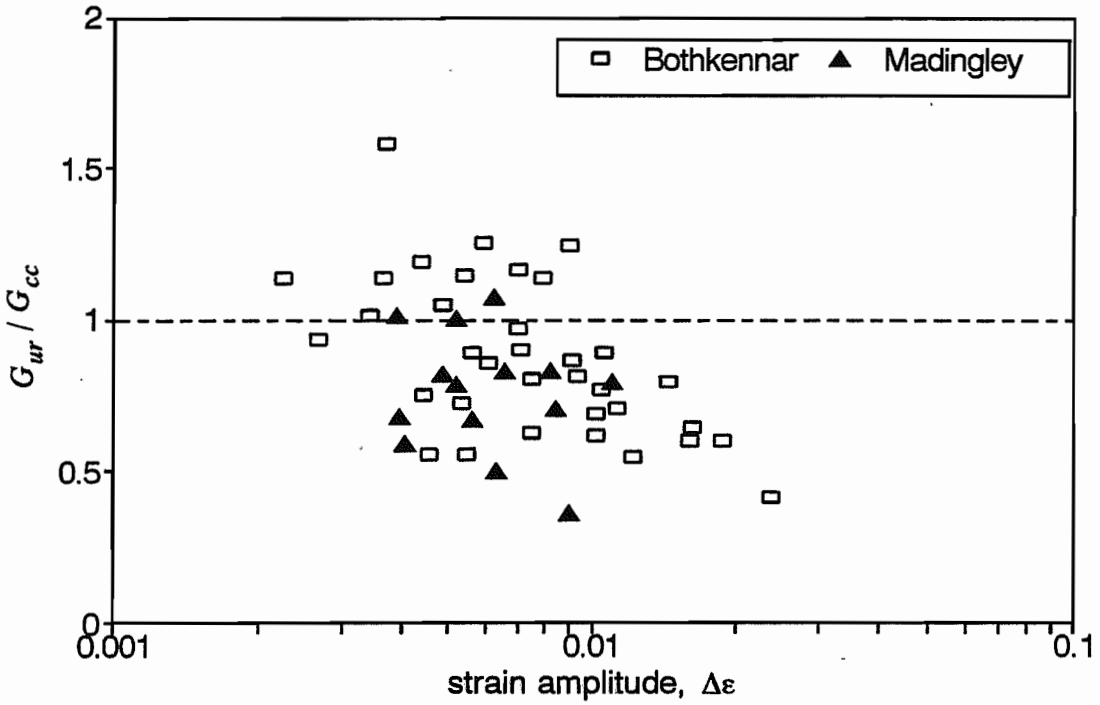

Figure 7.14 Relationship between G_{ur} and G_{cc} for tests at Bothkennar and Madingley

7.5.3 Comparisons with other field tests

A comparison between G_{ur} determined by the cone pressuremeter and the self-boring pressuremeter is shown in Figure 7.15 for tests at Bothkennar. Shear moduli have been normalised by the *in situ* mean effective stress, p_0'. Nash *et al.* (1992) report that all the SBPM unload-reload loops were carried out with a strain amplitude of 0.34%, and hence the results appear in the figure as upper and lower limits. The figure shows that G_{ur} values measured from the CPM are lower than G_{ur} values measured from the SBPM. The difference may be due to the initial soil disturbance caused by CPM insertion. Evidence for this is provided by G_{ur} values in Table 7.3 that systematically decrease from loop 1 to loop 3.

The trend of decreasing shear modulus with increasing strain amplitude is also evident in the Figure 7.15. When the moduli measured from the seismic cone are included as representative

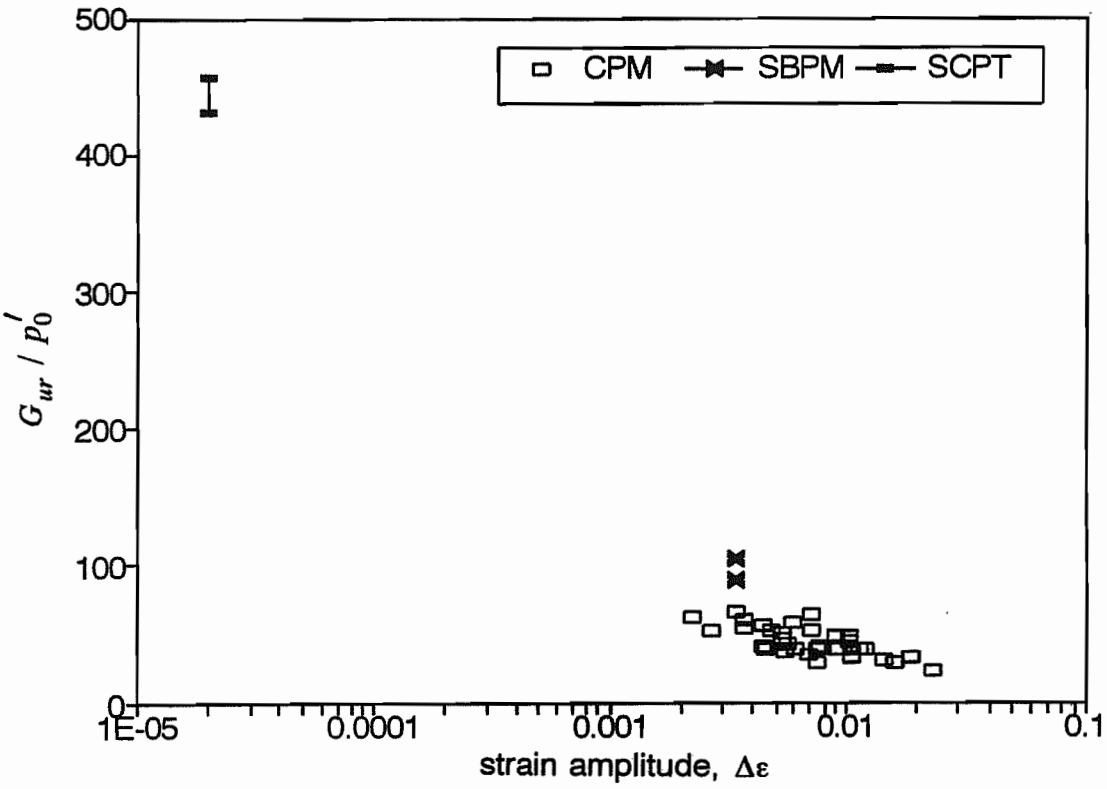

Figure 7.15 G_{ur} determined from field tests at Bothkennar

of a very small strain amplitude (equivalent to $\Delta\varepsilon$ less than $2.5\text{x}10^{-5}$), the variation of modulus with strain amplitude is similar to that reported by Georgiannou *et al.* (1991). This variation will be explored further in the following section.

Values of G_{cc} obtained from the tests at Madingley were shown to compare well with values of G_{ur} from SBPM tests by Houlsby and Withers (1988). Since the variation of G_{cc} with G_{ur} from the CPM is shown in Figure 7.14, a comparison between G_{ur} from the SBPM and G_{ur} from the CPM is therefore similar.

7.5.4 Methods of interpretation

The design of geotechnical structures in clays usually depends upon soil parameters determined in the laboratory from good quality undisturbed samples. As discussed in section 7.1, the stress-strain behaviour of most soils is non-linear, usually from very small strains.

Moduli determined from pressuremeter tests need to be related to G_0 values that remain constant below a threshold strain. In sands, resonant column tests or *in situ* seismic tests can provide estimates of G_0 (Bellotti *et al.*, 1989). In clays, it is more important to relate pressuremeter moduli to small strain moduli determined from triaxial tests.

Undrained triaxial compression tests can be used to obtain either a tangential shear modulus, G_t where

$$3G_t = \frac{dq}{d\varepsilon} \qquad ...(7.11)$$

or a varying secant modulus, G_s defined as

$$3G_s = \frac{\Delta q}{\varepsilon_s} \qquad ...(7.12)$$

where q is a deviator stress $(\sigma_a - \sigma_r)$ and ε_s is triaxial shear strain, $2(\varepsilon_a - \varepsilon_r)/3$. Wood (1990) shows that the pressuremeter modulus, G_{ur} can be related to G_s by the equation

$$G_s = G_{ur} + \Delta\varepsilon_c \frac{dG_{ur}}{d\varepsilon_c} \qquad ...(7.13)$$

where ε_c is the strain amplitude of a pressuremeter unload-reload loop, related to ε_s by

$$\Delta\varepsilon_c = \frac{\sqrt{3}\varepsilon_s}{2} \qquad ...(7.14)$$

Jardine (1991) suggests that equations (7.13) and (7.14) can be applied in one of three ways:

(1) differentiating the $G_{ur} : \Delta\varepsilon_c$ data numerically

(2) differentiating an expression which best fits the $G_{ur} : \Delta\varepsilon_c$ data

(3) relating G_{ur} : $\Delta\varepsilon_c$ data to G_s :ε_s by an empirical relationship which could be applied to a wide range of soil types

Applying the first approach to the tests at Bothkennar would be impractical because all loops were carried out within a small range of strain amplitudes. Numerical differentiation of the G_{ur} : $\Delta\varepsilon_c$ curve would, therefore, result in significant scatter, making it difficult to resolve stiffness at small incremental strains.

The second approach requires a curve fitted to the G_{ur} : $\Delta\varepsilon_c$ data, and has been used by Huang *et al.* (1991), Wood (1990) and others. Wood (1990) shows how this approach can be applied using an expression first proposed by Jardine *et al.* (1986) given by

$$G_s = A + B \cos\left\{\alpha\left[\log_{10}\left(\frac{\varepsilon}{C}\right)\right]^{\gamma}\right\} \qquad ...(7.15)$$

where γ is taken as unity for simplification, A and B are parameters which control the magnitude of the moduli, C is an elastic threshold strain, and α is a parameter which controls the rate of degradation of stiffness with strain. Here, too there is a difficulty in adopting this approach with the data available from the tests at Bothkennar, because of the small range of strain amplitudes from which to generate the parameters A, B, C and α.

The simplest way to prepare pressuremeter test data for comparisons with other types of stiffness measurement is to use the third approach which requires a simple transformation of the pressuremeter strain amplitude as proposed by Jardine (1991, 1992).

It is shown that the relationship between the G_{ur} : $\Delta\varepsilon_c$ and G_s : ε_s functions depends only on their shape. Above an elastic threshold strain, this behaviour is illustrated in Figure 7.16. Purely linear elastic behaviour represents an upper bound, zero tangent stiffness at an extremely small strain represents a lower bound, and clays with different OCR values show different degrees of curvature within these limits.

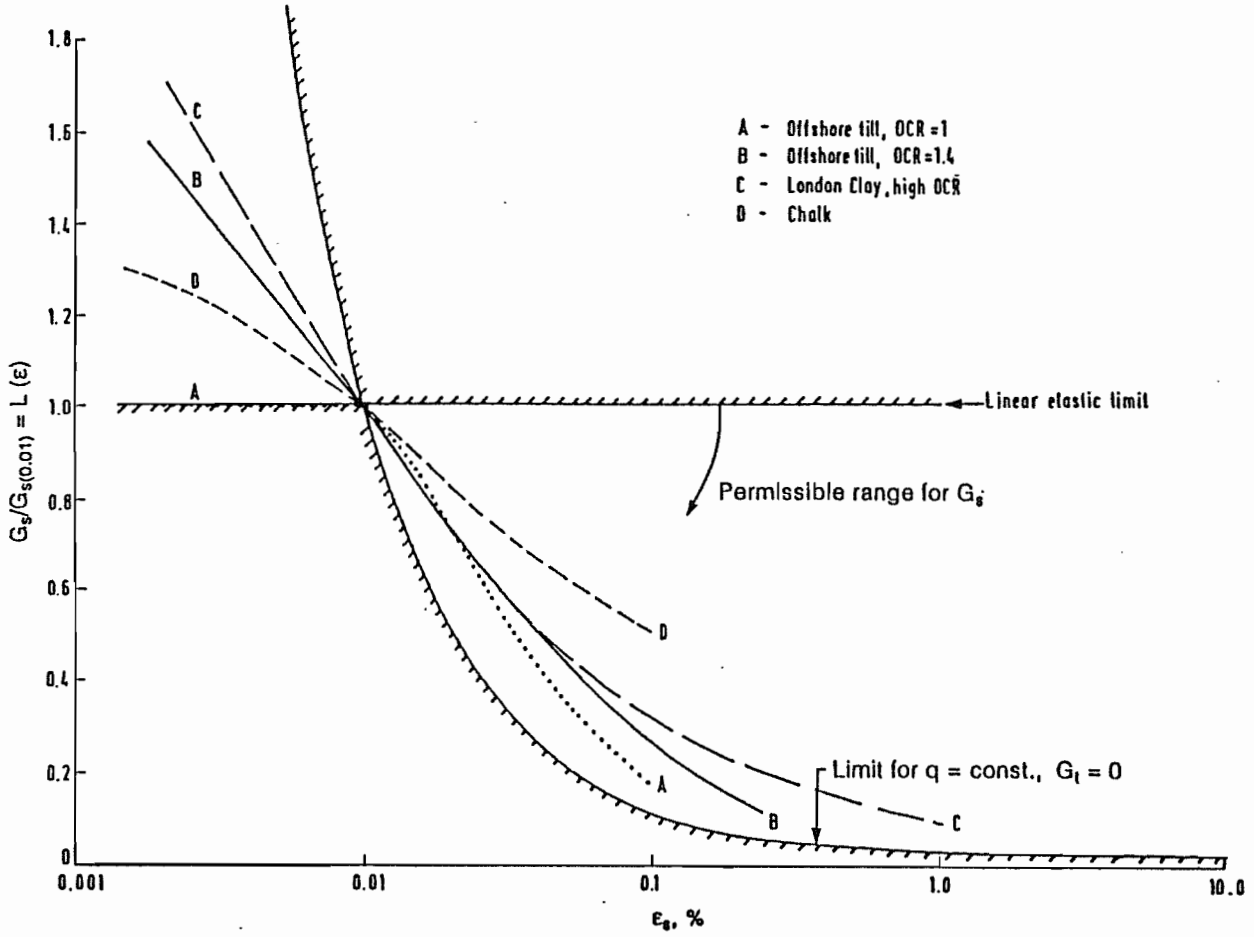

Figure 7.16 Possible forms of the normalised G_s-ε_s function (after Jardine, 1992)

Jardine presents pressuremeter data from two sites in very different clays (a normally consolidated offshore till and heavily overconsolidated London clay), and identifies the values of $\Delta\varepsilon_c$ at which G_{ur} and G_s are equal. An empirical relationship between ε_s and $\Delta\varepsilon_c$ is given by

$$\varepsilon_s = \frac{\Delta\varepsilon_c}{\left[1.2 + 0.8\log_{10}\left(\frac{\Delta\varepsilon_c}{10^{-5}}\right)\right]} \quad ...(7.16)$$

to give a strain amplitude, ε_s at which one would have G_s equal to the value of G_{ur} measured

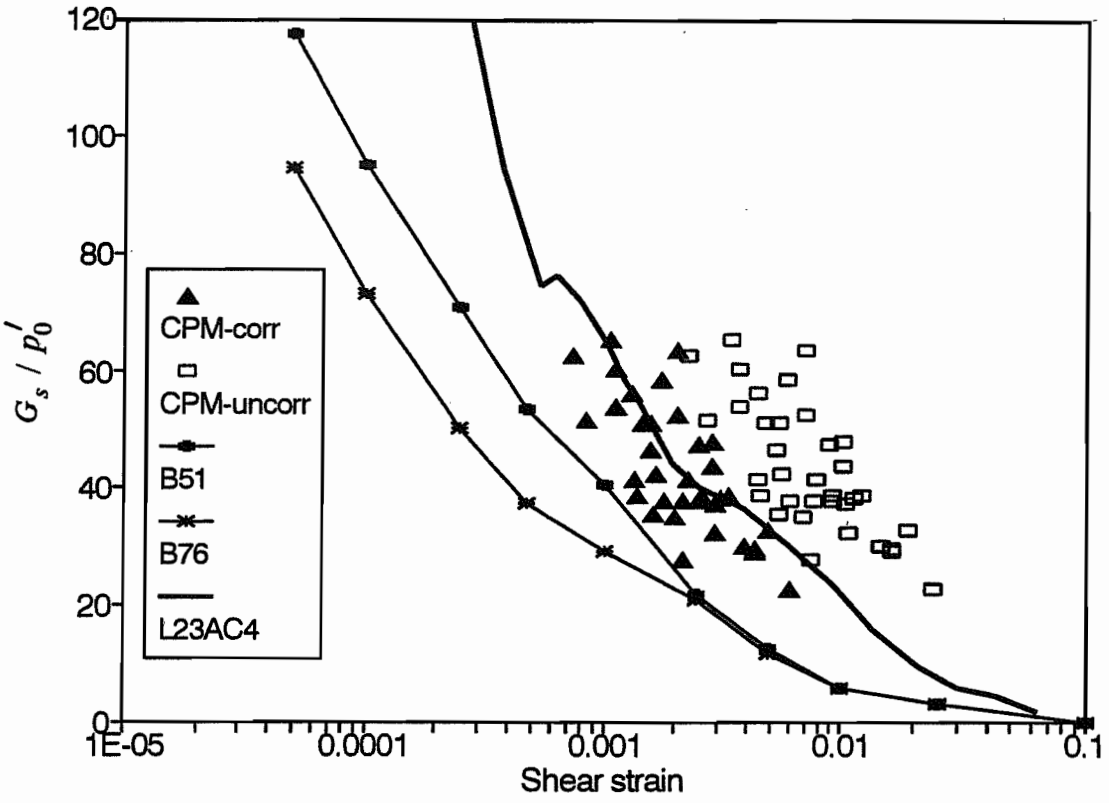

Figure 7.17 Shear moduli with transformed strain amplitudes from CPM tests at Bothkennar

the tests at Bothkennar. Secant stiffness of reconstituted Bothkennar clay has been reported by Allman and Atkinson (1992) in a set of K_0 consolidated, undrained triaxial tests, and undisturbed triaxial tests are reported by Atkinson *et al.* (1992). A comparison between the reported data and the transformed CPM data is presented in Figure 7.17. Tests B76 and B51 were carried out by Allman and Atkinson (1992) on reconstituted samples at initial mean effective stresses of 50 and 100kPa respectively. Test L23AC4 was carried out by Atkinson *et al.* (1992) using an intact specimen obtained from a Laval sampler. The transformation proposed by Jardine (1991, 1992) results in approximately a threefold change in the plotted

strain amplitudes as shown in the figure. In broad terms, without using such a correction, secant shear moduli could be overpredicted. With the correction applied, however, G_{ur} from cone pressuremeter tests can be brought to close agreement with G_s.

7.6 Conclusions

The stress-strain behaviour of most soils is highly non-linear from very small strains, so that soil stiffness, measured in terms of a shear modulus, G, is dependent upon both the stress level and strain amplitude over which the measurement was made.

Interpretation of shear modulus from CPM unload-reload loops can be made from the gradients of either a least squares or a chord fit to the data, and it has been shown that the latter estimates are consistently higher than the former in both sands and clays. Corrections for instrument compliance are increasingly important in the stiffer soils.

For tests in sand, a relationship first proposed by Janbu (1963) has been used to show the influence of stress level on estimates of shear modulus. Unlike the response of silica sands, tests in Dogs Bay sand have revealed that such a relationship is independent of the relative density. Shear modulus was shown to decrease significantly with an increase in the strain amplitude over which the modulus was calculated, and a relationship proposed by Wroth *et al.* (1979) was shown to quantify successfully this variation in Dogs Bay sand. Further tests in Hokksund sand were carried out to isolate this behaviour from the variations in stress level.

Shear moduli measured from unload-reload loops in soft and stiff clay were compared with moduli, G_{cc}, calculated from the unloading portion of the pressure-strain curve. It is suggested that a single strain amplitude could be attributed to G_{cc}. The variation of modulus with strain amplitude has also been studied in clay, and an empirical transformation proposed by Jardine (1991, 1992) has been successfully applied to cone pressuremeter data from Bothkennar. The transformation relates unload-reload moduli from CPM tests to secant moduli from laboratory tests, and without such a correction, field estimates of shear modulus could be overpredicted.

CHAPTER 8

NUMERICAL ANALYSIS

8.1 Introduction

The experimental work presented in this thesis has brought to light some of the inaccuracies involved in applying closed form solutions to cone pressuremeter testing in sand. These solutions (*e.g.* Hughes *et al.*, 1977; Carter *et al.*, 1986; Yu and Houlsby, 1991) depend upon an important assumption: that the angles of internal friction, ϕ and dilation, ν are constant throughout the analysis. The consequences of this assumption are addressed in this chapter using finite element analyses and they are shown to explain, in part, some of the differences between observed and predicted cone pressuremeter behaviour.

Vesic and Clough (1968) showed from tests in granular soils at elevated pressures that particle crushing occurs, thereby reducing the observed maximum angles of friction and dilation for a given initial density. This phenomenon is of particular relevance to tests in carbonate sand, because particle crushing begins at lower stresses than in silica sands, as discussed in Chapter 4. A one-dimensional finite element program reported by Yu (1990) has been used as the basis for a model presented in this chapter. In the models, variable friction and dilation angles have been allowed to vary, and particle crushing has been incorporated into the cavity expansion calculation. The model is successful in showing that particle crushing has an influence on results of cone pressuremeter tests in carbonate sand.

8.2 Cavity expansion by finite element analysis

The principles of finite element analysis are well covered in standard texts, for example

Zienkiewicz (1986). As an introduction to the work presented in this chapter, however, it is necessary to discuss the nature of the solution scheme used in the one-dimensional FORTRAN program, CAVEXP, reported by Yu (1990). The structure of the program has not been changed, but a number of subroutines have been added which allow calculations to be made with variable friction and dilation angles, and particle crushing.

The soil continuum is treated as axisymetric and can be represented by a number of two-noded linear elements, and a finite outer boundary. An infinite medium is modelled using an outer infinite spring element. Expansion of a cavity occurs in increments from a finite internal radius and approximates non-linear soil behaviour using a modified Euler solution scheme as described by Burd (1986) and shown in Figure 8.1. At the start of the *i*th load step, a global stiffness matrix is calculated comprising the individual element stiffnesses. This matrix is used to solve a set of incremental nodal displacements, $\Delta\delta_i$. The stresses, $\Delta\sigma$ which occur at points within each element (Gauss points) due to nodal displacements, $\Delta\delta_i$ are then determined. The work done by these stresses is used to calculate an equivalent set of incremental forces acting at the element nodes, ΔF_i. The total forces, P_i are then determined and a correction is made to ensure that equilibrium is maintained.

During an infinitesmal increment of stress, changes of strain are assumed to be divisible into elastic and plastic parts so that

$$d\underline{\varepsilon} = d\underline{\varepsilon}^e + d\underline{\varepsilon}^p \qquad ...(8.1)$$

The vector of elastic strain increments, $d\underline{\varepsilon}^e$ is related to stress increments by a symmetric matrix of constants, $\boldsymbol{D}_e$. Plastic strain increments, $d\underline{\varepsilon}^p$ occur when the stresses satisify a general yield criterion of the form

$$f(\underline{\sigma}) = 0 \qquad ...(8.2)$$

From the normality rule of plasticity theory, originally developed for metals, the plastic strain

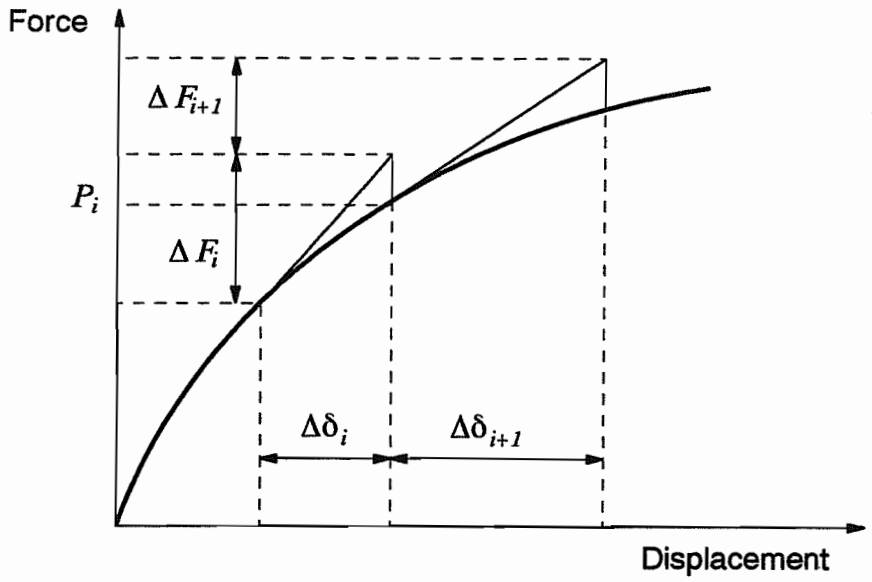

Figure 8.1 The modified Euler solution scheme

increments are in a direction normal to the yield surface defined by f so that

$$d\underline{\varepsilon}^p = \frac{\partial f}{\partial \underline{\sigma}} \qquad ...(8.3)$$

More realistic of granular soil behaviour, however, is the use of a separate function $g(\underline{\sigma})$, the plastic potential, to describe incremental plastic strain where

$$d\underline{\varepsilon}^p = \frac{\partial g}{\partial \underline{\sigma}} \qquad ...(8.4)$$

The particular case of $g = f$ is termed associated plasticity, otherwise the plastic flow is referred to as non-associated.

The stress changes can then be related to the imposed strain changes by an elastic-plastic stiffness matrix, $\boldsymbol{D}_{ep}$ which incorporates the additional terms due to plasticity, where

$$\boldsymbol{D}_{ep} = \boldsymbol{D}_e - \frac{\boldsymbol{D}_e \left[\frac{\partial g}{\partial \underline{\sigma}}\right] \left[\frac{\partial f}{\partial \underline{\sigma}}\right]^T \boldsymbol{D}_e}{\left[\frac{\partial f}{\partial \underline{\sigma}}\right]^T \boldsymbol{D}_e \left[\frac{\partial g}{\partial \underline{\sigma}}\right]} \qquad ...(8.5)$$

This approach has been used in developing a subroutine for CAVEXP which updates the stresses for each element using $\boldsymbol{D}_{ep}$ with sub-increments of strain. The models that had previously been implemented in CAVEXP used specific forms of the global stiffness matrix.

$\boldsymbol{D}_{ep}$ is calculated from one of several soil models. Within each soil model, a yield function, f is defined. The vector $\partial f/\partial \underline{\sigma}$ is calculated, and depending on the degree of association, the direction of the plastic strain increment is determined using equation (8.4).

Results from *in situ* tests are commonly expressed in terms of the stress parameters q and p where q is the deviator stress $(\sigma_1-\sigma_3)/2$ and p is the mean normal stress $(\sigma_1+\sigma_2+\sigma_3)/3$. Two basic models, one for clay and one for sand have been included to show that the finite element calculation is capable of determining the pressure-expansion curves and limit pressures of a pressuremeter test as predicted by large strain closed form solutions. The sand model has been developed further to incorporate variable friction and dilation angles which decrease to limiting values as the confining pressure, p' increases. To model particle crushing, the function defining the yield surface has been bounded by a normal stress, p_c' at which isotropic (*i.e.* $q = 0$) crushing occurs. A summary of the four soil models is given in Table 8.1.

Table 8.1 Numerical soil models

Model	Yield function	Application	Description of yield surface
12	von Mises	clay	f = constant, $g = f$
13	Matsuoka	sand	f increases linearly with p'
14	Matsuoka	sand	f increases non-linearly with p'
15	Matsouka	carbonate sand	f increases non-linearly with p' up to p_c'

8.3 Yield surfaces

8.3.1 von Mises yield surface (Model 12)

The von Mises yield surface was chosen rather than the Tresca yield surface to model clay behaviour, because the latter contains singularities where the function describing the surface is not differentiable without additional assumptions. Both these surfaces are represented in Figure 8.2 in the octahedral plane, where the Tresca model appears as a hexagon and the von Mises model as a circle.

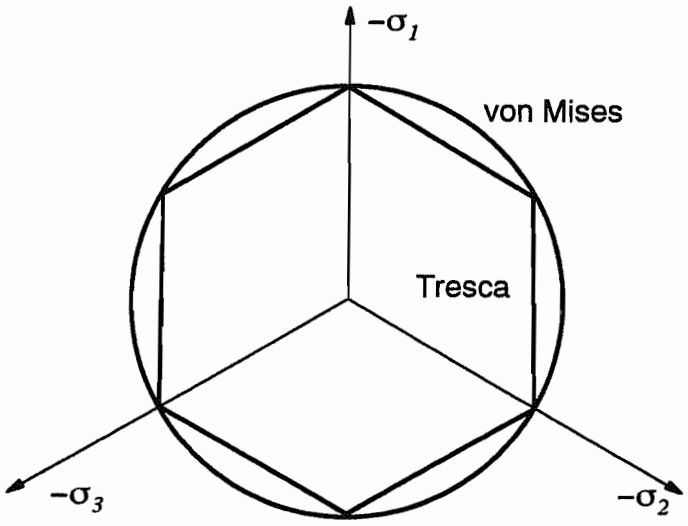

Figure 8.2 Yield surfaces for undrained behaviour

The von Mises yield surface can be expressed in terms of a function of the form

$$f = (\sigma_1-\sigma_2)^2 + (\sigma_2-\sigma_3)^2 + (\sigma_3-\sigma_1)^2 - 8s_u^2 \qquad ...(8.6)$$

where s_u is the triaxial undrained shear strength. The normals to the surface are then given by

$$\frac{\partial f}{\partial \sigma_1} = 2\,(2\sigma_1-\sigma_2-\sigma_3) \qquad ...(8.7)$$

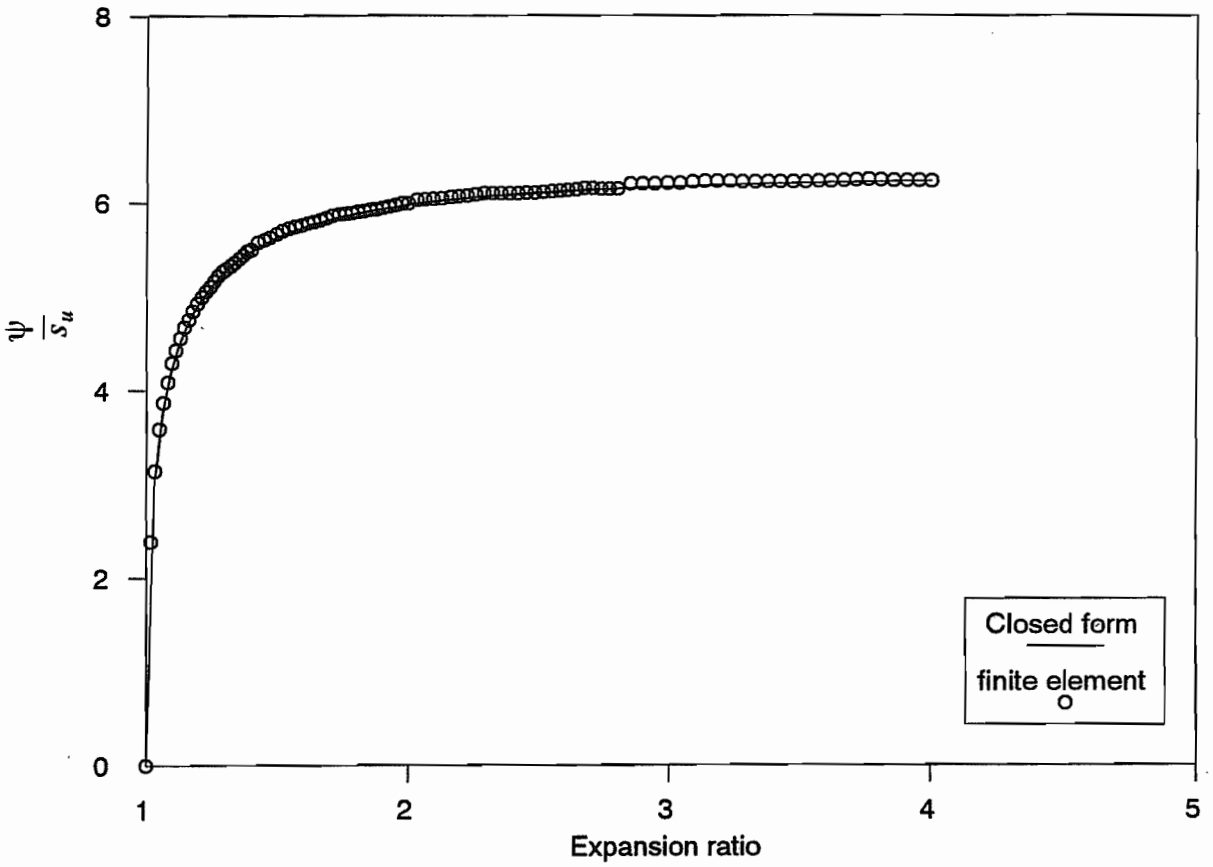

Figure 8.3 Pressure-expansion curve for Model 12 and the closed form solution of Sagaseta (1984)

and similarly for $\frac{\partial f}{\partial \sigma_2}$ and $\frac{\partial f}{\partial \sigma_3}$.

Because undrained soil behaviour is being described, the soil continuum does not experience volume change, and hence a fully associated flow rule can be applied so that

$$\frac{\partial g}{\partial \underline{\sigma}} = \frac{\partial f}{\partial \underline{\sigma}} \qquad ...(8.8)$$

The model was checked against the large strain cavity expansion solution of Sagaseta (1984) which was discussed in Chapter 1, and a comparison of the pressure-expansion curves is presented in Figure 8.3. Incompressible material behaviour was approximated by using a Poisson's ratio, υ of 0.49. An undrained triaxial shear strength of 200kPa and an elastic shear

modulus of $100s_u$, *i.e.* 20MPa were used, and an expansion ratio of 4 was given to the cavity. There is clearly a good agreement between Model 12 and the closed form solution.

8.3.2 Matsuoka yield surface (Model 13)

In a similar way to the clay model described in the previous section, it is more convenient to use a yield function for sand which is differentiable for all combinations of principal stresses, and so the Matsuoka surface has been chosen in preference to the Mohr-Coulomb surface which contains singularities at the corners. Both surfaces are shown in the octahedral plane in Figure 8.4.

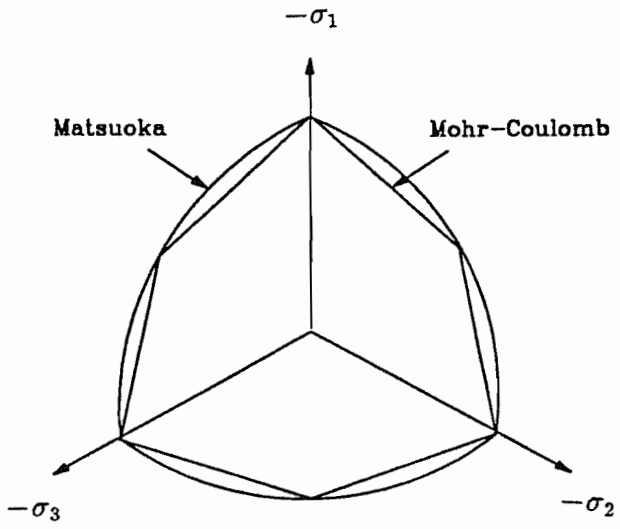

Figure 8.4 Yield surfaces used for drained behaviour

In terms of principal stresses, the Matsuoka yield surface can be defined by the function

$$f = \frac{(\sigma_1'-\sigma_3')^2}{\sigma_1'\sigma_3'} + \frac{(\sigma_2'-\sigma_3')^2}{\sigma_2'\sigma_3'} + \frac{(\sigma_3'-\sigma_1')^2}{\sigma_3'\sigma_1'} - 8\tan^2\phi_{tc} \qquad ...(8.9)$$

where ϕ_{tc} is the triaxial compression friction angle. In terms of the stress invariants

$$f = I_1I_2 - I_3\varsigma \qquad ...(8.10)$$

where $$I_1 = \sigma_1' + \sigma_2' + \sigma_3' \quad ...(8.11)$$

$$I_2 = \sigma_1'\sigma_2' + \sigma_2'\sigma_3' + \sigma_3'\sigma_1' \quad ...(8.12)$$

$$I_3 = \sigma_1'\sigma_2'\sigma_3' \quad ...(8.13)$$

$$\varsigma = 9 + 8\tan^2\phi_{tc} \quad ...(8.14)$$

The normal to this surface is then given by

$$\frac{\partial f}{\partial \sigma_1'} = 2\sigma_1'(\sigma_2'+\sigma_3') + \sigma_2'^2 + \sigma_3'^2 - \sigma_2'\sigma_3'(6+8\tan^2\phi_{tc}) \quad ...(8.15)$$

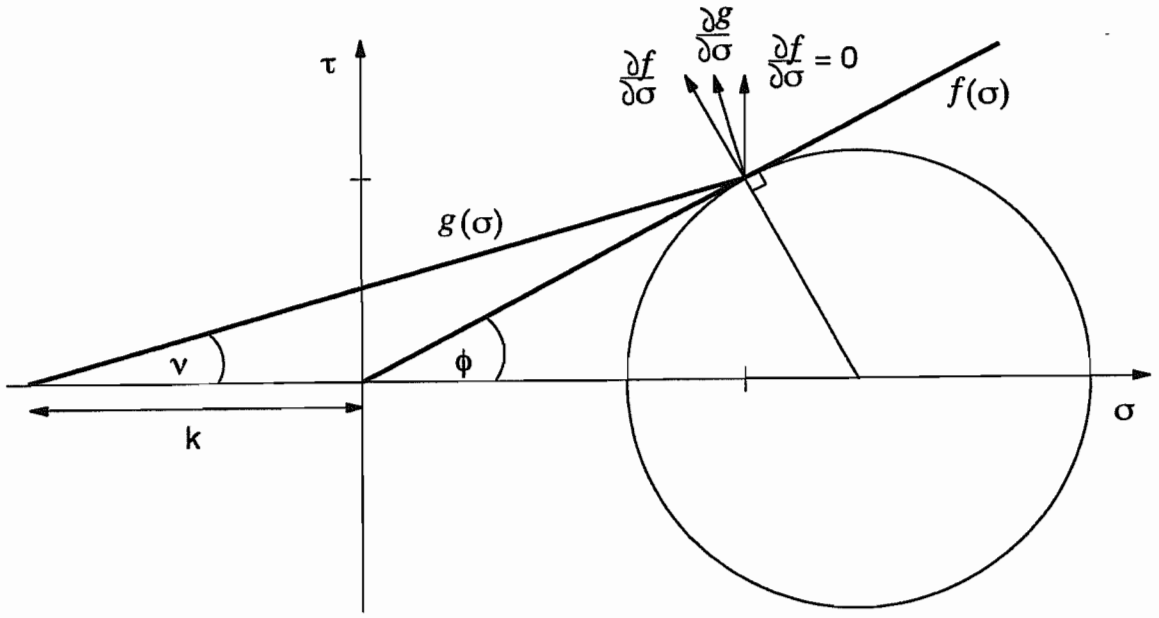

Figure 8.5 Plastic potential calculated from dilation angle and the yield function

When a dilation angle, ν is specified, the plastic potential, g can be calculated from the yield function, f. This can be done using one of two approaches, and is discussed here with the aid of Figure 8.5. In the figure, the yield function, f is shown in $\tau : \sigma$ space where τ is shear stress, with a constant friction angle, ϕ. Full association occurs when the plastic strain increment, $\partial g/\partial \underline{\sigma}$ coincides with the normal to the surface f for a particular stress level. Zero association, which results in zero volume change, occurs when the plastic strain increment is

vertical. In the first approach, as proposed by Burd (1986), the plastic strain increment can be calculated from a linear interpolation between full and zero association. In the second approach, adopted by Yu (1990), an assumption is made that the plastic potential function, g is similar to the yield function, f but ϕ_{tc} is replaced by ν_{tc}. Since f and g must intersect at the current stress state, the apex of the surface g is shifted from the origin a distance $-k$ so that

$$g(\underline{\sigma}^*) = I_1^* I_2^* - I_3^* \varsigma^* \qquad ...(8.16)$$

where

$$\underline{\sigma}^* = \underline{\sigma} + k\boldsymbol{I} \qquad ...(8.17)$$

$$\varsigma^* = 9 + 8\tan^2\nu \qquad ...(8.18)$$

and $\boldsymbol{I}$ is the unit vector. This condition is used to derive a cubic equation in terms of the principal stresses from which k can be solved.

The friction angle, ϕ and dilation angle, ν remain constant throughout the analysis, and hence the yield surface continues to expand indefinitely with increasing mean effective stress.

The pressure-expansion curve for a typical run using Model 13 is presented in Figure 8.6. Using a Poisson's ratio, υ of 0.2, an initial isotropic stress, p_0 of 100kPa and a stiffness, G of 10MPa, a cylindrical cavity was expanded by a ratio of 4. The triaxial friction and dilation angles used in the finite element runs were $\phi_{tc} = 35.83°$ and $\nu_{tc} = 6.16°$, which correspond to plane strain angles of $\phi_{ps} = 40.0°$ and $\nu_{ps} = 7.1°$ (Yu, 1990). For comparison, the Yu and Houlsby (1991) closed form solution has been plotted in the figure as a solid line, and the two solutions clearly agree well.

8.4 Variable friction and dilation angles (Model 14)

It is unrealistic to assume that peak friction angle remains constant in sand at increasingly high normal stresses, or that volumetric strains continue indefinitely. Barden *et al.* (1969)

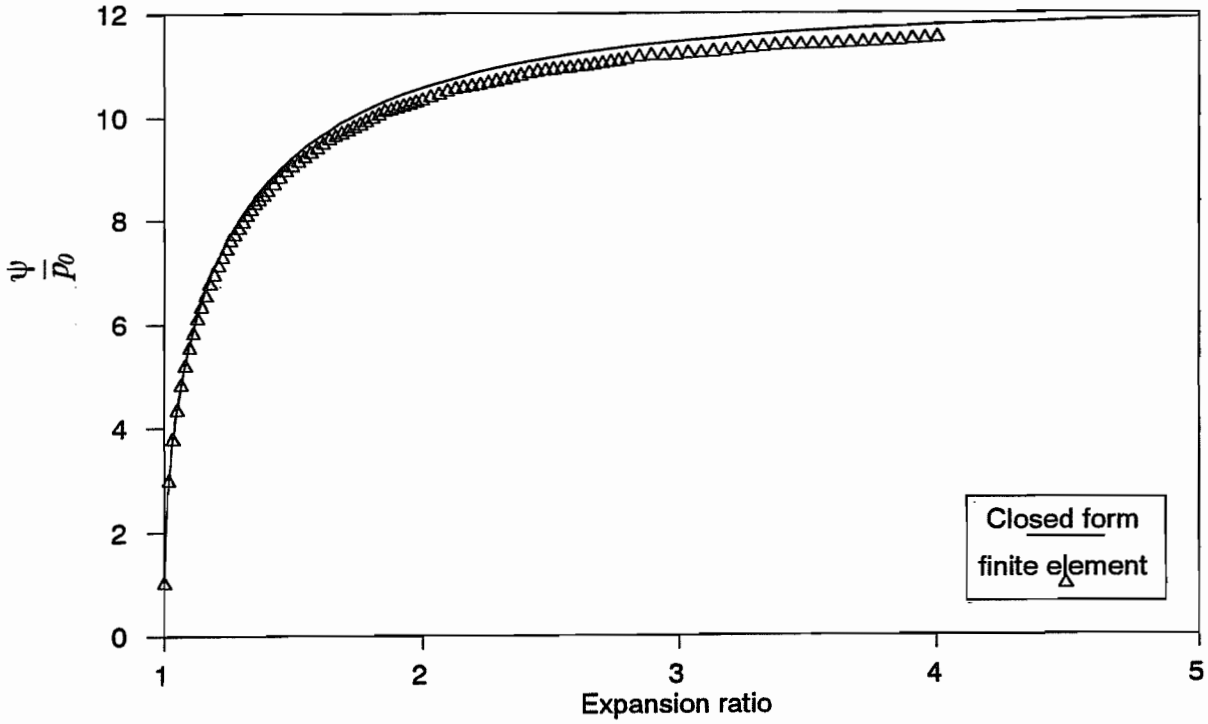

Figure 8.6 Pressure-expansion curve for Model 13

showed from drained, plane strain compression tests on sand at the same density that the peak stress ratio at failure and the angle of dilation were significantly affected by the confining stress. From low stress level tests in the Simple Shear Apparatus, Stroud (1971) showed that the peak stress ratio at failure and the angle of dilation were significantly affected by the relative density. The influence of both of these parameters has been quantified empirically by Bolton (1986) with correlations made from data obtained from 17 silica based sands. Bolton's correlation is given by equation (4.1) but is repeated here for clarity as

$$\phi_p - \phi_{cv} = 3I_R \qquad ...(8.19)$$

where ϕ_p and ϕ_{cv} are the triaxial peak and constant volume triaxial friction angles respectively, and I_R is a relative dilatancy index defined by

$$I_R = D_r (Q - \log_e p') - 1 \qquad ...(8.20)$$

This correlation was found by Bolton (1986) to be applicable within the range $0 < I_R < 4$. The parameter, Q is a measure of how rapidly the friction angle drops to a critical value. The relationship between ϕ_p and the maximum dilation angle, ν_{max} was given as

$$\phi_p - \phi_{cv} = 0.8\nu_{max} \qquad ...(8.21)$$

Bolton showed that equation (8.21) agrees well with the stress-dilatancy relationship of Rowe (1962).

Equations (8.19) to (8.21) have been used with Matsuoka's yield function as defined previously to model a more realistic yield surface as shown in Figure 8.7. The failure surface remains unbounded, and with any increases beyond a critical pressure, the friction angle remains constant at ϕ_{cv} and the dilation is zero.

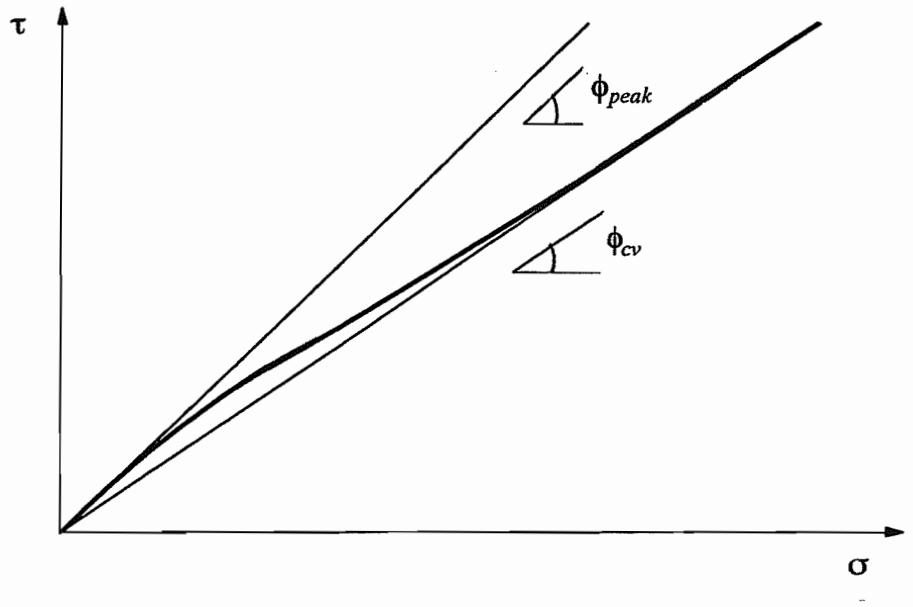

Figure 8.7 Curved failure envelope in shear stress : normal stress space

Variations in ϕ and ν are accounted for in Model 14 by specifying ϕ_{cv}, Q and initial D_r where D_r is continually updated during the calculation. An additional term is also necessary in determining the normal to the failure surface, $\partial f/\partial\sigma$ given in equation (8.15), because of the dependency of ϕ on σ. This term is given by

$$\frac{\partial f}{\partial \phi}.\frac{\partial \phi}{\partial p'}.\frac{\partial p'}{\partial \underline{\sigma}} = \frac{I_3 16\tan\phi}{\cos^2\phi}.\frac{-3D_r}{p'}.\frac{1}{3} \qquad ...(8.22a)$$

$$= \frac{48 I_3 D_r \tan\phi}{I_1 \cos^2\phi} \qquad ...(8.22b)$$

Tensile stresses and strains are taken as positive, and therefore care needs to be taken in choosing the correct sign convention for the mean stress, p'.

A series of runs using Model 14 was carried out to assess the influence of a curved failure envelope on the calculated values of cavity expansion limit pressure. The input parameters for the model included maximum voids ratio, 1.79, minimum voids ratio, 1.49, a ϕ_{cv} of 35°, and a Q of 10, which are typical values for a silica sand. The variation of limit pressure with relative density and mean stress is presented in Figure 8.8.

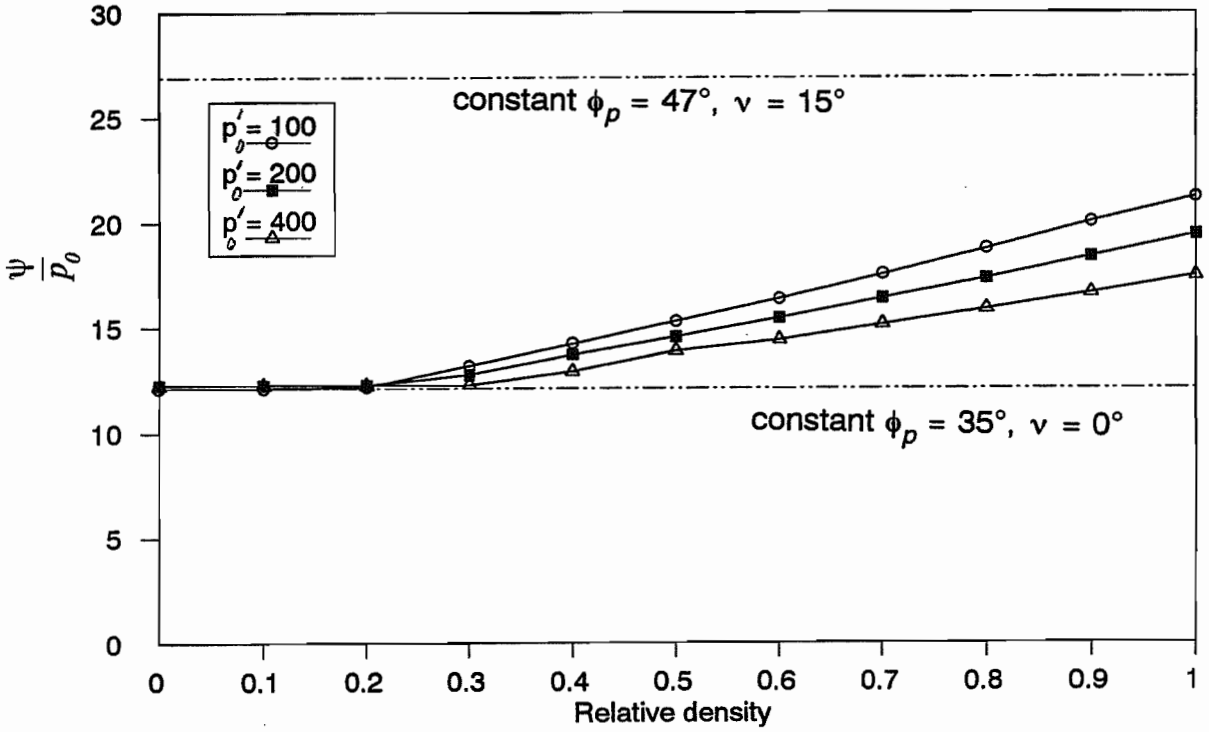

Figure 8.8 Variation of limit pressure with D_r and mean stress from Model 14

From equation (8.19) and the constraint that I_R varies between 0 and 4, the initial peak friction angle, $\phi_p = \phi_{cv} + 12° = 47°$. The initial dilation angle was then calculated from equation (8.21). Hence an upper and lower bound has been imposed on Model 14. The limit pressures representing the upper and lower bounds were calculated using Model 13 with ϕ_p of 47° and 35° and ν_{max} of 15° and 0° respectively, and are shown in the figure, normalised by the initial mean stress. It is clear that limit pressures calculated using the curved failure envelope of Model 14 fall within the expected bounds defined by a linear failure envelope. It is also

evident that for decreasing densities and increasing confining stresses, the additional strength due to a peak friction angle is almost completely lost. From this observation, it can be concluded that it is significantly unconservative to estimate limit pressures based upon a peak friction angle.

8.5 Particle crushing (Model 15)

An unbounded failure surface such as that of Model 14 is applicable to most silica sands because, within the range of stresses at which pressuremeter testing is normally carried out, it is unlikely that particle crushing will influence the observed strength. Further refinement must be given to the model, however, when considering carbonate sands.

Coop (1990) has observed the crushing behaviour of Dogs Bay carbonate sand from a series of isotropic and one-dimensional triaxial compression tests. From Coop's data, particle crushing is evident from a mean effective stress of between 300kPa and 800kPa (although it is difficult to attribute a more specific stress level which signifies the onset of crushing). This observation is supported by results from oedometer tests reported in Chapter 4. Considering that the effective stress level experienced by Dogs Bay sand from several CPM tests reached this range (see Table 7.1), it is of value to incorporate this feature into a numerical soil model.

It has been assumed for Model 15 that particle crushing begins when the friction angle reaches ϕ_{cv} at a critical pressure, p_x'. Using the empirical correlation of Bolton (1986) from equation (8.20), p_x' can then be defined at $I_R = 0$ by

$$p_x' = \exp\left(Q - \frac{1}{D_r}\right) \qquad ...(8.23)$$

For $p' > p_x'$, a new function is used to define the yield surface, given by

$$\phi = \phi_{cv}\left(\frac{2p_x'-p'}{p_x'}\right)^n \qquad ...(8.24)$$

where n is a material constant in the range $0 < n < 1$. This function is presented in Figure 8.9 for the particular case of $n = 0.6$. Continuity of the slope of the yield function at $p' = p_x'$ is not observed, however, the finite element calculation remains stable for a reasonable choice of the parameter n. For comparison, the surfaces defined by $n = 0.1$ and $n = 0.9$ are chain-dotted in the figure. The function crosses the p-axis vertically at $p_c' = 2p_x'$, and this point represents the isotropic stress level at which crushing commences.

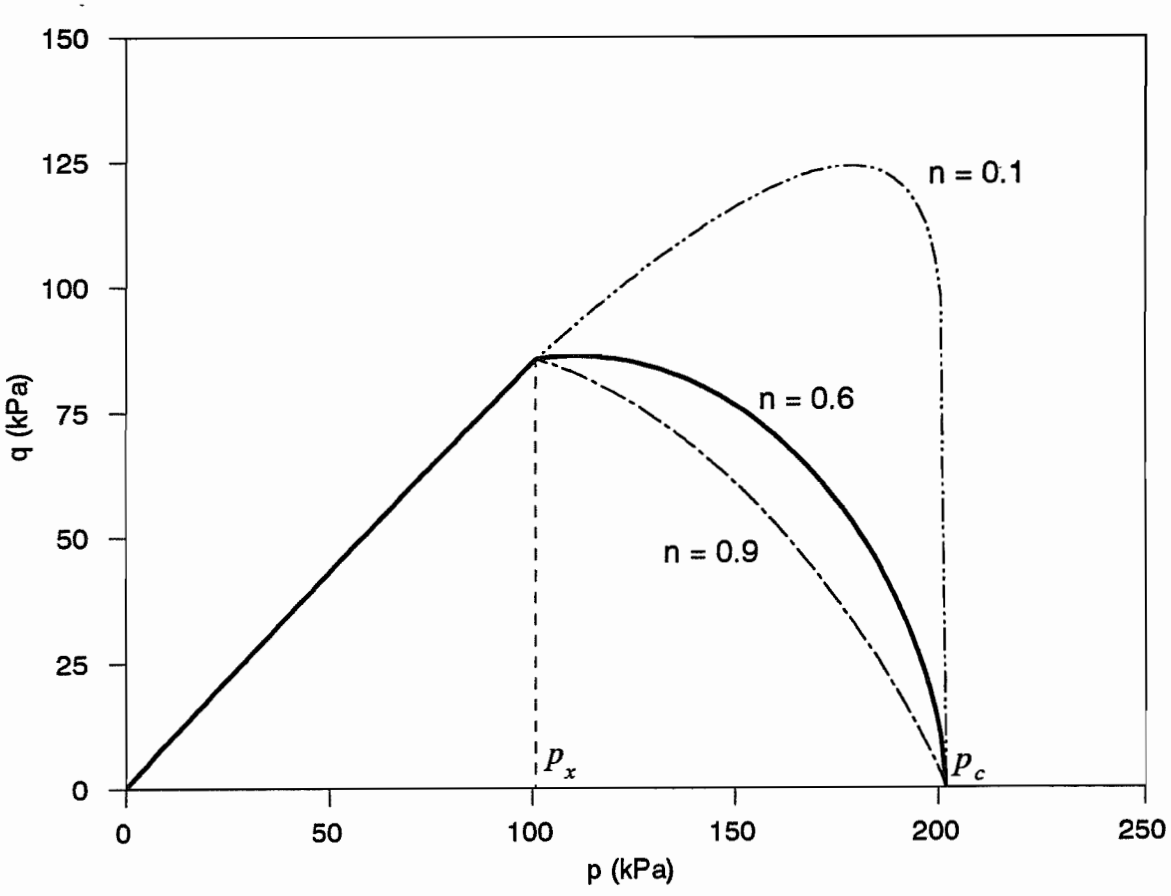

Figure 8.9 The yield surface of Model 15 in *q* : *p* space

The dilation angle, which becomes negative for $p' > p'_x$, can be modelled by the function

$$\sin\nu = \frac{p'_x - p'}{p'_x} \qquad ...(8.25)$$

The normal to the yield surface for $p > p'_x$ depends upon $\partial\phi/\partial p'$ determined by differentiation of equation (8.24) to give

$$\frac{\partial\phi}{\partial p'} = \phi_{cv}\left(\frac{2p'_x - p'}{p'_x}\right)^{n-1} \cdot \frac{-n}{p'_x} \qquad ...(8.26)$$

The additional term to $\partial f/\partial \underline{\sigma}$ given in equation (8.22) can be modified accordingly.

The model places a new emphasis on the importance of the parameter, Q because from equation (8.23), p'_x is exponentially sensitive to variations in Q. It is not intended, however, for the model to supersede Bolton's correlation; rather it is designed to capture the features of particle crushing at relatively low stress levels in a numerically convenient form.

Particle crushing has been used to explain, in part, the differences between observed limit pressures from cone pressuremeter tests in Dogs Bay sand and the limit pressures predicted from a cavity expansion model. In a simulation of the CPM tests reported in Chapter 4, two relative densities were used; 0.25 (loose) and 0.55 (dense). The stiffness index, G/p'_0 was estimated to be 100 for both loose and dense sands (see Chapter 7), and a ϕ_{cv} value of 40.3° was used. Difficulty arose in selecting a suitable value for the crushing pressure, p'_c and hence p'_x from which Bolton's parameter, Q could be determined. The variation of limit pressure with p'_c is clarified in Figure 8.10 for a series of runs at two initial confining stresses, p'_0 = 40kPa and

150kPa, and two relative densities, D_r = 0.25 and 0.55. The limit pressure calculated from Model 15 has been normalised by the limit pressure calculated from Model 14. As p_c' is decreased, limit pressure decreases significantly, and this effect is more pronounced at higher confining stresses, and for denser materials (because the limit pressures are higher in this case). It was assumed that crushing begins in loose sand at an isotropic stress, p_c of 200kPa. This value is somewhat lower than that suggested by Coop (1990) of 800kPa, but it was found that at higher values of p_c' the predicted limit pressures were almost insensitive to the presence of a bounded failure envelope.

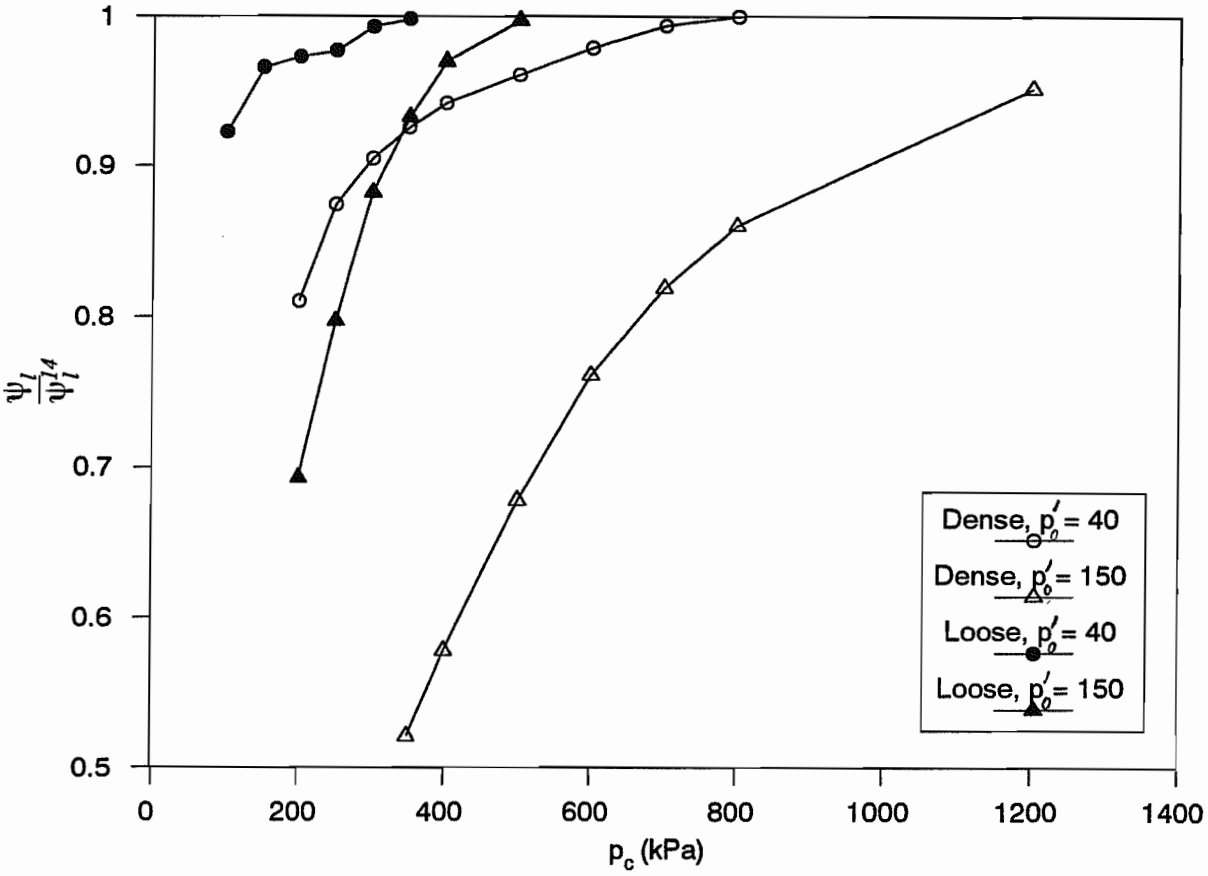

Figure 8.10 Variation of limit pressure and density with the crushing pressure

The results of a set of runs simulating the CPM tests in loose Dogs Bay sand are presented in Figure 8.11. Included in the figure are the CPM limit pressures. When particle crushing was not considered, limit pressures were predicted using the unbounded, curved failure

envelope of Model 14, and are shown as the top line in the figure. The influence of crushing as predicted by Model 15 is shown in the figure as the lower line. It is clear that the presence of a bounded failure envelope greatly improves the numerical estimation of CPM limit pressure. That the observed limit pressures were not predicted exactly by Model 15 is an indication, firstly of the sensitivity of calculated limit pressures to estimates of p_x', and secondly that the cone pressuremeter test is not truly modelled by a single continuous cavity expansion, as discussed in Chapter 5, and that the model is approximate in nature.

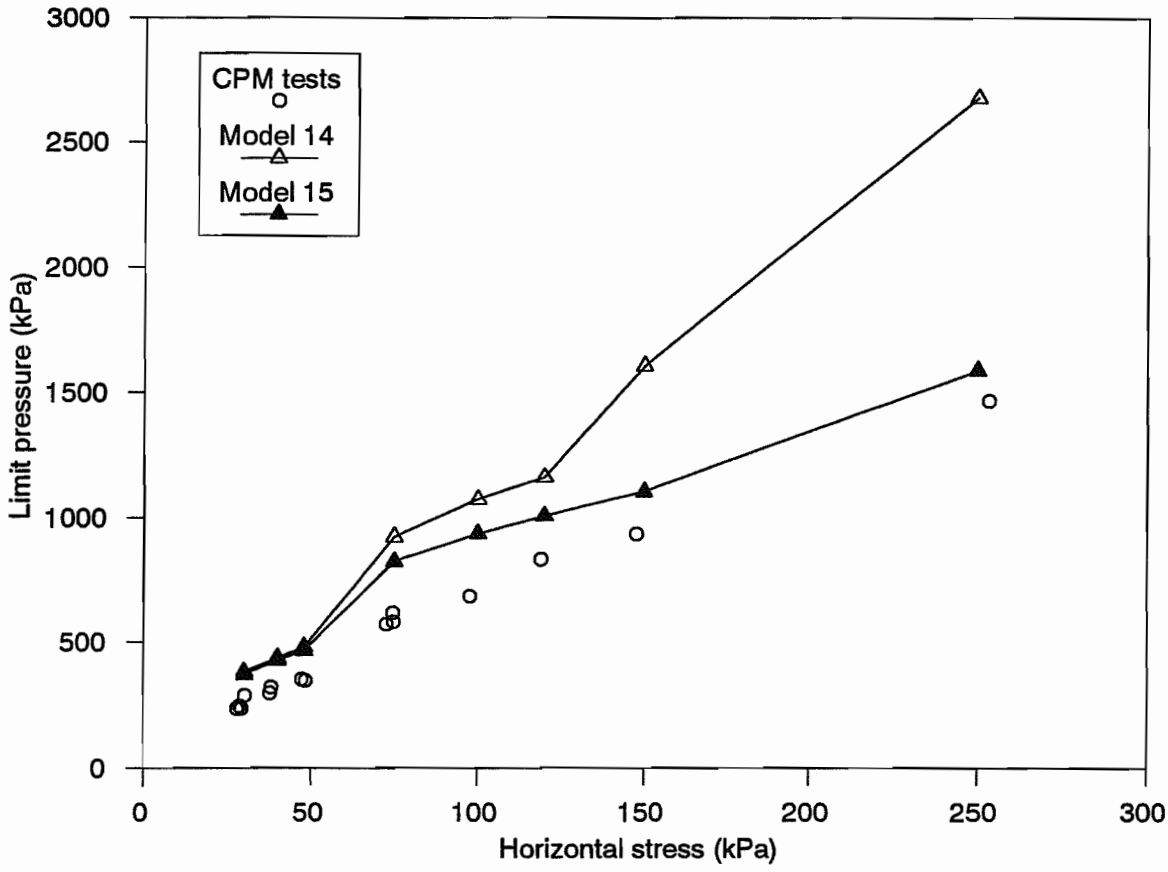

Figure 8.11 Prediction of limit pressures in loose Dogs Bay sand using Model 15

A similar process was carried out for the CPM tests in dense Dogs Bay sand. Based on the oedometer tests of Chapter 4, a value of p_c' of 450kPa has been used, which is greater than p_c' for loose sand. The results are shown in Figure 8.12, where it is evident that limit pressures predicted from Model 15 slightly underpredict those observed from CPM tests.

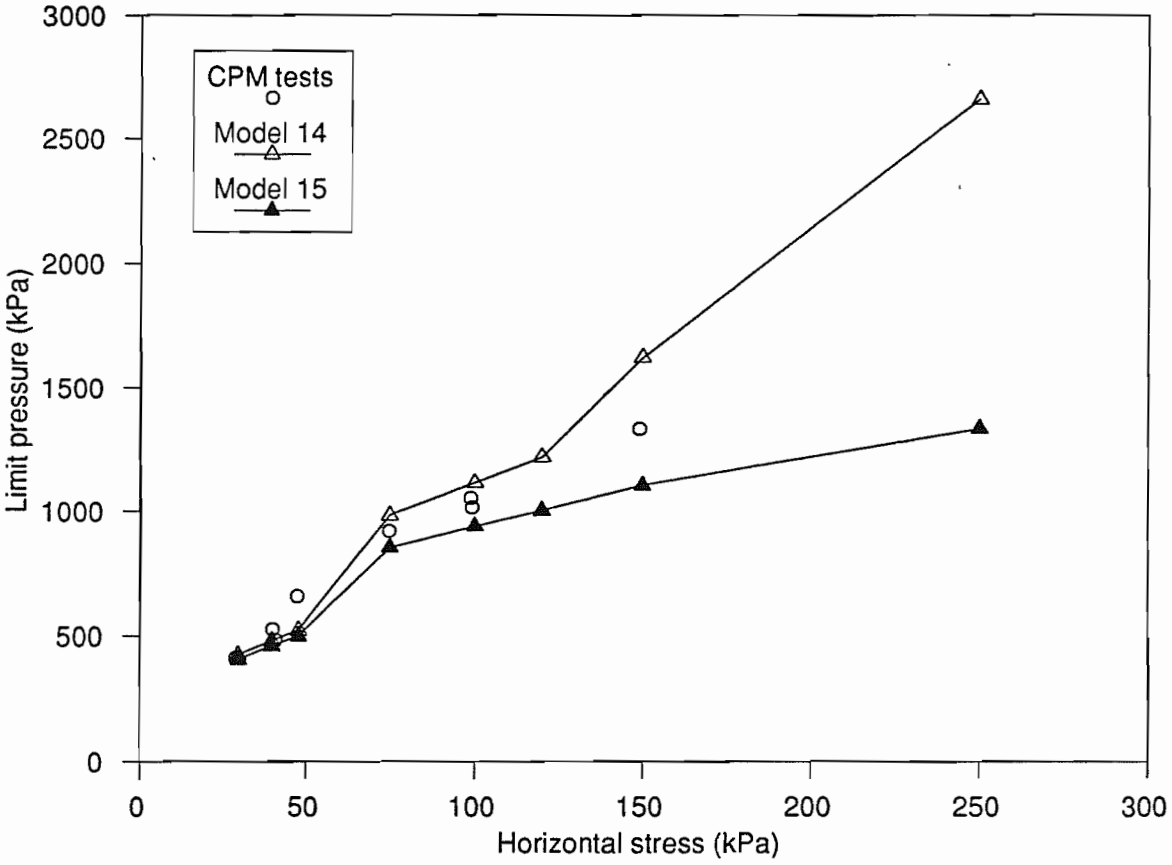

Figure 8.12 Prediction of limit pressure in dense Dogs Bay sand using Model 15

8.6 Conclusions

It appears that predictions of pressuremeter test behaviour in sands can be improved with the use of finite element models. A relatively simple yield function has been presented which incorporates a curved failure envelope up to a critical isotropic stress. At stresses greater than this critical value, a finite boundary to the failure surface is defined which extends to the normal stress axis. This feature has been illustrated with a numerical simulation of the cone pressuremeter tests carried out in the calibration chamber, and estimates obtained of CPM limit pressure were found to be improved.

CHAPTER 9

APPLICATIONS, SUMMARY AND CONCLUSIONS

9.1 General remarks

In this chapter, some of the practical applications of the cone pressuremeter are discussed, with particular emphasis placed on the efficiency of the device compared to the cone penetrometer and the self-boring pressuremeter. This takes the form of a time/cost analysis of the CPM, CPT and SBPM, using the example of a typical field situation.

The work presented in this thesis has been aimed at developing interpretation methods for the cone pressuremeter and has centred upon three areas of research:

(1) an extension of the database of cone pressuremeter tests to a variety of soil types

(2) the measurement of fundamental soil properties with the cone pressuremeter, specifically strength, *in situ* stress and stiffness

(3) an assessment of the application of cavity expansion theory to cone pressuremeter testing, with improvements or alternatives presented where necessary.

In following sections, conclusions which address these points are presented, based on a programme of calibration chamber tests in two types of sand, field tests in soft clay and numerical assessment. This includes a summary of procedures adopted, comments on methods of interpretation and comparisons with results reported in the literature. Finally, some suggestions are presented for the areas of cone pressuremeter development that require further research. It is concluded that the cone pressuremeter is an efficient and reliable tool for the

measurement of strength, stiffness and *in situ* horizontal stress in most types of sand, and strength and stiffness in clay.

9.2 Practical applications

9.2.1 Time/cost analysis

Most *in situ* test methods can be divided into two groups; logging methods and specific test methods (Campanella and Robertson, 1983). Logging methods, for example the CPT, are best suited for stratigraphic logging and preliminary evaluation of soil parameters, and there is usually a strong emphasis placed on speed and operational convenience of the test. In contrast, specific test methods are used to obtain soil parameters at selected depth locations. Operational convenience is often sacrificed for accuracy and reliability of measurements. The self-boring pressuremeter is an important example of a specific test device.

The cone pressuremeter is a device that fits into both categories. As a logging tool, it is identical to the cone penetrometer. As a specific test device, it has been shown in this thesis that it is capable of providing reliable information on a number of fundamental soil parameters. To this end, the cone pressuremeter is presented in this section as a competitor to the self-boring pressuremeter, and as a supplement to the cone penetrometer.

Aside from the measurement of soil parameters, the relative merits of the three devices, the CPT, CPM and SBPM, are best presented in terms of equipment needs and operational time rather than a direct examination of costs. The following comparisons, however, should be regarded as approximate.

Cone testing involves a significant investment in capital equipment to drive the cone and log the data. In addition, the cone pressuremeter requires very little. Apart from the device itself and pressure development equipment, only additional datalogging capacity is needed. After an initial site mobilisation, a CPT to 20m can be completed in about 1.5 hours, say six

soundings per working day. Each pressuremeter test takes approximately one hour, so a CPM sounding with six pressuremeter tests would also take about one day. A programme of 12 CPT soundings and one CPM sounding would, therefore, take 50% longer in time than the CPT soundings alone.

The equipment needed to install the SBPM is simple and relatively inexpensive. The drilling process is, however, relatively slow, so that a 20m hole with six tests may take two to three days, *i.e* at least twice as long as the CPM. An example of the combinations of testing that could be carried out in two days to a depth of 20m is presented in Table 9.1

Table 9.1 A comparison of the operating efficiency of the CPT, CPM and SBPM

2 days of testing to 20m depth		
CPT	CPM	SBPM
12 soundings	7 soundings + 6 tests or 2 soundings + 12 tests	6 tests

In terms of offshore *in situ* testing, the cone pressuremeter is particularly well adapted (indeed, this was one of the original purposes of the device) because it can be installed using the same equipment as that required for a cone penetrometer. In contrast, most of the self-boring pressuremeter systems in use are not suitable for use offshore, although some systems have been developed specifically for this purpose (Brucy and le Tirant, 1986; Fahey, 1988).

9.2.2 Limitations

While the cone pressuremeter seems a cost effective alternative to the self-boring pressuremeter, there exist, at this stage of its development, two main limitations to its use. Firstly, the measurement of strength and *in situ* horizontal stress in sand depend upon empirical correlations. Confidence can only be placed in empirical correlations when there

exists an extensive database of tests in a variety of soil types (note that this was one of the primary objectives of this thesis). Secondly, the cone pressuremeter cannot provide information about *in situ* horizontal stress in clays. The first of these limitations can be removed with continued use of the CPM; the second of these limitations, it is suggested, should be a topic addressed in future research.

9.3 Summary of CPM testing in sand

9.3.1 Procedures

Development of the cone pressuremeter in sand has been carried out using the results of tests in a large calibration chamber. The primary advantage of calibration chamber testing over field testing is that conditions of *in situ* stress and relative density can be controlled. Field tests, however, require comparisons with other *in situ* tests because of the difficulty in obtaining undisturbed samples for small scale laboratory testing. For this reason, a programme of chamber tests was carried out to assess the influence of stress and relative density on measured values of cone resistance and limit pressure. Schnaid (1990) reported a set of CPM tests in a calibration chamber in Leighton Buzzard silica sand. In this thesis, two further sands of very different mineralogical composition and grain size/shape were used in the testing programme - Dogs Bay carbonate sand and Hokksund felspathic sand.

Pluviation was used for the preparation of samples in the calibration chamber in two ranges of relative density, labelled as loose and dense, with the exception of dense Dogs Bay sand which was prepared using a vibration technique. The samples were found to be of a high uniformity, as indicated both from cone resistance profiles and the densities measured from rigid containers. Horizontal and vertical stresses were then applied to the sample using water filled membranes at the walls and base of the chamber.

The cone pressuremeter was jacked continuously into the sample at a constant speed, with readings taken automatically at fixed intervals. When the pressuremeter module was at mid-height of the chamber, insertion was stopped, and pressuremeter inflation was commenced. Cavity strain was measured using three instrumented strain arms located at mid-height of the module, and also from a measurement of the volume of silicon oil required to expand the membrane. At strain levels of 12%, 21% and 31%, the pressure was held constant until soil creep strains had decayed to a sufficiently low rate. An unload-reload cycle was then carried out, at a pre-determined strain amplitude. It is recommended that any large site investigation with the CPM should incorporate unload-reload loops at a fixed strain amplitude with some loops carried out at half and double that amplitude. At about 40% strain, the cavity strain was held constant for about 3 minutes while the cavity pressure was allowed to relax. The pressuremeter was then deflated to its original state.

It was necessary to make two corrections to the recorded data. The first correction was to account for the stiffness of the pressuremeter membrane, which was determined by performing an inflation in air. This correction is of most significance in soft soils. The second correction was for instrument compliance and was determined by performing an inflation in a very stiff tube. This correction is of most importance in stiff soils and can influence the measurement of shear modulus.

Cone resistance was measured at the same depth at which a pressuremeter test was carried out. Limit pressure was defined as the pressure at a particular cavity strain, and in each case was close to the maximum pressure achieved. The gradients of the unload-reload loops were used to determine the shear modulus of the soil. These measurements obtained from a series of cone pressuremeter tests have been used to make estimates of fundamental soil properties.

9.3.2 Strength and horizontal stress

In a review of recent methods of interpretation of cone pressuremeter tests in sand, it was found that cavity expansion theories have only a limited success in predicting cone resistance and limit pressure. This is for two reasons. Firstly, the mechanism of cone penetration followed by pressuremeter expansion in disturbed soil is not represented adequately by the continuous expansion of a single cavity, as assumed by theory. A small unloading, or cavity contraction, is experienced as the shoulder of the cone passes a soil element, then as pressuremeter expansion proceeds, there is a transition from a mechanism of cylindrical cavity expansion to spherical cavity expansion. Secondly, the assumption of constant angles of friction and dilation throughout the analysis is inaccurate due both to the large shear strains induced by a cone pressuremeter, and due to the crushability of the carbonate sand that has been tested.

In an undisturbed soil, the lift-off pressure (the pressure at which readings of the strain arms are first observed to increase) is a direct measurement of the *in situ* horizontal stress. The gross disturbance caused to the soil during CPM insertion, however, prevents the measurement of *in situ* horizontal stress by this method.

An alternative approach to interpretation of cone pressuremeter tests in sand was reported by Schnaid (1990) and has been used in this thesis with further success. The approach is based on the empirical relationship between cone pressuremeter measurements of q_c and ψ_l, and *in situ* horizontal stress, σ_h and relative density, D_r. From tests in Dogs Bay sand and Hokksund sand, it was shown that both q_c and ψ_l were more sensitive to σ_h than to the vertical stress, σ_v for each density tested. Horizontal stress was, therefore, used to normalise q_c and ψ_l in the

form $(q_c-\sigma_h)/\sigma'_h$ and $(\psi_l-\sigma_h)/\sigma'_h$. The combination of these factors in the form $(q_c-\sigma_h)/(\psi_l-\sigma_h)$ was shown to be dependent only upon D_r. A pair of linear empirical correlations were presented between D_r and $(\psi_l-\sigma_h)/\sigma'_h$, and D_r and $(q_c-\sigma_h)/(\psi_l-\sigma_h)$ based on all CPM data available from calibration chamber tests. On rearrangement, these correlations were used to solve for estimated values of σ_h and D_r. Horizontal stress was estimated to within 15% of the applied values, and relative density was estimated to within 15% of measured values. This approach is successful, considering the very different mineralogical components of the sands tested. To obtain values of friction angle from estimates of relative density, the empirical correlation proposed by Bolton (1986) has been considered most applicable.

Additional tests were carried out in Dogs Bay sand to assess the influence of a cycle of overconsolidation on the sample to cone pressuremeter measurements. It was found that q_c and ψ_l were sensitive to the horizontal overconsolidation ratio, such that these values were shown to be up to 60% higher than for equivalent tests in a normally consolidated sample. This is attributed to the additional degree of particle crushing caused to the soil by the application of higher stresses.

Application of strength measurements made from calibration chamber tests to field conditions must be used with caution. In dense, hard grained sands it was shown that chamber size effects can result in an underprediction of q_c and ψ_l by up to 30%, and hence an overprediction of the friction angle. Tests in carbonate sands, however, were generally insensitive to chamber size effects and hence applicable to field conditions.

9.3.3 Time-dependent behaviour

Time-dependent behaviour has been observed and quantified with the cone pressuremeter using three types of test: pressure holding tests and strain holding tests, both as described in the test procedure, and variable strain rate tests, where in place of unload-reload loops, different rates of strain were applied during pressuremeter inflation. A theory proposed by Singh and Mitchell (1968), used to describe the creep behaviour of soils, has been extended to explain the phenomena observed in all three types of test carried out with the cone pressuremeter. Creep has been recorded from pressure holding tests, stress relaxation has been recorded from strain holding tests, and from the variable strain rate tests, it is concluded that there exists a family of pressure-expansion curves for a constant strain rate and a given set of initial soil conditions. Limit pressure was shown to depend upon the rate of strain at which a test was carried out. Furthermore, soil creep can effect the observed gradient of an unload-reload loop, from which shear modulus is determined, and it is recommended that creep strains be allowed to decay prior to each unload-reload loop.

9.3.4 Stiffness

The stress-strain behaviour of most soils is highly non-linear from very small strains, so that soil stiffness, measured in terms of a shear modulus, G, is dependent upon both the stress level and the strain amplitude over which the measurement was made. It was shown in the literature that at a given stress level, there exists an elastic threshold shear strain, typically about 10^{-4} above which G decreases with increasing strain amplitude.

Shear modulus was measured with the cone pressuremeter from unload-reload loops carried out during pressuremeter inflation. As long as the change in cavity pressure during a loop was not too large to cause reverse plasticity of the soil, then from cavity expansion theory, the

shear modulus is directly proportional to the gradient of the loop. There was a consistent tendency for this gradient to be slightly lower when calculated by a least squares regression of the data in the loop than when calculated from the gradient of a line connecting the extremeties of the loop, and the latter approach was used in all analyses. The stress level at the pressuremeter-soil interface was calculated after making an assumption that the intermediate principal stress could be determined using an associated flow rule with the Matsuoka plasticity model. Shear modulus was then related to the stress level by a two parameter power law. The parameters were found to be insensitive to relative density.

Strain amplitudes of cone pressuremeter unload-reload loops typically ranged from 0.001 to 0.004, and were shown to account for large variations in shear modulus. Using a procedure proposed by Wroth *et al.* (1979), which is applicable to most types of sand, the shear moduli calculated from the unload-reload loops were related to shear moduli below the elastic threshold strain.

9.3.5 Particle crushing

In comparison to silica sands, carbonate sands exist at higher void ratios, their particles are structurally angular and weak, and they contain intraparticle voids. Although they develop higher peak strengths than silica sands, on shearing, dilation of these soils is suppressed at relatively low stress levels because of compression and crushing of grains.

This feature of carbonate sand behaviour has been addressed numerically in the development of a set of finite element models based on elastic-plastic cavity expansion theory. In place of the assumption of constant friction and dilation angles throughout an analysis, these parameters have been allowed to decrease to a critical value with the increase in confining

stress according to the relationship proposed by Bolton (1986). The Matsuoka failure surface defining the boundary between elastic and plastic soil behaviour was then extended to isotropic stress conditions, so that beyond a critical crushing pressure, a yield surface was defined which closed to the p' axis, so that even isotropic stresses would be treated as causing yield of the soil.

These models were used to estimate limit pressures based upon cone pressuremeter tests carried out in Dogs Bay sand in the calibration chamber. By incorporating particle crushing into the analysis, a great improvement was shown between predicted and observed limit pressures, although predicted values were found to be very sensitive to the choice of a critical crushing pressure.

9.4 Summary of CPM testing in clay

9.4.1 Procedures

Very little data exists in the literature on cone pressuremeter testing in soft clay. A set of 12 cone pressuremeter tests were carried out at a well documented soft clay site at Bothkennar, in Scotland. A 15cm^2 cone pressuremeter was used for testing and the results were compared to results from a number of other *in situ* devices and laboratory tests.

The cone pressuremeter was jacked into the ground using a standard cone truck, and at 3m intervals, penetration was stopped and a pressuremeter inflation was carried out. At three intervals during the test, inflation was stopped, and the strain held for one to two minutes followed by a rapid unload-reload loop. Upon reaching maximum expansion the pressuremeter was then deflated at the same rate. The corrections to the pressure-expansion data due to membrane stiffness were found to be significant, because of the low limit pressures recorded,

especially close to the surface.

9.4.2 Strength

The Houlsby and Withers (1988) analysis was used for interpretation of cone pressuremeter tests in clay. It is a graphical method applied to the unloading portion of the pressure-strain curve, developed from large strain cavity contraction theory. Estimates of undrained shear strength using this analysis were found to be in good agreement with published data from self-boring pressuremeter tests, field vane tests and undrained triaxial tests, considering that these tests subject the soil to very different modes of deformation, strain rates and strain levels. A reasonable comparison was also evident from strength measurements made with the cone results, however, it is concluded that confidence in these measurements could have been improved if a piezocone had been used, with an appropriate end area correction.

9.4.3 Horizontal stress

After making a correction to account for the finite length of the pressuremeter, estimates of horizontal stress using the Houlsby and Withers (1988) analysis were still found to be significantly higher than estimates made from self-boring pressuremeter tests and the dilatometer. This implies that a fundamental approach of interpretation is not applicable to this parameter, and it is more likely that an empirical correlation in the form of a correction factor could be developed to improve this estimate, but this would require further calibration testing of the cone pressuremeter.

9.4.4 Stiffness

Three unload-reload loops were performed during each pressuremeter inflation at Bothkennar, and estimates of shear modulus, G_{ur} were made from the gradient of the lines connecting the

extremeties of the loop and from a least squares regression of the data in the loop. The former approach was found to give consistently higher estimates of G_{ur} by about 14%. Shear modulus, G_{cc} was also estimated from the cavity contraction analysis of Houlsby and Withers (1988), although it was difficult to attribute a particular strain amplitude to this measurement. From a comparison between G_{ur} and G_{cc} made from data at Bothkennar and a stiff clay site at Madingley, it was found that a strain amplitude of around 0.006 is appropriate for interpretation of G_{cc}.

In order to relate pressuremeter moduli to triaxial moduli (which are determined at significantly lower strain amplitudes), an empirical correction proposed by Jardine (1992) was applied. A comparison of G_{ur} with a corrected strain amplitude was made with a secant triaxial modulus, G_s reported from tests on reconstituted and intact samples of Bothkennar clay and found to be in remarkably good agreement with the latter. It is concluded that the cone pressuremeter provides reliable measurements of stiffness from unload-reload loops when the strain amplitude is correctly accounted for.

9.5 Future research

The direction of future research can be divided into two categories; research into methods of interpretation and research into development of the equipment. In terms of the methods of interpretation, there is a need for field tests in sand. The primary aim of these tests would be to verify and/or improve the correlations presented in Chapter 5 for the estimation of density and *in situ* horizontal stress. There is also a need for these correlations to be tested at higher stress levels than were applied in the calibration chamber. A numerical analysis to assess the influence of the length to diameter ratio on cone pressuremeter tests in sand should be undertaken. Such an analysis in clay has already been reported by Yu (1990). This was

commenced during the course of this research, but difficulties were encountered in modelling the process of cone penetration followed by pressuremeter expansion in sand, and no results are therefore reported. The measurement of *in situ* horizontal stress in clay should be addressed. Cavity expansion theory does not produce reliable estimates of this parameter, and an empirical correlation is likely to be the way to estimate this. Further fields tests in clay are also strongly recommended.

In terms of equipment development, improvements to the protective outer membrane, the Chinese lantern, should be made. Due to high abrasive forces experienced, particularly in sands, wear and tear on the Chinese lanterns was found to be more damaging than on any other component of the cone pressuremeter. A possible solution to this is to use a cone with a diameter slightly larger than the pressuremeter module. As long as the induced contraction is sufficiently small, the methods of interpretation presented in this thesis, which are dependent upon cavity expansions at large strain, should not be influenced.

9.6 Conclusions

As a result of the research presented in this thesis, the following conclusions have been made relating to the development of the cone pressuremeter.

(1) Methods of interpretation of the cone pressuremeter test based on the assumptions of constant friction and dilation angles and a single continuous cavity expansion have been shown to be inaccurate.

(2) Cone pressuremeter tests in the calibration chamber have revealed that empirical correlations can be used to estimate relative density and horizontal stress in sands. These correlations are applicable to a wide range of sand types.

(3) Time-dependent behaviour in carbonate sand was studied by performing pressure and strain holding tests, and varying the test procedure during cone pressuremeter inflation. A creep model was successfully applied and extended to provide a framework for this behaviour. The rate of pressuremeter inflation can influence the observed values of CPM limit pressure.

(4) Horizontal overconsolidation in carbonate sand has a much greater influence on cone resistance and limit pressure than vertical overconsolidation. This is due to the angular nature of the particles resulting in local crushing at interparticle contacts. Overconsolidation in silica sands does not influence observed cone resistance or limit pressure.

(5) Limit pressures from CPM tests in carbonate sand in the calibration chamber can be estimated more accurately when consideration is given to particle crushing and the variation of friction and dilation angles during CPM inflation. This was verified with the aid of a finite element soil model.

(6) Shear modulus in sand can be measured with the cone pressuremeter by incorporating unload-reload loops in the test procedure. Moduli values are sensitive to both the stress level and strain amplitude of the loop.

(7) The cone pressuremeter can be used to obtain reliable estimates of undrained shear strength and shear modulus in clay, but estimates of *in situ* horizontal stress are unreliable.

(8) The strain amplitudes over which shear moduli in clay are measured from unload-reload loops need to be corrected if comparisons with laboratory data are to be made. An empirical correction has been applied successfully to cone pressuremeter data from Bothkennar.

(9) The cone pressuremeter can be used as both a profiling tool and an instrument for measuring specific soil properties. One of its main advantages is speed of installation compared with the self-boring pressuremeter, and for this reason it has a particular application to offshore investigations.

As a final statement, the author believes the cone pressuremeter to be a reliable and cost effective *in situ* testing device. The success of this research will be in its practical application.

References

Where references do not appear in this list, consult Bibliography

Aas, G., Lacasse, S., Lunne, T. and Hoeg, K. (1986) - Use of *in situ* tests for foundation design on clay. *Proc. In situ '86*, ASCE Spec. Conf., Blacksburg, Virginia, June, 1-30.

Airey, D.W., Randolph, M.F. and Hyden, A.M. (1988) - The strength and stiffness of two calcareous sands. *Proc. Int. Conf. Calcareous Sediments,* Perth, Vol. 1, 43-50.

Al-Douri, R., Hull, T.S. and Poulos, H.G. (1990) - Preparation and measurement of uniform sand beds in the laboratory. *Research report R609*, Univ. Sydney.

Allman, M.A. and Atkinson, J.H. (1992) - Mechanical properties of reconstituted Bothkennar soil. *Géotechnique*, Vol. 42, No. 2, 289-302.

Almeida, M.S.S., Jamiolkowski, M. and Peterson, R.W. (1991) - Preliminary results of CPT tests in calcareous Quiou sand. *Proc. First Int. Symp. Calibration Chamber Testing*, ISOCCT1, Potsdam, U.S.A., 41-53.

Anderson, W.F. and Pyrah, I. (1989) - Consolidation and creep effects in the PMT in clay. *Proc 12th ICSMFE*, Rio de Janeiro, Vol. 1, 153-156.

Anderson, W.F. and Pyrah, I. (1991) - Pressuremeter testing in a clay calibration chamber. *Proc. First Int. Symp. Calibration Chamber Testing*, ISOCCT1, Potsdam, U.S.A., 55-66.

Angemeer, J., Carlson, E. and Klick, J.H. (1973) - Techniques and results of offshore pile load testing in calcareous soils. 5th *Offshore Technology Conference*, OTC 1894, Vol. 2, 677-692.

Atkinson, J.H., Allman, M.A. and Böese, R.J. (1992) - Influence of laboratory sample preparation procedures on the strength and stiffness of intact Bothkennar soil recovered using the Laval Sampler. *Géotechnique*, Vol. 42, No. 2, 349-354.

Baguelin, F., Jézéquel, J.F., Le Mee, H. and Le Mehaute, A. (1972) - Expansion of cylindrical probes in cohesive soils. *Journ. Soil Mech. Found. Div., ASCE*, Vol. 98, No. SM11, 1129-1142.

Baguelin, F., Jézéquel, J.F. and Shields, D.H. (1978) - The pressuremeter and foundation engineering. *Trans. Tech. Publications,* Clausthall.

Baldi, G., Bellotti, R., Ghionna, N., Jamiolkowski, M. and Pasqualini, E. (1982) - Design parameters for sands from CPT. *Proc. 2nd European Symp. Penetration Testing*, Amsterdam, Vol. 2, 425-432.

Baldi, G., Bellotti, R., Ghionna, N., Jamiolkowski, M. and Pasqualini, E. (1986) - Interpretation of CPT's and CPTU's, 2nd part: Drained penetration of sands. *Proc. 4th Int. Geotechnical Seminar*, Singapore.

Baligh, M.M. (1975) - Theory of deep site static cone penetration resistance. *Research report No. 875-76,* Dept. Civil Eng., M.I.T., Cambridge, U.S.A.

Baligh, M.M. (1976) - Cavity expansion in sands with curved envelopes. *Proc. ASCE Journ. Geotechnical Engineering*, GT11, Vol. 102, 1131-1145.

Baligh, M.M. (1986) - Undrained deep penetration, I: shear stresses; II: pore pressures. *Géotechnique*, Vol. 36, 471-485, 487-501.

Baligh, M.M., Vivatrat, V. and Ladd, C.C. (1980) - Cone penetration testing in soil profiling. *ASCE Journ. Geo. Eng. Div.,* Vol. 106, 447-461.

Barden, L., Ismial, H. and Tong, P. (1969) - Plane strain deformation of granular material at low and high pressures. *Géotechnique*, Vol. 19, No.4, 441-452.

Barentsen, P. (1936) - Short description of a field testing method with a cone shaped apparatus. *First Int. Conf. Soil Mech. Found. Eng.*, Vol. 1, Cambridge, U.S.A.

Barton, M.E. and Palmer, S.N. (1989) - The relative density of geologically aged, British fine and fine-medium sands. *Quart. Journ. Eng. Geology*, Vol. 22, 49-58.

Been, K., Crooks, J.H.A., Becker, D.A. and Jefferies, M.G. (1986) - The cone penetration test in sands, part 1: state parameter and interpretation. *Géotechnique,* Vol. 36, No. 2, 239-249.

Been, K. and Jefferies, M.G. (1985) - A state parameter for sands. *Géotechnique*, Vol. 35, No. 2, 99-112.

Begemann, H.K.S. (1953) - Improved method of determining resistance to adhesion by sounding through a loose sleeve placed behind the cone. *Third Int. Conf. Soil Mech. Found. Eng.*, Vol. 1, Zurich.

Belotti, R. (1984) - Chamber size effects and boundary condition effects. *Sem. Cone Penetration Testing in the Laboratory*, Univ. Southampton.

Belotti, R., Bizzi, G. and Ghionna, V.N. (1982) - Design, construction and use of a calibration chamber. *Proc. Second European Symp. Penetration Testing*, Amsterdam, 439-446.

Belotti, R., Ghionna, V., Jamiolkowski, M., Lancellotta, R. and Manfredini, G. (1986) - Deformation characteristics of cohesionless soils from *in situ* tests. *Proc. ASCE Spec. Conf., In situ '86*, Blacksburg.

Belotti, R., Ghionna, V., Jamiolkowski, M., Robertson, P.K. and Peterson, R.W. (1989) - Interpretation of moduli from self-boring pressuremeter tests in sand. *Géotechnique*, Vol. 39, No. 2, 269-292.

Beringen, F.L., Kolk, H.J. and Windle, D. (1982) - Cone penetration and laboratory testing in marine calcareous sediments. *ASTM Spec. Tech. Publ. 777*, 179-209.

Bieganousky, W.A. and Marcusson, W.F., III (1976) - Uniform placement of sand. *Journ. Geotech. Eng. Div., ASCE*, No. GT3, 229-233.

Bishop, A.W. (1971) - Shear strength parameters for undisturbed and remoulded soil specimens. *Proc. Roscoe Memorial Symp.*, 3-58.

Bolton, M.D. (1986) - The strength and dilatancy of sands. *Géotechnique*, Vol. 36, No. 1, 65-78.

Borsetto, M., Imperato, L., Nova, R. and Peano, A. (1983) - Effects of pressuremeters of finite length in soft clay. *Proc. Int. Symp. Soil and rock investigations by in situ testing*, Paris, Vol. 2, 211-215.

Brucy, F. and le Tirant, P. (1986) - Use of PAM and pressuremeters in offshore foundation design. *Proc. 2nd Int. Symp. Pressuremeter and its Marine Applications*, Texas, 5-21.

Bruzzi, D., Ghionna, V.N., Jamiolkowski, M., Lancellotta, R. and Manfredini, G. (1986) - Self-boring pressuremeter in Po River sand. *Proc. 2nd Symp. Pressuremeter and its Marine applications*, ASTM SPT 950, 57-73.

Burd, H.J. (1986) - A large displacement finite element analysis of a reinforced unpaved road. *DPhil Thesis*, University of Oxford.

Burd, H.J. and Houlsby, G.T. (1990) - Finite element analysis of two cylindrical expansion problems involving nearly incompressible material behaviour. *Int. Journ. Num. and Anal. Meth. Geomechanics*, Vol. 14, 351-366.

Campanella, R.G. and Robertson, P.K. (1983) - Flat plate dilatometer testing: Research and development. *Soil Mech. Series No. 68.* University of British Columbia.

Carter, J.P., Booker, J.R. and Yeung, S.K. (1986) - Cavity expansion in cohesive frictional soils. *Géotechnique*, Vol. 36, 349-358.

Carter, J.P., Randolph, M.F. and Wroth, C.P. (1979) - Stress and pore changes in clay during and after the expansion of a cylindrical cavity. *Int. Journ. Num. Anal. Meth. Geomech.*, Vol. 3, 305-322.

Chaney, R.C., Slonim, S.M. and Slonim, S.S. (1982) - Determination of calcium carbonate content in soils. *ASTM STP 777*, 3-15.

Clarke, A.R. and Walker, B.F. (1977) - A proposed scheme for the classification and nomenclature for use in the engineering description of Middle Eastern sedimentary rocks. *Géotechnique*, Vol. 27, No. 1, 93-99.

Cole, E.R.L. (1967) - The behaviour of soils in the simple shear apparatus. *Ph.D thesis*, University of Cambridge.

Collins, I.F., Pender, M.J. and Wang Yan (1992) - Cavity expansion in sands under drained loading conditions. *Int. Journ. Num. Anal. Meth. Geomech.*, Vol 16, 3-23.

Coop, M.R. (1990) - The mechanics of uncemented carbonate sands. *Géotechnique*, Vol. 40, No. 4, 607-626.

Crippa, V., Lo Presti, D.C.F. and Pedroni, S. (1990) - Maximum dry density of cohesionless soils by pluviation and by ASTM D4253-83: a comparative study. *Fourth Sem. Research involving validation of in situ devices in large calibration chambers*, Grenoble.

Datta, M., Gulhati, S.K. and Rao, G.V. (1979) - Crushing of calcareous sands during shear. *Proc. 11th OTC*, Texas, Vol. 3, 1459-1467.

De Beer, E.E., Goelen, E., Heynen, W.J. and Joustra, K. (1988) - Cone penetration test (CPT): International reference test procedure. *Proc. First Int. Symp. Penetration Testing*, ISOPT-1, Orlando, 27-52.

Demars, K.R. (1982) - Unique engineering properties and compression behaviour of deep sea calcareous sediments. *ASTM STP 777*, 97-112.

Demars, K.R., Nacci, V.A., Kelly, W.E. and Wang, M.C. (1976) - Carbonate content: an index property for ocean sediments. *Proc. 8th OTC*, Texas, 97-106.

Durgunoglu, H.T. and Mitchell, J.K. (1975) - Static penetration resistance of soils: I-Analyses, II-Evaluation of theory and implications for practice. *Proc. ASCE Spec. Conf. In situ measurement of soil properties*, Vol. 1.

Dutt, R.N., Moore, J.E., Mudd, R.W. and Rees, T.E. (1985) - Behaviour of piles in granular carbonate sediments from offshore Phillipines. *Offshore Technology Conference*, OTC 4899, Vol. 1, 73-82.

Evans, K.M. (1987) - A model study of the end bearing capacity of piles in layered carbonate soils. *D.Phil thesis*, Oxford University.

Fahey, M. (1986) - Expansion of a thick cylinder of sand: a laboratory simulation of the pressuremeter test. *Géotechnique*, Vol. 36, No. 3, 397-424.

Fahey, M. (1988) - Self-boring pressuremeter testing in calcareous soil. *Proc. Int Conf. Calcareous sediments*, Perth, Vol. 1, 165-172.

Fahey, M. and Jewell, R.J. (1990) - Effect of pressuremeter compliance on measurement of shear modulus. *Proc. Third Int. Symp. on Pressuremeters*, British Geotechnical Society, Oxford, 115-124.

Fioravante, V., Jamiolkowski, M., Tanizawa, F. and Tatsuoka, F. (1991) - Results of CPT's in Toyoura quartz sand. *Proc. 1st ISOCCT1*, Potsdam, 135-146.

Fookes, P.G. and Higginbottom, I.E. (1975) - The classification of description of near shore carbonate sediments for engineering purposes. *Géotechnique*, Vol. 25, No.2, 406-411.

Fukagawa, R., Ohta, H., Iizuka, A., Nishihara, A. and Morita, Y. (1990) - Effects of drainage on interpretation of pressuremeter tests in clay. *Proc. Third Int. Symp. on Pressuremeters*, British Geotechnical Society, Oxford, 189-198.

Géotechnique (1992) - Eighth Symposium in Print, Vol. 42, No. 2.

Georgiannou, V.N., Rampello, S. and Silvestri, F. (1991) - Static and dynamic measurements of undrained stiffness on natural overconsolidated clays. *Proc. 10th European Conf. SMFE*, Vol. 1, 91-96.

Ghionna, V.N. and Jamiolkowski, M. (1991) - A critical appraisal of calibration chamber testing of sands. *Proc. First Int. Symp. Calibration Chamber Testing*, Potsdam, U.S.A., 13-39.

Ghionna, V. *et al.* (1983) - Evaluation of self-boring pressuremeter. *Proc. Int. Symp. on In situ testing*. Paris, Vol. 2, 294-301.

Gibson, R.E. and Andersen, W.F. (1961) - *In situ* measurement of soil properties with the pressuremeter. *Civil Eng. and Public Works Review,* Vol. 56, 615-618.

Golightly, C.R. (1988) - Engineering properties of carbonate sands. *PhD Thesis*, University of Bradford.

Golightly, C.R. and Hyde, A.F.L. (1988) - Some fundamental properties of carbonate sands. *Proc. Int. Conf. Calcareous Sediments*, Perth, Vol. 1, 69-78.

Hagenaar, J. (1982) - The use and interpretation of SPT results for the determination of axial bearing capacities of piles driven into carbonate soils and coral. *Proc. 2nd European Symp. Penetration Testing*, Amstredam, 51-55.

Hardin, B.O. and Drnevich, V.P. (1972) - Shear modulus and damping in soils: Design equations and curves. *Journ. Soil Mech. Div. ASCE*, Vol. 98, No. SM7, 667-692.

Houlsby, G.T. and Carter, J.P. (1990) - The effects of pressuremeter geometry on the results of tests in clay. *Internal report, OUEL 1928/92*, Oxford University.

Houlsby, G.T., Clarke, B.G. and Wroth, C.P. (1986) - Analysis of the unloading of a pressuremeter in sand. *Proc. Second Int. Symp. Pressuremeter and its Marine Applications.*, ASTM STP 950, 245-262.

Houlsby, G.T. and Hitchman, R.C. (1988) - Calibration tests of a cone penetrometer in sand. *Géotechnique*, Vol. 38, No. 1, 39-44.

Houlsby, G.T. and Wroth, C.P. (1982) - Determination of undrained strengths by cone penetration tests. *Proc. 2nd European Symp. Penetration testing*, Amsterdam, Vol. 2, 585-590.

Huang, A.B., Holtz, R.D. and Chameau, J.L. (1991) - Laboratory study of pressuremeter tests in clays. *ASCE Journ. Geotech. Eng.*, Vol. 117, 1549-1567.

Hughes, J.M.O. (1982) - Interpretation of pressuremeter tests for the determination of elastic shear modulus. *Proc. Eng. Found. Conf. Updating subsurface sampling of soils and rocks and their in situ testing*. Santa Barbara, 279-289.

Hughes, J.M.O., Wroth, C.P. and Windle, D. (1977) - Pressuremeter tests in sands. *Géotechnique*, Vol. 27, No. 4, 455-477.

Hull, T.S., Poulos, H.G. and Alehossein, H. (1988) - The static behaviour of various calcareous sediments. *Proc. Int. Conf. Calcareous Sediments*, Perth, Vol. 1, 87-96.

Iwasaki,T., Tatsuoka, F. and Yoshikau, T. (1978) - Shear moduli of sands under cyclic torsional shear loading. *Soils and Foundations*, Vol. 18, No. 1, 40-56.

Jaky, J. (1944) - The coefficient of earth pressure at rest. *Journ. Soc. Hungarian Architects and Engineers, Budapest*, 355-358.

Jamiolkowski, M., Ladd, C.C., Germaine, J.T. and Lancellotta, R. (1985) - New developments in field and laboratory testing of soils. *Proc. 11th Conf. Soil Mech. Found. Eng.*, San Fransisco, Vol. 1, 57-154.

Jamiolkowski, M., Lancellotta, R., Tordella, L. and Battaglio, M. (1982) - Undrained strength from CPT. *Proc. Europ. Symp. Penetration Testing*, ESOPT-2, Amsterdam.

Jamiolkowski, M., Ghionna, V.N., Lancellotta, R. and Pasqualini, E. (1988) - New correlations of penetration tests for design practice. *Proc. First Int. Symp. Penetration Testing*, ISOPT-1, Orlando, 263-296.

Janbu, N. (1963) - Soil compressibility as determined by oedometer and triaxial tests. *European Conf. SMFE*, Germany, Vol. 1.

Janbu, N. and Senneset, K. (1974) - Effective stress interpretation of *in situ* static penetration tests. *Proc. European Symp. Penetration Testing*, Stockholm, Vol. 2.2.

Jardine, R.J. (1991) - Discussion on Wood, D.M. (1990). *Géotechnique*, Vol. 41, 621-624.

Jardine, R.J. (1992) - Nonlinear stiffness parameters from undrained pressuremeter tests. *Can. Geotech. Journ.*, Vol. 29, 436-447.

Jardine, R.J., Potts, D.M., Fourie, A.B. and Burland, J.B. (1986) - Studies of the influence of non-linear stress-strain characteristics in soil structure interaction. *Géotechnique*, Vol. 36, No. 3, 377-396.

Jefferies, M.G. and Davies, M.P. (1991) - Discussion on soil classification by the cone penetration test. *Can. Geotech. Journ.*, Vol. 28, 173-176.

Jewell, R.J., Andrews, D.C. and Khorshid, M.S. (1988) - *Engineering for Calcareous Sediments*. A.A. Balkema, Rotterdam, Brookfield.

Keary, R. (1967) - Biogenic carbonate in beach sediments of the west coast of Ireland. *Scient. Proc. Royal Dublin Soc.*, Series A, Vol. 3, No. 7, 75-85.

Kildalen, S., Last, N., Lunne, T. and Parkin, A. (1982) - Results of triaxial tests on Hokksund sand. *Internal report S2108-13*, Norwegian Geotechnical Institute.

King, R.W., van Hooydonk, Kolk, H. and Windle, D. (1980) - Geotechnical investigations of calcareous soils on the North West shelf of Australia. *Proc. 12th OTC*, Texas, Vol. 3, 1459-1467.

Kolbuszewski, R.L. (1948) - An experimental study of the maximum and minimum porosities of sands. *Proc. Second Int. Conf. Soil Mech. Found. Eng.*, Rotterdam, 158-165.

Kolbuszewski, R.L. and Jones, R.H. (1961) - The preparation of sand samples for laboratory testing. *Proc. Midland Soil Mech. Found. Eng. Soc.*, Vol. 4, 108-123.

Lacasse, S. and Lunne, T. (1982) - Piezocone tests in two soft marine clays. *Internal report 52155-20*, NGI.

Lacasse, S., D'Orazio, T.B. and Bandis, C. (1990) - Interpretation of self-boring and push-in pressuremeter tests. *Proc. 3rd Int. Symp. Pressuremeters.* Oxford, 273-286.

Lacerda, W.A. and Houston, W.N. (1973) - Stress relaxation in soils. *Proc. 8th ICSMFE*, Moscow, Vol. 1, 221-227.

Ladanyi, B. (1963) - Evaluation of pressuremeter tests in granular soils. *Proc. Second Pan American Conf. Soil Mech. Found. Eng.*, Vol. 1, 3-20.

Ladd, C.C., Foott, R., Ishihara, K., Schlosser, F. and Poulos, H.G. (1977) - Stress-deformation and strength characteristics. *Proc. 9th Int. Conf. Soil Mech. Found. Eng.*, Tokyo.

Last, N.C. (1982) - The cone penetration test in granular materials. *Ph.D thesis*, University of London.

Last, N., Butterfield, R. and Harkness, R.M. (1987) - An investigation of full scale penetrometers in a large triaxial calibration chamber. *Internal report*, University of Southampton.

Lees, A. and Buller, A.T. (1972) - Modern temperate water and warm water shelf carbonate sediments contrasted. *Marine Geology*, Vol. 13, m67-m73.

Lo Presti, D. (1990) - Pluvial deposition - General aspects, problems, suggestions. *Fourth Sem. Research involving validation of in situ devices in large calibration chambers*, Grenoble.

Lunne, T. (1991) - Practical use of CPT correlations in sand based on calibration chamber tests. *Proc. First Int. Symp. Calibration Chamber Testing*, ISOCCT1, Potsdam, 225-236.

Lunne, T., Clausen, C.J.F. and Kjekstad, O. (1976) - Comparisons between cone penetration tests and borings at some North Sea locations. *Internal report 52155-6,* N.G.I., Oslo.

Mair, R.J. and Wood, D.M. (1987) - Pressuremeter testing - methods and interpretation. CIRIA *Ground Eng. Report; In situ testing*, Butterworths, London.

Marchetti, S. (1980) - In situ tests by flat dilatometer. *ASCE, Journ. Geotech. Eng. Div.*, Vol 106, GT3, 299-321.

Marsland, A. and Quarterman, R.S.T. (1982) - Factors affecting the measurements and interpretation of quasi static penetration tests in clays. *Proc. Second European Symp. Penetration Testing*, Amsterdam, 697-702.

Matos, S.F. and Mello, J.R. (1982) - Piling of Garoupa platform. *Offshore Technology Conference,* OTC 4207, Vol. 1, 495-510.

Matsuoka, H. (1976) - On the significance of the spatial mobilised plane. *Soils and Foundations*, Vol. 16, No. 1, 91-100.

McClelland, B. (1988) - Calcareous sediments: An engineering enigma. *Proc. Int. Conf. Calcareous Sediments*, Perth, Vol. 2, 777-784.

Meyerhof, G.G. (1961) - The ultimate bearing capacity of wedge shaped foundations. *Proc. 5th Int. Conf. Soil Mech. Found. Eng.*, Vol. 2, 105-109.

Mitchell, J.K. and Gardener, W.S. (1975) - In situ measurements of volume change characteristics. *Proc. ASCE Spec. Conf. In situ measurement of soil properties*, Raleigh, U.S.A.

Mitchell, J.K. and Keaveny, J.M. (1986) - Determining sand strength by cone penetrometer. *Proc. ASCE Spec. Conf., In situ '86*, Blacksburg.

Mitchell, J.K. and Lunne, T. (1978) - Cone resistance as measure of sand strength. *Journ. Geotech. Eng. Div., ASCE*, Vol. 104, No. GT7, 995-1012.

Mitchell, J.K. and Solymar, Z.V. (1984) - Time-dependent gain in freshly deposited and densified sand. *Journ. Geotech. Eng. Div., ASCE*, No. 11.

Miura, S. and Toki, S. (1982) - A sample preparation method and its effect on static and cyclic deformation-strength properties of sand. *Soils and Foundations*, ISSMFE, Vol. 22, No. 1, 61-77.

Morrison, M.J., McIntyre, P.D., Sauls, D.P. and Oosthuizen, M. (1988) - Laboratory test results for carbonate soils from offshore Africa. *Proc. Int. Conf. Calcareous Sediments*, Perth, Vol. 1, 109-118.

Mostyn, G. (1988) -Statistical evaluation of design parameters for gravity based anchor system. *Proc. Int. Conf. Calcareous Sediments*, Perth, Vol. 2, 711-718.

Murff, J.D. (1987) - Pile capacity in calcareous sands: state of the art report. *Journ. Geotech Eng., ASCE* Vol. 113, GT5, 490-507.

Nash, D.F.T., Powell, J.J.M. and Lloyd, I.M. (1992) - Initial investigations of the soft clay test site at Bothkennar. *Géotechnique*, Vol. 42, No. 2, 163-182.

Nauroy, J.F. and le Tirant, P. (1983) - Model tests of piles in calcareous sands. *Proc. Conf. Geotechnical practice in offshore engineering.*, ASCE, Texas, 356-369.

Noorany, I. (1985) - Side friction of piles in calcareous sands. *Proc. 11th ICSMFE*, San Fransisco, Vol. 3, 1611-1614.

Olsen, R.S. and Farr, J.V. (1986) - Site characterization using the cone penetration test. *Proc. ASCE Spec. Conf., In situ '86*, Blacksburg.

Palmer, A.C. (1972) - Undrained plane-strain expansion of a cylindrical cavity in clay: a simple interpretation of the pressuremeter test. *Géotechnique*, Vol. 22, No. 3, 451-457.

Parkin, A.K., Lunne, T. (1982) - Boundary effects in the laboratory calibration of a cone penetrometer for sand. *Proc. 2nd European Symp. Penetration Testing*, Amsterdam, Vol. 2, 761-768.

Poulos, H.G. (1980) - A review of the behaviour and engineering properties of carbonate soils. *Research Report R381*, Univ. Sydney.

Poulos, H.G., Uesugi, M. and Young, G.E. (1982) - Strength and deformation properties of Bass Strait carbonate sands, *Research Report R412*, Univ. Sydney.

Powell, J.J.M. and Quarterman, R.S.T. (1988) - The interpretation of cone penetration tests in clays, with particular reference to rate effects. *Proc. 1st Int. Symp. Penetration testing*, ISOPT1, Orlando, Vol. 2, 903-910.

Rad, N.S. and Tumay, M.T. (1987) - Factors affecting sand specimen preparation by raining. *Geotech. Testing. Journ.*, Vol. 10, No. 1, 31-37.

Reading, H.G. (1978) - *Sedimentary environments and facies*. London: Blackwell Scientific Publ.

Renfry, G.E., Waterton, C.A. and van Goudoever, P. (1988) - Geotechnical data used for the design of the North Rankin *A* platform foundation. *Proc. Int. Conf. Calcareous Sediments*, Perth, Vol. 2, 343-356.

Robertson, P.K. (1990) - Soil classification using the cone penetration test. *Can. Geotech. Journ.*, Vol. 27, 151-158.

Robertson, P.K. and Campanella, R.G. (1983) - Interpretation of cone penetration tests. *Canadian Geotech. Journ.*, Vol. 20, No. 4, 718-733.

Robertson, P.K. and Hughes, J.M.O. (1986) - Determination of properties of sand from self-boring pressuremeter tests. *Proc. 2nd Symp. Pressuremeter and its marine applications*. ASTM SPT 950, 283-302.

Rowe, P.W. (1962) - The stress-dilatancy relation for static equilibrium of an assembly of particles in contact. *Proc. Royal Soc.*, A 269, 500-527.

Sagaseta, S. (1984) - Personal communication to Oxford University.

Schmertmann, J. (1975) - The measurement of *in situ* shear strength. *Proc. ASCE Spec. Conf. In-situ measurements of soil properties, Vol. 2.*

Schmertmann, J. (1978) - Guidelines for cone penetration test performance and design. *Dept. Transportation, Federal Highway Administration,* Report No. FHWA-TS-78-209, Washington.

Scoffin, T.P. (1988) - The environments of production and deposition of calcareous sediments on the shelf west of Scotland. *Journ. Sedimentary Geology*, Vol. 60, 107-124.

Searle, I.W. (1979) - The interpretation of Begemann friction jacket cone results to give soil types and design parameters. *Proc. 7th European Conf. SMFE*, Brighton, Vol. 2, 265-270.

Seed, H.B., Wong, R.T., Idriss, I.M. and Tokimatsu, K. (1986) - Moduli and damping factors for dynamic analyses of cohesionless soils. *J. Geotech. Eng. Div., ASCE*, GT11, 1016-1032.

Semple, R.M. (1988) - The mechanical properties of carbonate soils. *Proc. Int. Conf. Calcareous Sediments*, Perth, Vol. 2, 807-836.

Senneset, K., Janbu, N. and Svano, G. (1982) - Strength and deformation parameters from cone penetration tests. *Proc. Second European Symp. Penetration Testing*, Amsterdam, 863-870.

Singh, A. and Mitchell, J.K. (1968) - General stress-strain time function for soils. *Journ. Soil Mech. Found. Div. ASCE*, Vol. 94, SM1, 21-46.

Smith, M.G. (1990) - First year report, Oxford University

Stroud, M.A. (1971) - Sand at low stress levels in the Simple Shear Apparatus. *PhD Thesis*, University of Cambridge.

Taylor, D.W. (1948) - *Fundamentals of Soil Mechanics*. Wiley, New York

Teh, C.I. (1987) - An analytical study of the cone penetration test. *D.Phil thesis*, Oxford University.

Vaid, Y.P. and Negussey, D. (1984) - Relative density of pluviated sand samples. *Soils and Foundations*, ISSMFE, Vol. 24, No. 2, 101-105.

Vesic, A.S. (1972) - Expansion of cavities in an infinite soil mass. *ASCE Journ. Soil Mechanics and Foundation Engineering*, Vol. 98, 265-290.

Vesic, A.S. (1975) - Principles of pile design. *Lecture series on Deep Foundations*, M.I.T., Cambridge, U.S.A.

Vesic, A.S. (1977) - Design of pile foundations. *Synthesis of Highway Practice No. 42*, National co-operative highway research programme, National Research Council, Washington D.C.

Vesic, A.S. and Clough, G.W. (1968) - Behaviour of granular materials under high stresses. *Journ. Soil Mech. Found. Div. ASCE*, Vol. 94, SM3, 661-688.

Villet, W.C.B. and Mitchell, J.K. (1981) - Cone resistance, relative density and friction angle. Cone penetration testing and experience. *Proc. ASCE National Convention*, St. Louis, 178-208.

Voyiadjis, G.Z., Tumay, M. and Kurup, P. (1991) - Minature piezocone penetration tests on soft soils in a calibration chamber system. *Proc. First Int. Symp. Calibration Chamber Testing*, ISOCCT1, Potsdam, U.S.A., 377-392.

Walker, B.P. and Whitaker, T. (1967) - An apparatus for forming uniform beds of sand for model foundation tests. *Géotechnique, Vol. 17, No. 2.*

Windle, D. (1976) - In situ testing of soils with a self-boring pressuremeter. *PhD. thesis*, University of Cambridge.

Windle, D. and Wroth, C.P. (1977) - In situ measurement of the properties of stiff clays. *Proc. 9th ICSMFE*, Tokyo, Vol. 1, 347-352.

Wood, D.M. (1990) - Strain-dependent moduli and pressuremeter tests. *Géotechnique*, Vol. 40, No. 3, 509-512

Wroth, C.P. (1982) - British experience with the self-boring pressuremeter. *Proc. Symp. on the pressuremeter and its marine applications*. Paris, 143-164.

Wroth, C.P. (1984) - The interpretation of *in situ* soil tests. *Géotechnique*, Vol. 34, No. 4, 449-489.

Wroth, C.P. (1988) - Penetration testing - A more rigorous approach to interpretation. *Proc. First Int. Symp. Penetration Testing*, ISOPT-1, Orlando, 303-314.

Wroth, C.P., Randolph, M.F., Houlsby, G.T. and Fahey, M. (1979) - A review of the engineering properties of soils with particular reference to the shear modulus. *Report CUED/D Soils TR75*, Cambridge University.

Wroth, C.P. and Windle, D. (1975) - Analysis of the pressuremeter test allowing for volume change. *Géotechnique*, Vol. 25, 598-604.

Yu, H.S. and Houlsby, G.T. (1991) - Finite cavity expansion in dilatant soils: loading analysis. *Géotechnique*, Vol. 41, No. 2, 173-183.

Zienkiewicz, O.C. (1986) - *The Finite Element Method.* 3rd Edition, McGraw-Hill, Maidenhead.

Bibliography

An exhaustive list of references relating to full-displacement pressuremeters

Baguelin, F. and Jezequel, J.F. (1986) - The LPC pressio penetrometer. *Proc. Symp. Offshore Engineering practice.* 203-219.

Campanella, R.G., Howie, J.A., Sully, J.P., Hers, I. and Robertson, P.K. (1990) - Evaluation of cone pressuremeter tests in soft cohesive soils. *Proc. Third Int. Symp. on Pressuremeters*, British Geotechnical Society, Oxford, 125-136.

Campanella, R.G. and Robertson, P.K. (1986) - Research and development of the UBC cone pressuremeter. *3rd Can. Conf. Marine Geotechnical Engineering*, MEM. Univ., St. John's, NFLD., June.

Hers, I. (1989) - The interpretation and analysis of the cone pressuremeter in cohesive soils. *MASc. Thesis*, Dept. Civil Eng., Univ British Columbia.

Houlsby, G.T. (1990) - Methods of interpretation of *in situ* tests. *Modern in situ testing of soil*, lecture 2, Course at Oxford University.

Houlsby, G.T. and Nutt, N.R.F. (1992) - Development of the cone pressuremeter. *Proc. Wroth Memorial Symp.*, Oxford, 254-271.

Houlsby, G.T. and Withers, N.J. (1988) - Analysis of the cone pressuremeter test in clay. *Géotechnique*, Vol. 38, No. 4, 575-587.

Houlsby, G.T. and Yu, H.S. (1990) - Finite element analysis of the cone pressuremeter test. *Proc. Third Int. Symp. on Pressuremeters*, British Geotechnical Society, Oxford, 221-230.

Howie, J.A. (1989) - *PhD thesis*, University of British Columbia

Howie, J.A., Robertson, P.K. and Campanella, R.G. (1990) - Influence of equipment and test procedures on interpretation of PM tests. *Proc. 3rd Int. Sypm. Pressuremeters.* Oxford, 104-114.

Hughes, J.M.O. and Robertson, P.K. (1985) - Full displacement pressuremeter testing in sand. *Canadian Geotech. Journ.*, No. 22, 298-307.

Jezequel, J.F., Lamy, J.L. and Perrier, M. (1982) - The LPC-TLM pressio-penetrometer. *Proc. Symp. Pressuremeter and its marine applications.* Paris, 275-288.

Nutt, N.R.F. and Houlsby, G.T. (1991) - Calibration tests on the cone pressuremeter in carbonate sand. *Proc. First Int. Symp. Calibration Chamber Testing*, ISOCCT1, Potsdam, U.S.A., 265-275.

Powell, J.J.M. (1990) - A comparison of four different pressuremeters and their methods of interpretation in a stiff, heavily overconsolidated clay. *Proc. 3rd Int Symp. Pressuremeters.* Oxford, 287-298.

Robertson, P.K., Hughes, J.M.O., Campanella, R.G. and Sy, A. (1984) - Design of laterally loaded displacement piles using a driven pressuremeter. *Laterally loaded deep foundations: analysis and performance*, ASTM STP 835, 229-238.

Schnaid, F. (1988) - A calibration chamber at Oxford University for testing granular materials. *Proc. Sem. Calibration of in situ tests in laboratory and field*, session 2, Oslo.

Schnaid, F. (1990) - A study of the cone pressuremeter test in sand. *D.Phil thesis,* Oxford University.

Schnaid, F. and Houlsby, G.T. (1990) - Calibration chamber tests of the cone pressuremeter in sand. *Proc. 3rd Int Symp. Pressuremeters.* Oxford, 263-272.

Schnaid, F. and Houlsby, G.T. (1991) - An assessment of chamber size effects in the calibration of in situ tests in sand. *Géotechnique*, Vol. 41, No. 3, 437-445.

Withers, N.J., Schaap, L.H.J. and Dalton, C.P. (1986) - The development of a full displacement pressuremeter. *Proc. Second Int. Symp. on The Pressuremeter and its Marine Applications.* ASTM SPT 950, 38-56.

Withers, N.J., Howie, J.A., Hughes, J.M.O. and Robertson, P.K. (1989) - Performance and analysis of cone pressuremeter tests in sands. *Géotechnique,* Vol. 39, No. 3, 433-454.

Yu, H.S. (1990) - Cavity expansion theory and its application to the analysis of pressuremeters. *D.Phil thesis,* Oxford University.